

University of New Mexico

**UNM Digital Repository**

---

Earth and Planetary Sciences ETDs

Electronic Theses and Dissertations

---

Summer 7-13-2020

## **NEOGENE DRAINAGE REVERSAL AND COLORADO PLATEAU UPLIFT IN THE SALT RIVER AREA**

Jordan Curtis Anderson

Follow this and additional works at: [https://digitalrepository.unm.edu/eps\\_etds](https://digitalrepository.unm.edu/eps_etds)



Part of the [Geology Commons](#)

---

### **Recommended Citation**

Anderson, Jordan Curtis. "NEOGENE DRAINAGE REVERSAL AND COLORADO PLATEAU UPLIFT IN THE SALT RIVER AREA." (2020). [https://digitalrepository.unm.edu/eps\\_etds/272](https://digitalrepository.unm.edu/eps_etds/272)

This Thesis is brought to you for free and open access by the Electronic Theses and Dissertations at UNM Digital Repository. It has been accepted for inclusion in Earth and Planetary Sciences ETDs by an authorized administrator of UNM Digital Repository. For more information, please contact [amywinter@unm.edu](mailto:amywinter@unm.edu), [lsloane@salud.unm.edu](mailto:lsloane@salud.unm.edu), [sahrk@unm.edu](mailto:sahrk@unm.edu).

Jordan C. Anderson

*Candidate*

---

Earth and Planetary Science

*Department*

---

This thesis is approved, and it is acceptable in quality and form for publication:

*Approved by the Thesis Committee:*

Dr. Karl Karlstrom, Chairperson

---

Dr. Laura Crossey

---

Dr. Louis Scuderi

---

Dr. Matthew Heizler

---

**NEOGENE DRAINAGE REVERSAL AND COLORADO  
PLATEAU UPLIFT IN THE SALT RIVER AREA**

**by**

**JORDAN C. ANDERSON**

**B.S. EARTH AND PLANETARY SCIENCE  
UNIVERSITY OF NEW MEXICO  
2016**

**M.S. THESIS**

Submitted in Partial Fulfillment of the  
Requirements for the Degree of

**Master of Science  
Earth and Planetary Sciences**

The University of New Mexico  
Albuquerque, New Mexico

**July, 2020**

## ACKNOWLEDGMENTS

I would like to acknowledge and thank my advisor Dr. Karl Karlstrom for his guidance and inspiration in this project. His passion and dedication to the field of geologic research inspired me to complete this thesis. I would not be the geologist I am today without his advisement.

I would also like to thank the members of my committee, Dr. Laura Crossey for her academic and financial support; Dr. Louis Scuderi for his GIS insights; Dr. Matthew Heizer and the members of the New Mexico Geochronology Research Laboratory in Socorro, NM for their technical expertise with the  $^{40}\text{Ar}/^{39}\text{Ar}$  analyses.

Finally, I would like to thank my family and Camille Dwyer for their support throughout my academic career.

**NEOGENE DRAINAGE REVERSAL AND COLORADO PLATEAU UPLIFT IN  
THE SALT RIVER AREA**

**by**

**Jordan Anderson**

**B.S., Earth and Planetary Science, University of New Mexico, 2016**

**M.S., Earth and Planetary Science, University of New Mexico, 2020**

**ABSTRACT**

The Salt River of east-central Arizona flows southwest across a diverse desert landscape. Its headwaters drain the southern Colorado Plateau and it ends in the Basin and Range where it is the largest tributary of the Gila River. Geology in this area is rich with sedimentological and structural data useful in understanding the evolution of the southern Colorado Plateau. The overall goal of this study is to constrain when the southern edge Colorado Plateau developed in this area and how it has changed since. This study examines the history of the Salt River and its precursors to evaluate drainage evolution of the southern Colorado Plateau

Rivers in the Salt River area flowed northeast during the Paleogene and Eocene. They drained the Mogollon Highlands and flowed onto the Colorado Plateau. This was followed by Oligocene and Basin and Range normal faulting that down-dropped the Mogollon Highlands relative to the Colorado Plateau. The combination of normal

faulting and Colorado Plateau uplift ended the northeast-flowing river systems and caused the regional drainage direction to reverse and flow toward the southwest. Chapter 1 of this study refines the timing of this drainage reversal by constraining the ages of paleoriver sediments deposited before and after the reversal. Maximum depositional ages of river sediments are determined by detrital zircon and sanidine. Minimum depositional ages are determined by overlying or interbedded volcanic units. River provenance is constrained by detrital grain studies and clast counts from previous studies. The overall result of Chapter 1 are multiple ages for northeast-flowing rivers (<59.38 Ma in the Flying V Canyon area and 37-33.55 Ma for the rest of the study area), a refined age for the initial sediments deposited by internal drainage in the Salt River paleocanyon (30-21.8 Ma), and distinctly different ages for southwest-flowing rivers in the Salt River paleocanyon (<12.49 Ma and <7.34 Ma). These results indicate the transition from northeast-flowing rivers to internal drainage occurred between 33.55 and 30 Ma.

The Colorado Plateau has experienced multiple stages of uplift since the late Cretaceous. The first occurred during the Laramide orogeny and the second occurred during the ignimbrite flareup. Chapter 2 of this study uses incision rates in the Salt River to quantify post-10 Ma stage of Colorado Plateau uplift. Incision rate of the Salt River's headwaters have been semi-steady at a rate of 95 m/Ma over the past 3 Ma as calculated using the age and height of four basalt flows from the Springerville Volcanic field emplaced in paleochannels of the Salt River and its tributaries between 3.0 to 0.52 Ma. These rates differ from rates of 10 m/Ma calculated for downstream incision rates near the Sentinel-Arlington volcanic field on the Gila River over the past 2.37 Ma. This differential incision rate of the headwaters relative to the base river of 85 m/Ma over 3

Ma is interpreted to reflect 255 m of surface uplift of young uplift of the Colorado Plateau uplift.

**TABLE OF CONTENTS**

**ABSTRACT..... IV**

**LIST OF FIGURES..... IX**

**LIST OF TABLES..... XI**

**CHAPTER 1 NEOGENE DRAINAGE REVERSAL IN THE SALT RIVER**

**AREA..... 1**

    ABSTRACT..... 1

    INTRODUCTION..... 3

    GEOLOGIC BACKGROUND AND PREVIOUS WORK..... 5

    GOAL OF THIS STUDY..... 20

    METHODS..... 21

    RESULTS..... 24

    INTERPRETATIONS..... 48

    DISCUSSION..... 54

    CONCLUSIONS..... 58

    REFERENCES..... 61

**CHAPTER 2 COLORADO PLATEAU UPLIFT IN THE SALT RIVER**

**AREA..... 69**

    ABSTRACT..... 69

    INTRODUCTION..... 70

    METHODS..... 74

    RESULTS..... 77

    INTERPRETATIONS..... 79

CONCLUSIONS.....	88
REFERENCES.....	89

# LIST OF FIGURES

## Chapter 1

Figure 1.....	4
Figure 2.....	5
Figure 3.....	6
Figure 4.....	7
Figure 5.....	9
Figure 6.....	15
Figure 7.....	18
Figure 8.....	22
Figure 9.....	26
Figure 10.....	27
Figure 11.....	28
Figure 12.....	29
Figure 13.....	30
Figure 14.....	32
Figure 15.....	33
Figure 16.....	34
Figure 17.....	35
Figure 18.....	36
Figure 19.....	37
Figure 20.....	39
Figure 21.....	40

Figure 22.....	41
Figure 23.....	42
Figure 24.....	44
Figure 25.....	45
Figure 26.....	47

## **Chapter 2**

Figure 1.....	73
Figure 2.....	74
Figure 3.....	78
Figure 4.....	81
Figure 5.....	84

## LIST OF TABLES

### Chapter 1

Table 1..... 25

Table 2..... 25

### Chapter 2

Table 1..... 77

## **CHAPTER 1: NEOGENE DRAINAGE REVERSAL IN THE SALT RIVER AREA**

### **ABSTRACT**

The modern Salt River flows southwest from the Colorado Plateau, through the Arizona Transition Zone and into to the Basin and Range. Rivers in this area flowed northeast during the Paleogene from the Laramide Mogollon Highlands into structural basins of the topographically lower southern Colorado Plateau area. One of these rivers carved the Salt River paleocanyon through a portion of the Mogollon Highlands known as the Apache Uplift to similar depths as the modern Grand Canyon. This study refines the timing of this drainage reversal in the Salt River area by constraining the ages of paleoriver sediments deposited during the time of northeast-flowing rivers, internal drainage and southwest-flowing rivers. These results provide insights into the evolution of the southern Colorado Plateau.

U-Pb dating of detrital zircon is used for maximum depositional ages and provenance analyses.  $^{40}\text{Ar}/^{39}\text{Ar}$  dating of detrital sanidine is used for higher precision maximum depositional ages. The majority of paleoriver samples that were analyzed with both detrital zircon and sanidine show similar maximum depositional ages. Minimum or direct depositional ages are determined by overlying or interbedded volcanic units.

The Mogollon Rim Formation is composed of river gravel, sandstone and mudstone on the southern rim of the Colorado Plateau that were deposited by northeast-flowing rivers. Results indicate deposition began after 59.38 Ma in the Flying V Canyon area and from 37 – 33.55 Ma in the Trout Creek section. The Whitetail Conglomerate represents the transition from northeast-flowing rivers to internal drainage in the Salt

River paleocanyon. Whitetail Conglomerate is as old as the interbedded 37.6 Ma dacite in Canyon Creek fault side drainages, but deposition in the axis of the Salt River paleocanyon occurred between 30 and 21.8 Ma. The transition from northeast-flowing rivers to internal drainage occurred between 33.55-30 Ma marking the age of initial development of the southern edge of the Colorado Plateau. Apache Leap tuff flowed NE down Salt River paleocanyon nearly to Canyon Creek fault at 18.6 Ma. Internal drainage is documented by the 14.67 Ma Black Mesa basalt that flowed onto underlying lake beds. The first southwest-flowing river system in the Salt River paleocanyon deposited the Dagger Canyon conglomerate after incising at least 200 m deep into the Whitetail Conglomerate. The lower Dagger Canyon conglomerate is present in tilted fault blocks on the eastern side of Tonto Basin and the western portion of the Salt River paleocanyon. The dip of bedding increases down-section from 0 to 27° providing evidence that deposition occurred while the faults were active. Lower Dagger Canyon conglomerate deposition began after 12.49 Ma, presumably due to base level fall associated with Basin and Range extension. The upper Dagger Canyon conglomerate is composed of flat-lying river gravels and sandstone located at higher elevations than the lower Dagger Canyon conglomerate in Tonto Basin and the Salt River paleocanyon. Deposition of the upper Dagger Canyon conglomerate began after 7.34 Ma and a possible a lag in fluvial deposition occurred between the two facies. If a lag in fluvial deposition occurred then the upper Dagger Canyon conglomerate represents a rejuvenation of the southwest-flowing river system in the Salt River paleocanyon after Basin and Range faulting waned. A likely driver for this rejuvenation would be southern Colorado Plateau uplift by the building of Mount Baldy volcanic field 12-8 Ma.

## **INTRODUCTION**

The Salt River area of central Arizona contains an informative record of the Cenozoic tectonism and geomorphic evolution of the Arizona Transition Zone and the southern Colorado Plateau region of the southwestern U.S. The 320-km-long river system drains an area of 35,480 square kilometers and is the largest tributary of the Gila River. It flows southwest from the southern edge of the Colorado Plateau, through the Arizona Transition Zone, and into the Basin and Range province where it meets the Gila River near Phoenix, Arizona (Figure 1). The Gila River continues southwest through the Basin and Range until it meets the Colorado River near Yuma, AZ. The name Salt River is applied below the confluence of the White and Black Rivers (Figure 2). These rivers and their tributaries have their headwaters in the erosional escarpment of the Mogollon Rim, the White Mountains, Mount Baldy and the Springerville volcanic field. The Salt River cuts a towering 600-m-deep canyon near the boundary between the Colorado Plateau and the Arizona Transition zone. Significant tributaries to the Salt River flow south from the Mogollon Rim escarpment.

The Salt River flows southwest, however rivers in this area flowed toward the northeast during the Paleogene. The regional drainage reversal was facilitated by the extensional collapse of the Laramide Mogollon Highlands and Colorado Plateau uplift (Hunt, 1956; Peirce et al., 1979; Faulds, 1986; Potochnik and Faulds, 1998). The northeast-flowing rivers drained the Mogollon Highlands and deposited sediment onto the topographically lower Colorado Plateau area (Cather and Johnson, 1984; Potochnik, 1989). Two episodes of extension, one during the Oligocene and another during Miocene Basin and Range deformation collapsed the Mogollon Highlands (Davis and Coney,

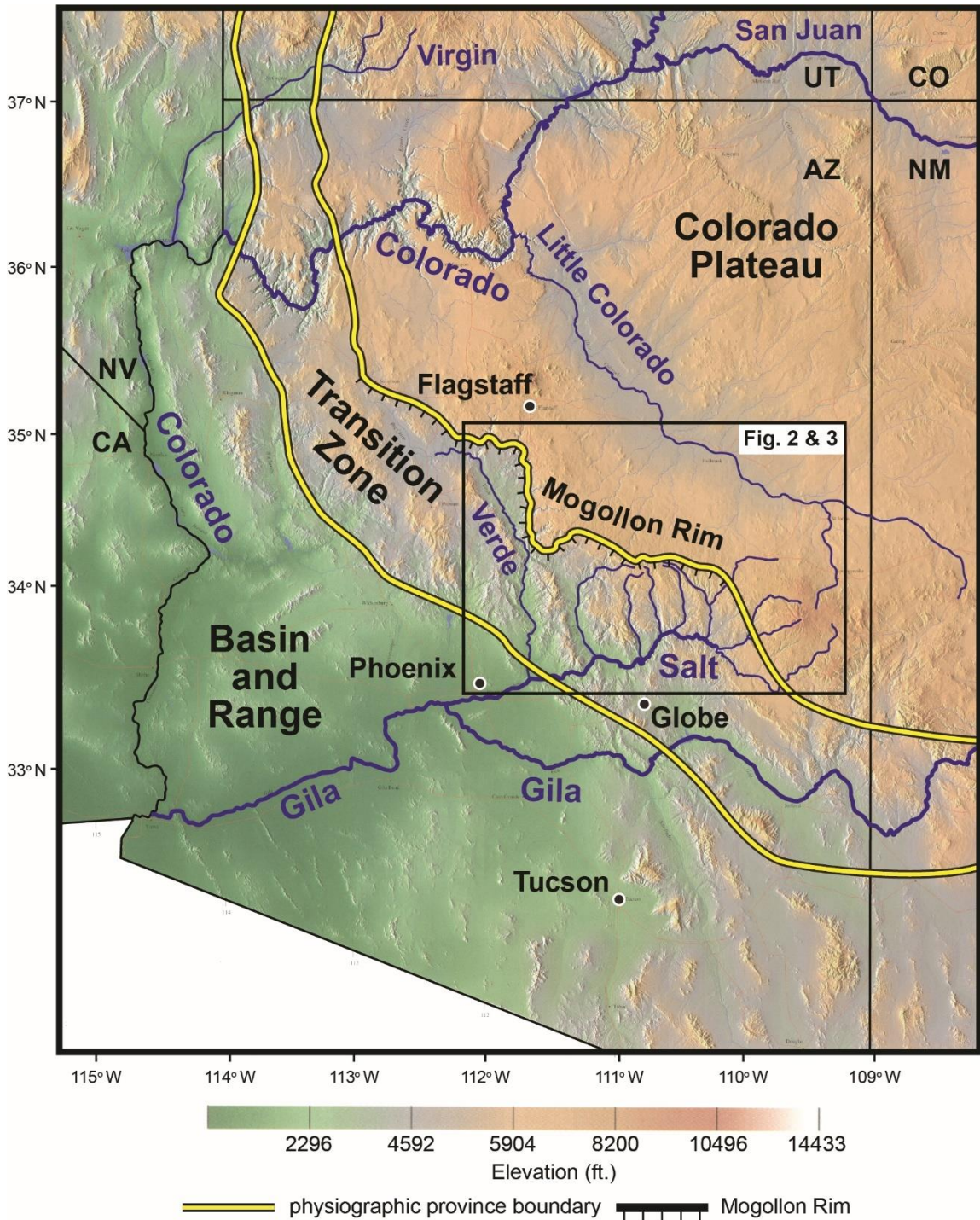


**Figure 1:** Digital elevation map of Arizona. Physiographic province boundaries outlined in yellow-black lines; Mogollon Rim escarpment shown by black ticks; major rivers shown with blue lines. The areas of Figures 2 and 3 are outlined by black boxes.

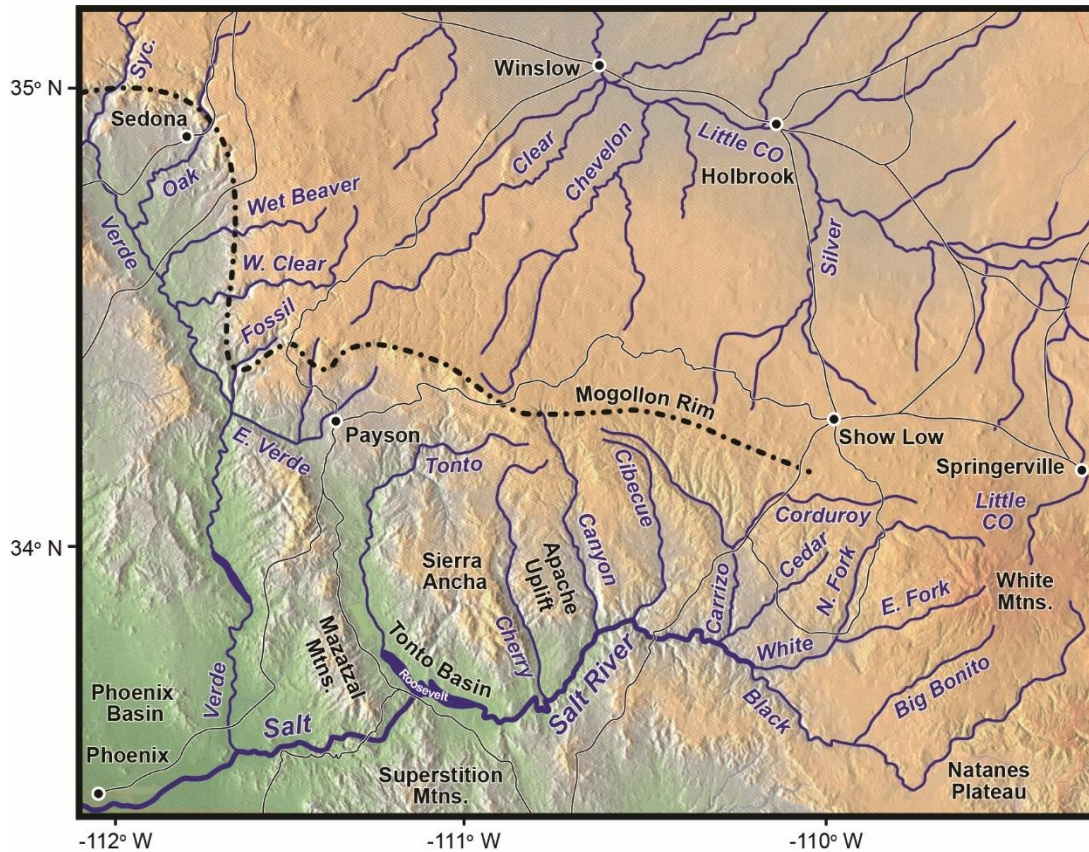


**Figure 2:** Digital elevation map of the Salt River drainage area and its major tributaries. Syc. stands for Sycamore Creek. Major highways are shown with white and black lines. Major cities are shown by black circles. The Mogollon Rim escarpment is shown with a black dashed line.

1979). This, combined with Colorado Plateau uplift to the northeast, forced rivers to flow southwest (Peirce, 1985; Faulds, 1986; Potochnik and Faulds, 1998). The goals of this study are to constrain the timing of the drainage reversal and to better understand Colorado Plateau evolution.

## **GEOLOGIC BACKGROUND AND PREVIOUS WORK**

The Colorado Plateau was near sea level during the Early Cretaceous. The Western Interior Seaway inundated much of North America in a north-south trending interior seaway that extended from the Arctic to the Gulf of Mexico (Williams and Stelck,

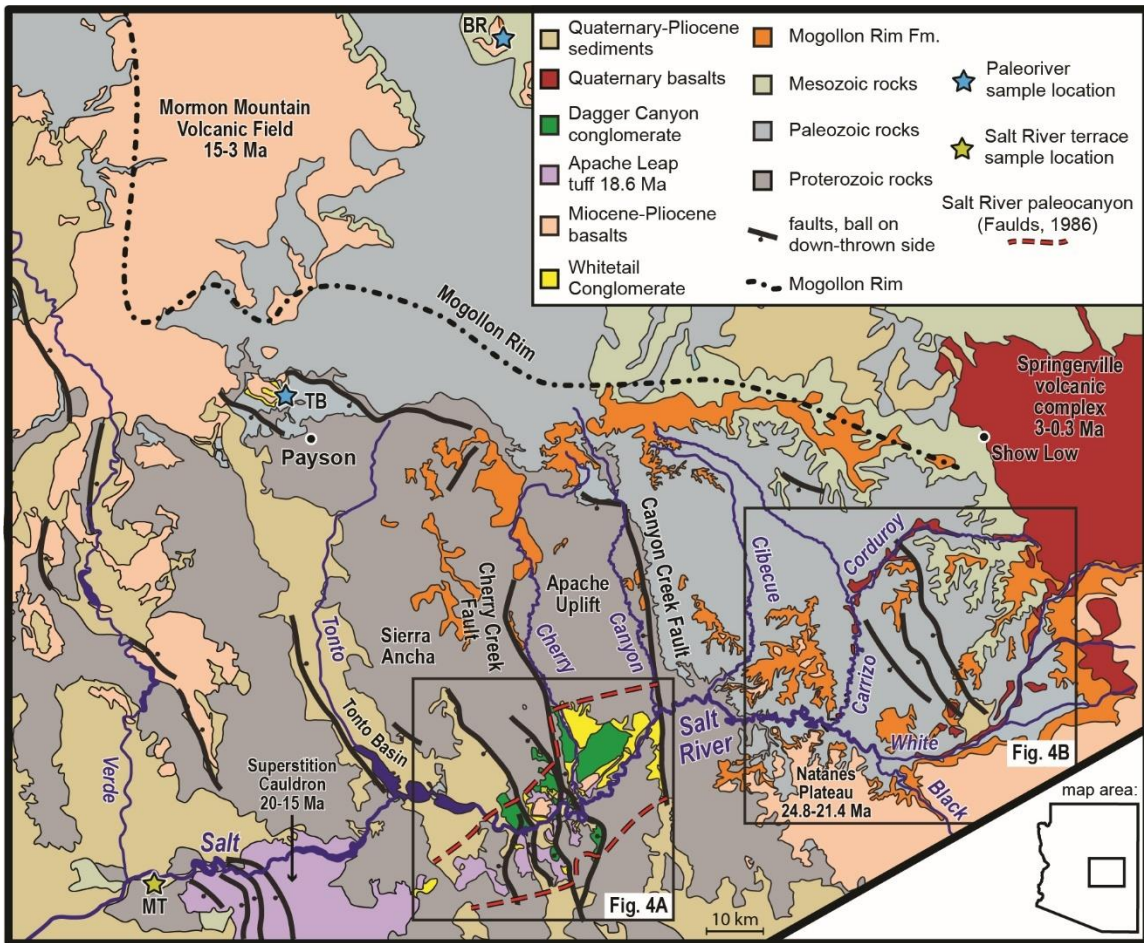


**Figure 3:** Simplified geologic map of the Salt River area showing the extent of the Salt River paleocanyon (Faulds, 1986); modified from Skotnicki, 2002 and state county geologic maps. BR is the Blue Ridge sample location. TB is the Tonto Natural Bridge Sample location. MT is the Mesa terrace sample location. Block boxes show the extent of Figures 4A and 4B.

1975; Nations, 1989; Eaton and Nations, 1991; Cobban et al., 1994; Slattery et al., 2015).

This seaway deposited the Dakota Formation and the Mancos Shale. The base of the Dakota sandstone in Arizona creates a regional angular unconformity overlying older Precambrian rocks to the south and younger Jurassic sediments to the north (Bilodeau, 1986; Dickinson et al., 1989; Potochnik, 2001b). The final Western Interior Seaway regression in the San Juan Basin area occurred around 74 Ma (Cather, 2004). Upper Cretaceous strata are preserved in the Salt River headwaters on the edge of the Colorado

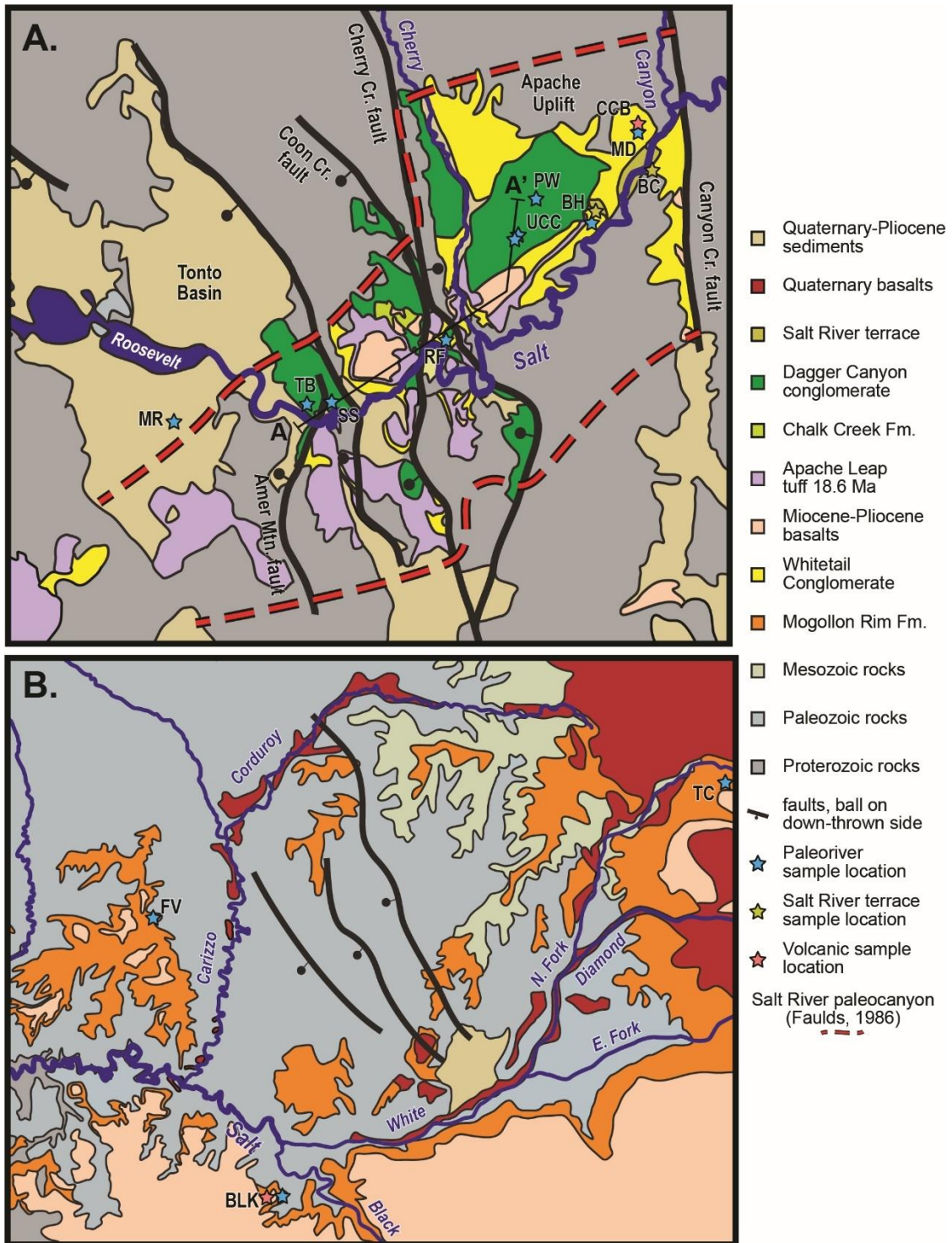


**Figure 4A:** Simplified geologic map of the Salt River paleocanyon area modified from Faulds and Potochnik 2001; and Skotnicki, 2002. Sample locations are: CCB, Canyon Creek Butte; MD, Mud Springs Draw; BC, Butte Creek; BH, Beehive Rock; PW, Pringle Wash; UCC, Upper Corral Canyon; RF, Redmond Flat; SS, ShuteSprings; TB, Tonto Basin; MR, samples K18-MR1-3. Cross section line for Figure 16 outlined from A-A'. **Figure 4B:** Simplified geologic map of the Salt River headwaters modified from Faulds and Potochnik 2001; and Skotnicki, 2002. Sample locations: TC, Trout Creek; BLK, Black River; FV, Flying V Canyon.

Plateau (Figures 3 and 4), but were eroded from the Mogollon Highlands during Laramide uplift.

Laramide orogeny deformation and lower global sea levels forced the Western Interior Seaway to recede from the southern Colorado Plateau area during the Late Cretaceous (Cumella, 1983; Bilodeau, 1986; Haq et al., 1987; Eaton and Nations, 1991). The Laramide was responsible for regional uplift, and east to northeast crustal shortening and tilting Mesozoic and Paleozoic strata focused on the steep limbs of monoclines that bound basement-cored uplifts (Davis, 1979; Keith and Wilt, 1985; Huntoon, 1990). The orogeny also formed the Mogollon Highlands, a northwest to southeast trending mountain range that stretched across Arizona in the location of the modern Arizona Transition Zone (Cooley and Davidson, 1963; Nations et al., 1985; Gastil et al., 1992).

The Apache uplift was one part of the Mogollon Highlands formed by a horst block between the Cherry Creek and Canyon Creek faults (Davis et al., 1982) (Figure 5). These north-south trending faults initially formed during the Late Proterozoic as normal faults and were reactivated during Laramide deformation forming outward facing monoclines (Davis, 1981; Davis et al., 1981; Faulds, 1986). The exact extent of the Apache uplift is not known because of middle to late Cenozoic normal faulting; however, the exposed lengths of the Cherry Creek and Canyon Creek fault zones suggests they extended at least 70 km in length from the Globe-Miami, AZ area to the vicinity of the Mogollon Rim (Faulds, 1986). The uplift was responsible for an estimated 1675 m of Laramide structural relief (Davis et al., 1982). A northeast flowing paleoriver system draining the Mogollon Highlands cut the Salt River paleocanyon at least 1000-1400 m

A. <59-33 Ma

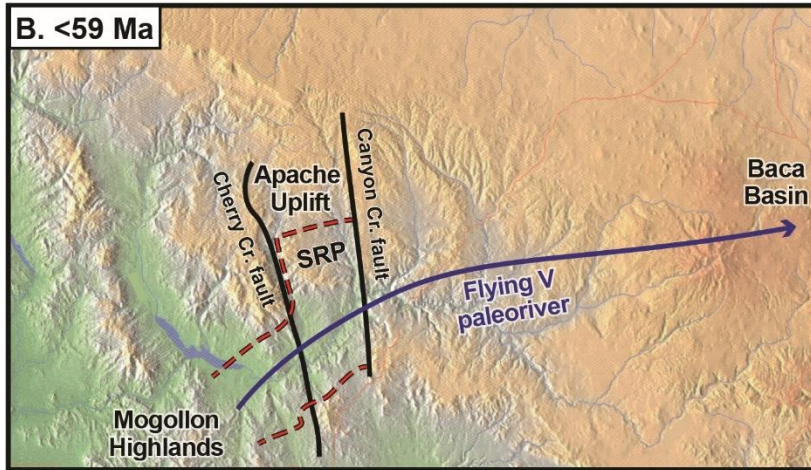
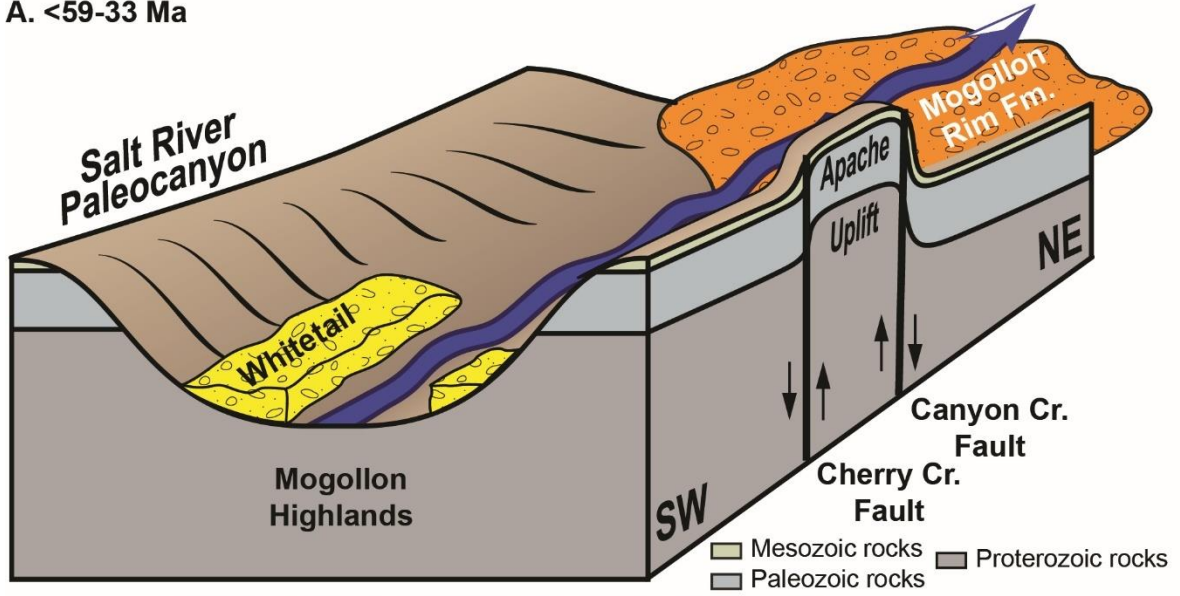


**Figure 5A:** Schematic representation of the Salt River paleocanyon, the Apache uplift, Mogollon Highlands, and northeast-flowing rivers during the Eocene including the relative positions of the Whitetail Conglomerate and Mogollon Rim Formation; modified from Faults, 1986.

**Figure 5B:** Digital elevation map showing approximate location of the NE-flowing Flying V paleoriver that cut the Salt River paleocanyon (SRP) and deposited the gravels at Flying V Canyon after 59 Ma. River paleocurrent directions are from Potochnik, 1989.

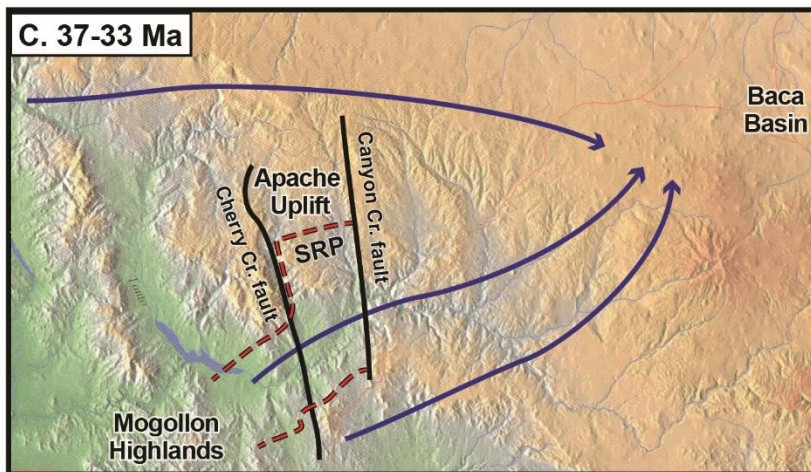


**Figure 5C:** Digital elevation map showing approximate locations of northeast-flowing rivers that deposited the rest of the Mogollon Rim Formation between 37-33 Ma. Locations and paleocurrent directions are from Potochnik, 1989.

deep across the Apache uplift (Peirce, 1985; Faulds, 1986; Potochnik and Faulds, 1998; Potochnik, 2001a). The axis of this paleocanyon is almost parallel to the modern Salt River (Figures 3 and 4A). Using the axis of the paleocanyon as a piercing point, Faulds (1986) determined that the Canyon Creek fault zone must have accommodated at least 1100 m of west-side-up reverse displacement and the Cherry Creek fault zone accommodated at least 600 m of east-side up reverse displacement during the Laramide. The Salt River paleocanyon extended west from Cherry Creek fault to the Superior, Arizona area. (Faulds, 1986).

Several paleoriver systems flowed north and northeast off of the Mogollon Highlands onto basins in the topographically lower Colorado Plateau area (Cooley and Davidson, 1963; Peirce et al., 1979; Faulds, 1986; Potochnik, 1989). These paleorivers beveled Laramide structures and a created a regionally extensive, low to moderate relief pediment surface across the Four Corners area over multiple erosional episodes (Cooley, 1958; Potochnik, 1989; Schmidt, 1991; Potochnik, 2001a; Cather et al., 2012). The paleorivers deposited sets of discontinuous river gravels originally known as “rim gravels” that are located on the rim of the Colorado Plateau and contain basement clasts derived from the Mogollon Highlands to the south (Mckee and Mckee, 1972; Young and Mckee, 1978; Peirce, 1985).

Northeast-flowing paleorivers in the Salt River area deposited the gravels and sandstone known as the Mogollon Rim Formation (Potochnik, 1989) (Figure 5). The Mogollon Rim Formation ranges in thickness from 375 m near Trout Creek, to 45 m at Blue Ridge (Potochnik, 1989, 2001a). The basal member of the Mogollon Rim Formation consists of rounded, cobble to boulder, moderately sorted, clast-supported conglomerates

and river sands with horizontal to massive bedding and lenses of channel sands (Facies A Potochnik, 1989). Clast imbrication and the presence of Precambrian clasts from the Mogollon Highlands and volcanic porphyry clasts from the Miami-Globe porphyry-copper mining district area indicate these gravels were deposited by northeast flowing streams (Potochnik, 1989, 2001a). The upper members of the Mogollon Rim Formation are composed of conglomeratic sandstone, along with subangular to subrounded well sorted sandstone interpreted to represent migrating bedforms in braided bedload streams (Facies B), channel sandstone to mudstone fining-upward sequences interpreted to represent meandering streams (Facies C) and fine-grained sandstone to mudstone sequences represent floodplain deposits (Facies D and E Potochnik, 1989). The transition from mature river gravels to sandstone and mudstone indicates the northeast-flowing rivers lost competency after depositing the basal conglomerate member (Potochnik, 1989). The clast composition changes up-section from predominantly Paleozoic limestone in the lower sections to Proterozoic and Laramide igneous clast in the upper sections indicating that the source area in the Mogollon Highlands was undergoing erosional unroofing (Potochnik, 1989). The ultimate depocenters for these northeast flowing rivers was likely the Baca Basin in western New Mexico (Cather and Johnson, 1984; Cather et al., 1994; Potochnik, 2001b; Donahue, 2016; Pecha et al., 2018) (Figure 5).

Prior to this study, the depositional age of the southeast rim gravels was constrained between  $54.6 \pm 1.2$  to  $33.55 \pm 0.41$  Ma based on the whole rock K-Ar age of a latite clast from the Round Top Mountain area (Peirce et al., 1979) and the  $^{40}\text{Ar}/^{39}\text{Ar}$  age of an overlying tuff in the Trout Creek section (Potochnik and Faulds, 1998). Also, a

33.32 ± 0.59 Ma tuff overlies the section at Blue Ridge (Potochnik, 2001a). A 35.22 ± 0.90 ash is interbedded midway in the section near Trout Creek above the basal conglomerate member (Potochnik and Faulds, 1998).

The Mogollon Rim Formation is conformably overlain by the Spears Group (Figures 6) a debris flow volcanoclastic conglomerate sequence formed by the detritus and pyroclastic material shed from the emerging Mogollon-Datil volcanic field (Cather et al., 1987, 1994). Mogollon-Datil caldera eruptions occurred episodically between 36 and 24 Ma (McIntosh et al., 1992). This volcanic field was one of several to erupt along the edges of the Colorado Plateau during the Ignimbrite Flareup. The Ignimbrite Flare up was responsible for uplifting the Colorado Plateau and defining its edges (Lipman and Glazner, 1991; Humphreys, 1995; Farmer et al., 2008; Roy et al., 2009; Cather et al., 2012; Karlstrom et al., 2012). The Datil Group is overlain by the 25.3 to 17.7 Ma Natanes Plateau flood basalts and basaltic andesites (Damon et al., 1996; Wrucke et al., 2004).

Reverse faults of the Apache Uplift and the Mogollon Highlands were reactivated as normal faults during the Oligocene (Faulds, 1986; Potochnik, 2001a). The Cherry Creek fault's east-down offset and the Canyon Creek fault's west-down offset structurally inverted the Apache Uplift into a broad graben structure (Faulds, 1986; Potochnik, 2001a) (Figure 6). This period of normal faulting lowered the Arizona Transition Zone 760 m relative the Colorado Plateau (Peirce et al., 1979; Faulds, 1986; Potochnik, 1989). The Canyon Creek fault zone experienced a total of 940 m of west-down normal offset (Potochnik and Faulds, 1998).

Regional Oligocene normal faulting facilitated the deposition of the Whitetail Conglomerate in the Salt River paleocanyon (Faulds, 1986; Potochnik and Faulds, 1998;

Potochnik, 2001a) (Figure 4A). This unit represents the transition from erosion to aggradation in the Salt River paleocanyon (Potochnik and Faulds, 1998). The majority of the Whitetail Conglomerate was deposited after northeast-flowing rivers were no longer present in the paleocanyon (Faulds, 1986; Potochnik and Faulds, 1998; Potochnik, 2001a). A  $37.60 \pm 0.60$  Ma rhyodacite flow interbedded in the lower Whitetail Conglomerate along the Canyon Creek fault paleotributary indicates deposition in paleocanyon's tributaries began while northeast-flowing paleorivers were still present in the area and possibly still present in the paleocanyon (Potochnik and Faulds, 1998; Potochnik, 2001a). The Whitetail Conglomerate is a 300-m-thick succession primarily composed of matrix supported, poorly sorted, poorly consolidated, angular, pebble to cobble, conglomerate locally derived from the Salt River paleocanyon with thin beds of coarse sandstone (Faulds, 1986; Potochnik, 2001a). Several distinct facies indicate depositional environments ranged from main channel fluvial, to alluvial fan, and debris flow (Faulds, 1986; Potochnik and Faulds, 1998; Potochnik, 2001a). The thickest accumulations occur along the axis of the Salt River paleocanyon. Thick deposits are also present along the fault bounded paleocanyon tributaries along the Cherry Creek and Canyon Creek faults (Faulds, 1986; Potochnik and Faulds, 1998; Potochnik, 2001a). The regionally distributed Apache Leap Tuff conformably overlies the Whitetail Conglomerate (Faulds, 1986; Potochnik, 2001a) (Figure 6). The Apache Leap Tuff flowed northeast into the Salt River paleocanyon from the Superstition Volcanic Complex at  $18.63 \pm 0.07$  Ma (Faulds, 1986; McIntosh and Ferguson, 1998; Potochnik, 2001a). Paleocurrent directions in the Whitetail Conglomerate, and the thinning of the Apache Leap Tuff toward the northeast indicate that a weak, northeast-flowing drainage

in the Salt River paleocanyon persisted during the Oligocene and that the paleocanyon's headwaters extended to Superior, AZ area (Faulds, 1986; Potochnik, 2001a). The absence of both units east of the Canyon Creek fault indicates that the northeast, through-flowing river system had previously been severed (Faulds, 1986; Potochnik, 2001a). The Whitetail Conglomerate is also locally overlain by two dacite flows located at Canyon Creek Butte and Medicine Butte. Similar deposits are located in the Tonto Natural Bridge area that Pierce (1979) identified as "valley gravels" deposited after the development of the Mogollon Rim escarpment (Figure 3).

The Apache Leap Tuff is disconformably overlain by the Chalk Creek Formation in the Salt River paleocanyon (Figure 6). It contains three interfingering members, a lower fanglomerate and sandstone member, a middle dolomite member and an upper member of mudstone along with volcanoclastic sandstone and conglomerate (Faulds, 1986). The lower fanglomerate and sandstone member is similar to the fanglomerates of the Whitetail Conglomerate except they include clasts of the Apache Leap Tuff. A localized basalt flow from the Coon Creek volcanic center interrupted the deposition of the fanglomerate facies forming topographic barriers that facilitated the formation of lakes in the Salt River paleocanyon at  $16.21 \pm 0.45$  Ma (Faulds, 1986; Potochnik and Faulds, 1998) (Figure 6). These lakes deposited the dolomite and mudstone facies of the Chalk Creek Formation (Faulds, 1986; Potochnik and Faulds, 1998). The thickest accumulations of dolostone are 50 meters thick and occur along the axis of the Salt River paleocanyon indicating the paleocanyon was still a major topographic feature effecting deposition in this area (Faulds, 1986; Potochnik and Faulds, 1998). The  $14.67 \pm 0.34$  Ma Black Mesa basalt flow interfingers the upper member of the Chalk Creek Formation and

A. 18.6-14.7 Ma

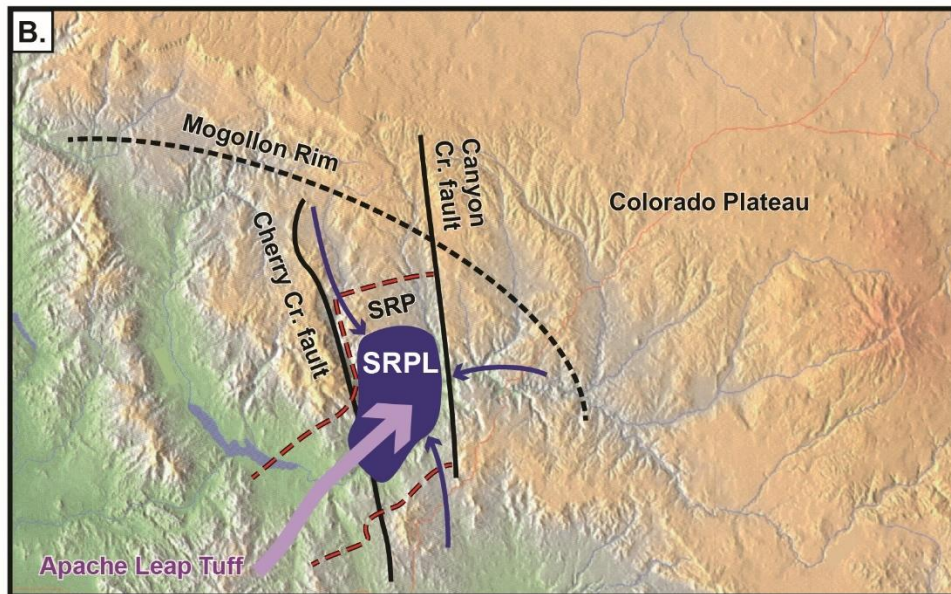
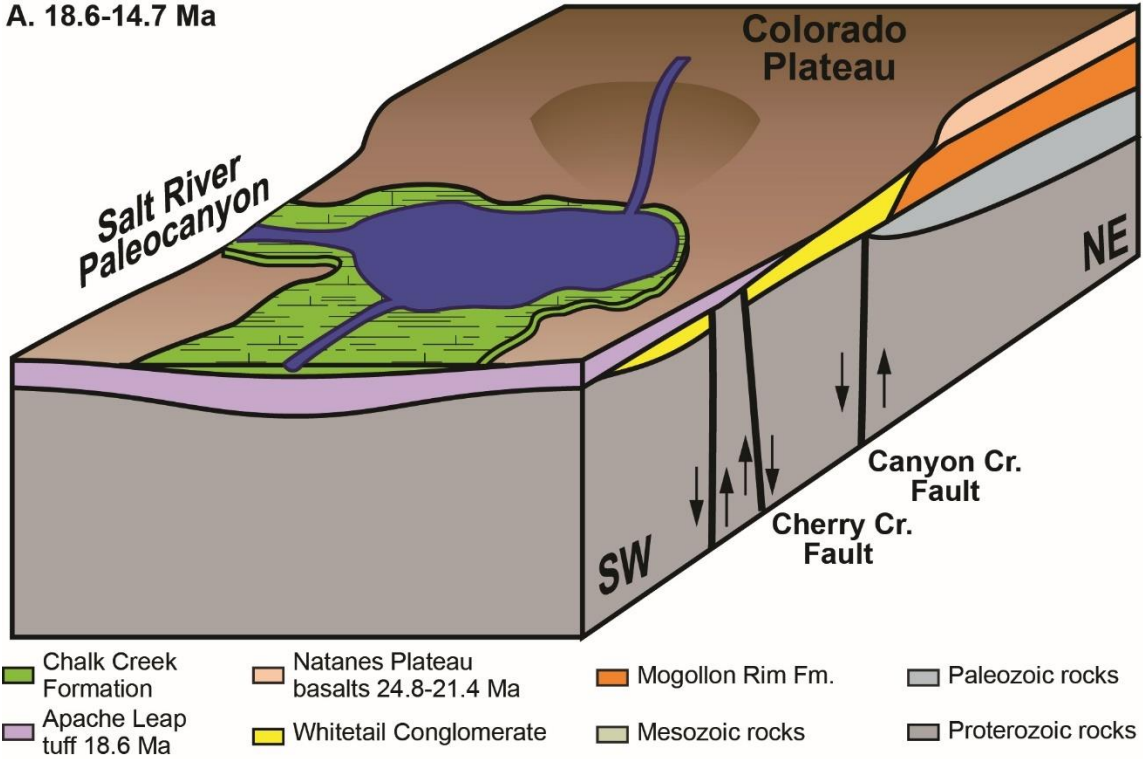


**Figure 6A:** Schematic representation of the internally draining Salt River paleocanyon geology and the Salt River paleocanyon lake during the Oligocene-Miocene including the Salt River paleocanyon and the initial Mogollon Rim escarpment that defined the southern Colorado Plateau boundary; modified from Faults, 1986. **Figure 6B:** Digital elevation map showing approximate locations the Salt River paleocanyon (SRP), the Salt River paleocanyon lake (SRPL), and its tributaries. The approximate path of the NE-flowing Apache Leap Tuff from the Superstition Cauldron to the Salt River paleocanyon is outlined by the purple line. Approximate location of the Mogollon Rim escarpment outlined by black dashed line.

was also sourced from the Coon Creek volcanic center (Faulds, 1986; Potochnik and Faulds, 1998).

Basin and Range faulting significantly deformed the Salt River area between 14 and 12 Ma (Faulds, 1986; Menges and Pearthree, 1989; Potochnik and Faulds, 1998). The Canyon Creek and Cherry Creek faults were again reactivated with normal offset due to southwest-northeast regional extension (Faulds, 1986; Potochnik and Faulds, 1998; Potochnik, 2001a). This faulting equally offsets Black Mesa basalt flows and the Apache Leap Tuff and the lack of middle Miocene conglomerate deposits above the Black Mesa basalt indicate that fault movement here began soon after 14 Ma (Faulds, 1986). The end of this extension likely corresponds with the waning of Basin and Range deformation around 12 Ma (Shafiqullah et al., 1980; Faulds, 1986). The amount of offset along the faults in the Salt River area increases from east to west with a few hundred meters along faults near the Mogollon Rim, to 1150 m at Canyon Creek fault, 1500 m at Cherry Creek fault and more than 1600 m at the edge of the Tonto Basin (Faulds, 1986). Fault angles also decline toward the southwest from sub-vertical near the Mogollon Rim to around 65 degrees at Tonto Basin causing extension values to increase toward the southwest from 1% near the Mogollon Rim to 15% near Tonto Basin (Faulds, 1986). Combined normal offset of these faults during the Oligocene and Miocene canceled out much of the Laramide offset leaving the Apache block 485 m structurally higher than block east of Canyon Creek fault (Faulds, 1986). Tilt-fanning of the dip of Miocene strata relative to faults is observed in the Tonto Basin and elsewhere that records syn-faulting sedimentation. The Tonto Basin to the west and north of the Salt River paleocanyon began subsiding during Oligocene extension based on an angular unconformity between

late Tertiary sedimentary rocks and older cobble to boulder conglomerate likely correlative with the Whitetail Conglomerate (Lance et al., 1962; Faulds, 1986; Nations, 1987). However, most of its subsidence occurred during middle Miocene Basin and Range extension since the basin contains only small amounts of the Whitetail Conglomerate and Apache Leap Tuff and thick deposits of late Cenozoic sedimentary rocks (Faulds, 1986). This basin overtook the Salt River paleocanyon as the deepest largest topographic depression in the area during this time (Faulds, 1986).

Basin and Range extension initiated the first southwest-flowing river system in the Salt River paleocanyon (Faulds, 1986; Potochnik and Faulds, 1998; Potochnik, 2001a). This river system ran a similar course as the modern Salt River east of Tonto Basin (Faulds, 1986; Potochnik, 2001a) and is referred to as the proto-Salt River in this study (Figure 7). The proto-Salt River triggered an erosional episode in the Salt River paleocanyon and formed an angular unconformity between tilted Oligocene to middle Miocene deposits and flat overlying post-14 Ma conglomerates (Faulds, 1986; Potochnik and Faulds, 1998; Potochnik, 2001a). It integrated the majority of the Salt River paleocanyon area and incised 200 m into the Black Mesa basalts and Chalk Creek Formation (Faulds, 1986; Potochnik and Faulds, 1998; Potochnik, 2001a, 2001b). No tilted conglomerates are present above the Black Mesa basalts, this erosional episode must have begun after Black Mesa volcanism and during Basin and Range normal faulting (Faulds, 1986). Potochnik (2001a; 2001b) estimated the proto-Salt River began between  $11.74 \pm 0.94$  and  $8.97 \pm 0.19$  Ma. The older constraint is based on a basalt flow overlying the Mogollon Rim Formation at Flying V Canyon (Damon et al., 1996). The Mogollon Rim Formation at this location was not significantly weathered before

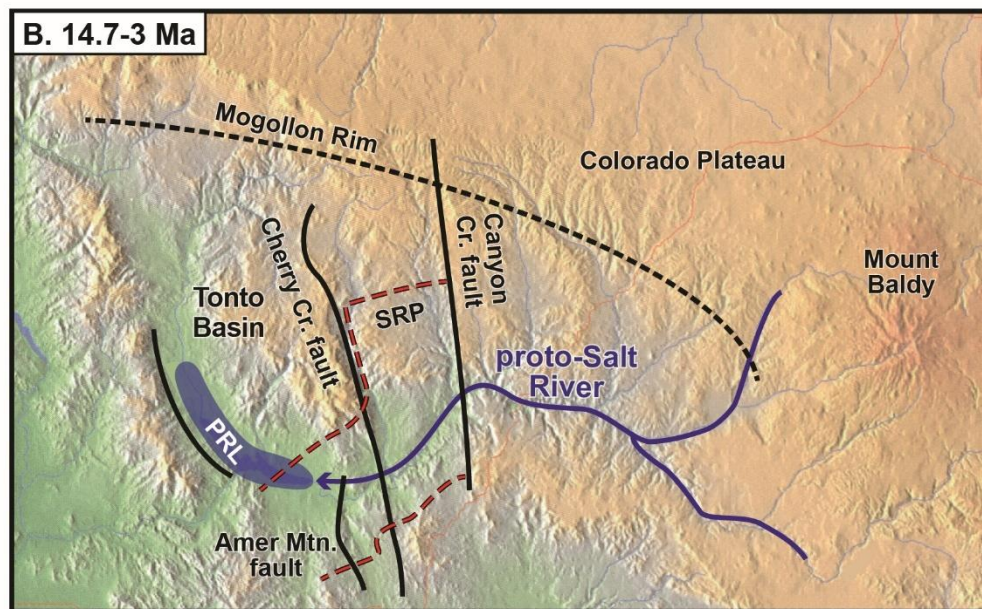
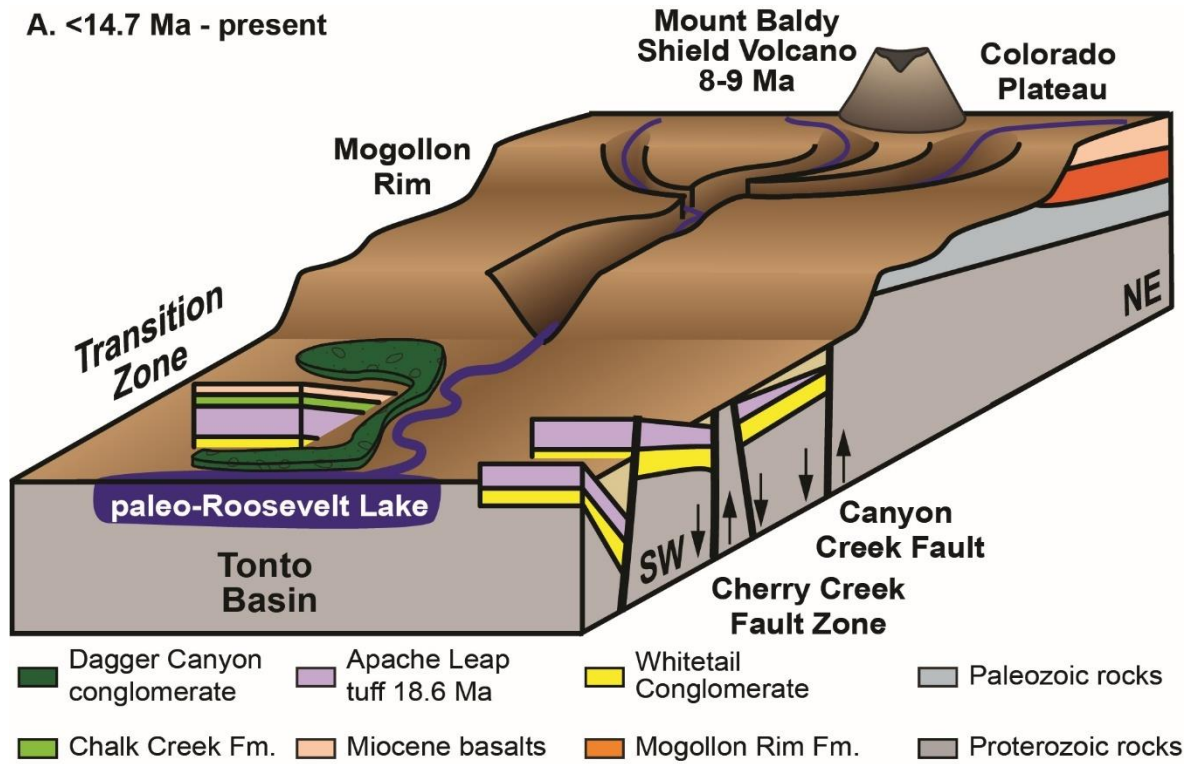


**Figure 7A:** Schematic representation of the SW-flowing proto-Salt River; modified from Faults, 1986. **Figure 7B:** Digital elevation map showing approximate location of the southwest-flowing proto-Salt draining the Mogollon Rim escarpment into the proto-Roosevelt Lake (PRL). Mogollon Rim escarpment is shown as black dashed line.

emplacement of the basalt flow suggesting the proto-Salt River system did not exist in this area before 11.74 Ma. The younger constraint is based on a latite flow from Mount Baldy (Condit and Shafiqullah, 1985) that overlies a 200 m erosional surface near the Mogollon Rim escarpment, suggesting the proto-Salt River existed in this area before 8.97 Ma.

The proto-Salt River deposited the Dagger Canyon conglomerate after incising the Black Mesa basalt and Chalk Creek Formation (Potochnik and Faulds, 1998; Potochnik, 2001a, 2001b) (Figures 7). The Dagger Canyon conglomerate (Cook Creek conglomerate Faulds, 1986) thickens from east to west in the Salt River paleocanyon and is not present east of the Canyon Creek Fault (Faulds, 1986; Potochnik and Faulds, 1998; Potochnik, 2001a) (Figure 4). It contains clasts derived from the Mogollon Rim Formation along with clasts of Miocene volcanics (Faulds, 1986; Potochnik, 2001a). Pebble imbrication and crossbedding indicate a southwest paleoflow direction (Faulds, 1986; Potochnik, 2001a). The lower Dagger Canyon conglomerate (Shute Springs Member Potochnik, 2001a) is 180 m thick and located in east dipping fault blocks bounded by the Cherry Creek and Armer Mountain Fault zones (Potochnik, 2001a). It consists of well-lithified, well rounded, pebble to boulder volcanoclastic conglomerate with a supporting matrix of subangular to subrounded, moderately sorted, lithic arkose sandstone (Faulds, 1986). It is well exposed in drainages south and north of the modern Salt River near Shute Spring Creek. It is also exposed on the east side of Highway 288 north of the Salt River Bridge (Potochnik, 2001a). Deposition of the lower Dagger Canyon conglomerate coincided with movement along the Armer Mountain fault block based on the decreasing dip of bedding up-section from 27° to 0° (Potochnik, 2001a).

The upper Dagger Canyon conglomerate (Devore Springs member Potochnik, 2001a) is 300 m thick and exposed in tributaries between of the Cherry Creek and Canyon Creek fault zones and north of the modern Salt River near the Salt River paleocanyon axis (Faulds, 1986; Potochnik, 2001a). It consists of flat-lying, poorly-lithified, subangular to rounded, pebble to cobble clast, with locally matrix supported conglomerate interbedded with poorly sorted, fine to coarse-grained, lithic arkose sandstone (Faulds, 1986).

The proto-Salt River continued feed a paleolake in the Tonto Basin unit the lake overtopped the topographic barrier of the Mazatzal Highlands to the west (Douglass et al., 2009; Larson et al., 2010; Skotnicki et al., 2016; Hilgendorf et al., 2020). The Salt River then became a tributary of the established Gila River based on the now buried envelope of Salt River gravels inset in Gila River gravels (Skotnicki et al., 2016). The overflow event occurred before 2.8 Ma according to cosmogenic burial ages of these gravels in the Phoenix Basin (Skotnicki et al., 2016). The event was likely driven in part due to onset of North American glaciation around 3 Ma (Huybers and Molnar, 2007) and post-10 Ma uplift of the Colorado Plateau (Morgan and Swanberg, 1985; Lowry et al., 2000; Karlstrom et al., 2008, 2012; Moucha et al., 2008, 2009; Wijk et al., 2010; Crow et al., 2011, 2014; Levander et al., 2011; Cather et al., 2012). This marks the final major base level lowering event to occur along the Salt River because the Gila River was fully integrated from the Safford Basin to sea level by this time (Dickinson, 2015; Skotnicki et al., 2016; Gootee, 2019). The paleo-Salt River then deposited a series of strath terraces in the Phoenix Basin (Péwé, 1978) and in the Salt River paleocanyon.

## **GOAL OF THIS STUDY**

The goal of this study is to determine when the drainage reversal from major NE-flowing rivers, to major SW-flowing rivers occurred in the Salt River area. This study provides additional age constraints for sediments deposited before, during and after the reversal to accomplish this goal. Detrital zircon and sanidine are utilized to provide maximum depositional ages and the ages of overlying and interbedded volcanic units provide minimum depositional ages. Five samples of the Mogollon Rim Formation, three samples of the Whitetail Conglomerate, seven samples of the Dagger Canyon conglomerate, one sample of Tonto Basin sandstone, one sample of Tonto Basin mudstone were analyzed for this study (Figure 8). This study also provides an additional age constraint for the Salt River's spill over event from the Arizona Transition Zone into the Basin and Range by constraining the maximum depositional ages of three Salt River terraces. The Canyon Creek Butte dacite overlying the Whitetail Conglomerate at Mud Springs Draw and Natanes Plateau Basalt overlying the Mogollon Rim Formation near the Black River were analyzed for minimum depositional ages. These constraints provide insight into the evolution of the Colorado Plateau.

## **METHODS**

Zircon is a nesosilicate accessory mineral in igneous and metamorphic rocks. The age of a zircon crystal is determined by measuring the ratio of the parent uranium isotope to the daughter lead isotope for  $^{238}\text{U}$  and  $^{235}\text{U}$  and multiplying the ratio by their half-life (Gehrels, 2011). Grains of zircon are commonly found in sedimentary rocks (Gehrels et al., 2011). They can survive erosional processes and are resistant to diagenesis making them ideal for provenance studies (Dickinson and Gehrels, 2010). Detrital zircon analyses were run on 11 paleoriver samples for this study at the Arizona Laserchron

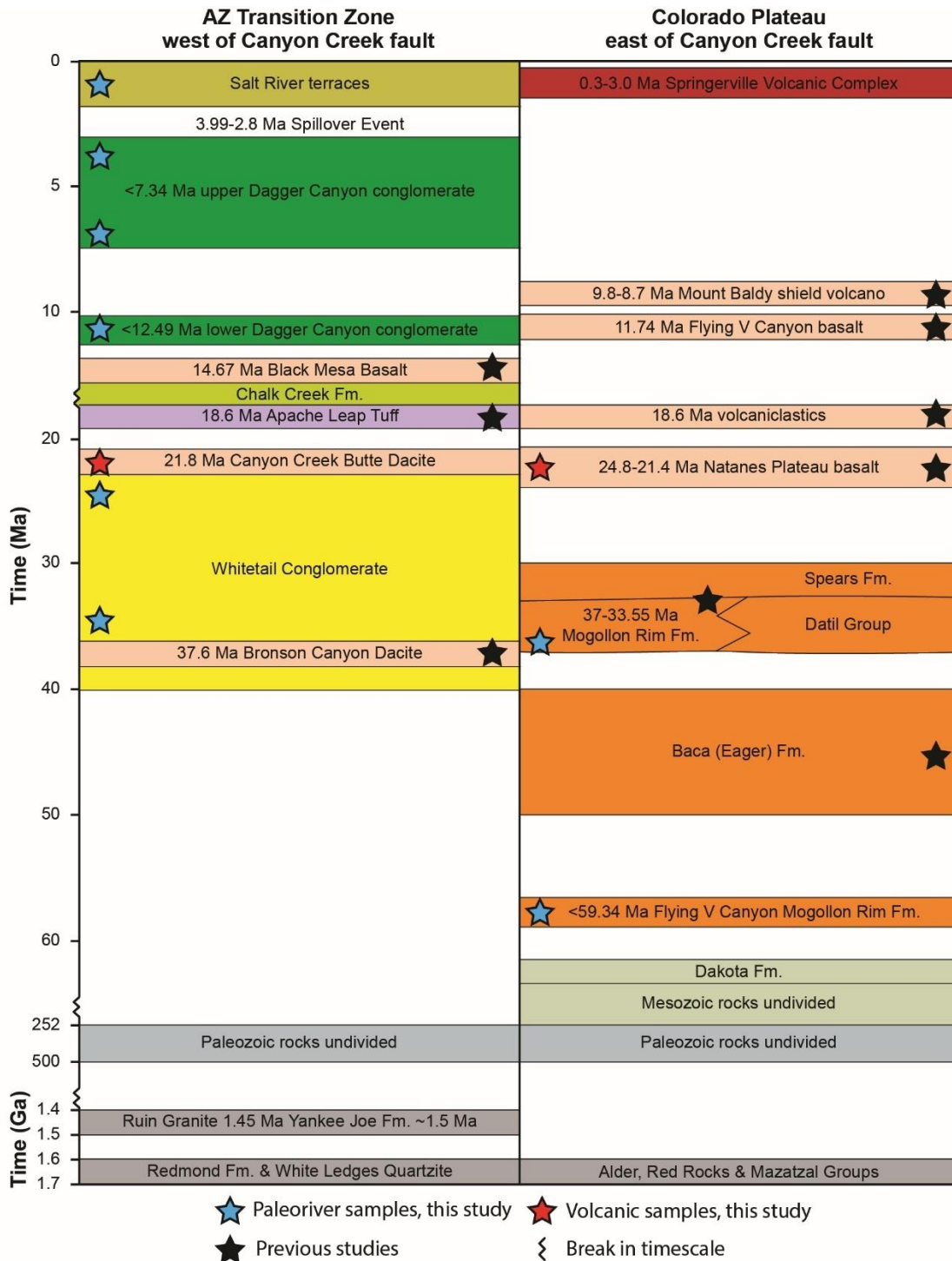


**Figure 8:** Geochronology constraints for stratigraphy in the Salt River area. Blue stars represent paleoriver samples analyzed for this study. Red stars represent volcanic samples analyzed for this study. Black stars represent paleoriver and volcanic samples analyzed by other studies.

Center in Tucson following the Laser-ablation inductively coupled plasma mass spectrometry laboratory methods of Gehrels (2011).  $^{206}\text{Pb}/^{238}\text{U}$  ages are used for grains younger than 1.2 Ga and  $^{206}\text{Pb}/^{207}\text{Pb}$  ages are used for grains older than 1.2 Ga (Gehrels, 2011).

Sanidine is a high temperature polymorph of potassium feldspar formed in felsic volcanic eruptions. Detrital grains of sanidine are also commonly found in paleoriver sediments. Sanidine is dateable using the  $^{40}\text{Ar}/^{39}\text{Ar}$  method (Merrihue and Turner, 1966; Heizler, 2012) and was analyzed at the New Mexico Geochronology Research Laboratory. High precision age measurements of detrital sanidine ( $\pm 0.07\text{-}0.01$  Ma) and their K/Ca ratios can be used to link individual grains to specific caldera sources (Hereford et al., 2016). Sanidine grains were irradiated in the USGS TRIGA reactor in Denver, CO. Argon gas was extracted by single crystal laser fusion using a  $\text{CO}_2$  laser. Age analysis was conducted using a Thermo Scientific Helix Multicollector noble gas mass spectrometer.

Dating a high number ( $n > 100$ ) of zircon and sanidine detrital grains from paleoriver samples gives an age distribution of zircon and sanidine grains present in the sample. The weighted mean of the sample's youngest grains determines its maximum depositional age. The depositional age of the paleoriver deposit is younger than its maximum depositional age because these minerals formed before they were incorporated into the river sediments. Determining the minimum depositional age of a paleoriver deposit is possible when volcanic deposit like basalt, dacite, or ash tuff overlie or are interbedded with the river sediments.

Paleoriver samples were collected from sand lenses interbedded in conglomeratic facies from each unit. Samples of paleoriver sand were retrieved from holes dug at least 50 cm deep into the formation to avoid contamination from younger detrital grains settling on the formation after exposure by erosion. Fluvial sand was collected from each site and split in equal proportions for detrital zircon and sanidine analyses.

Two volcanic samples were dated for this study to constrain the minimum depositional ages of paleoriver samples. This work was completed at the New Mexico Geochronology Research Laboratory using  $^{40}\text{Ar}/^{39}\text{Ar}$  methods (McIntosh et al., 2003). Samples were crushed and cleaned with hydrochloric acid before grains of the groundmass were separated from phenocrysts. Argon gas was extracted from the groundmass by a process of step heating using a resistance furnace and analyzed using a Thermo Scientific Helix Multicollector noble gas mass spectrometer. Ages were calculated by weighting each heating step by the inverse of the variance to test the statistical precision of contiguous heating steps (Mahon, 1996).

## **RESULTS**

Geologic maps with sample locations are presented in Figures 3 and 4. The location, description and maximum depositional ages of paleoriver samples are listed in Table 1. The location, description and ages of volcanic samples are listed on Table 2.

Detrital zircon and sanidine data are presented as age-distribution relative probability curve diagrams. These graphs are constructed by assigning a Gaussian distribution to each grain analyzed based on the grain's age and associated analytical error. The sum of each grain's probability distribution forms an individual curve which is

Sample	Latitude	Longitude	Elev. (m)	DZ (Ma)	DS (Ma)	Description
K16-Salt-13	33.92960	-110.35632	1764	64	60.02	Mogollon Rim Formation from road cut in Flying V Canyon
JA19-Salt-15	33.92969	-110.35528	1754		59.38	Mogollon Rim Formation taken 5 m beneath Salt-13
JA17-TC-1	34.02062	-109.82017	2018	37		Mogollon Rim Formation near Trout Creek
JA18-BLK-1	33.69040	-110.23469	1620	33		Mogollon Rim Formation near Black River
JA17-BR-1	34.62026	-111.25763	2088	30		Mogollon Rim Formation from Blue Ridge
K16-Salt-6	33.72950	-110.71964	829	30		Whitetail Formation from Beehive Rock
JA17-MD-1	33.79428	-110.67433	1115	26		Whitetail Formation at Mud Springs Draw underling Canyon Creek Butte dacite
JA17-TB-1	34.32834	-111.44829	1552	25		Whitetail Formation at Tonto Natural Bridge
JA18-DC-3	33.62425	-110.92812	675		15.33	lower Dagger Canyon conglomerate in Tonto Basin
JA19-RF-1	33.66407	-110.82720	719		15.69	lower Dagger Canyon conglomerate from Redmond Flat
JA19-SS-1	33.62533	-110.90917	685		12.49	lower Dagger Canyon conglomerate near Shute Springs Creek
K16-Salt-9	33.72795	-110.76206	1011	8	7.34	upper Dagger Canyon conglomerate in Upper Corral Canyon
K16-Salt-10	33.73163	-110.76190	1049	8		upper Dagger Canyon conglomerate in Upper Corral Canyon
JA17-DC-1	33.75233	-110.74876	1235	8	7.21	upper Dagger Canyon conglomerate at Pringle Wash
K18-Salt-MR1	33.59840	-110.99107	794		8.83	Tonto Basin mudstone below MR2
K18-Salt-MR2	33.59875	-110.99084	794		17.01	upper Dagger Canyon conglomerate in Tonto Basin
K18-Salt-MR3	33.59871	-110.99161	784		7.19	Tonto Basin sandstone below MR1
JA19-BH-2	33.73262	-110.71846	911		7.05	Salt River terrace at Beehive Rock
K18-MT	33.53959	-111.62830	460		3.99	Mesa Terrace off of N. Bush Hwy
JA18-BC-1	33.77234	-110.67508	866	76	3.61	Salt River terrace at Butte Creek

**Table 1:** Locations and descriptions of paleoriver samples. The Elev. column represents the sample's elevation above sea level in meters. The DZ column represents the maximum depositional age in Ma based on detrital zircon. The DS column represents the maximum depositional age in Ma based on detrital sanidine.

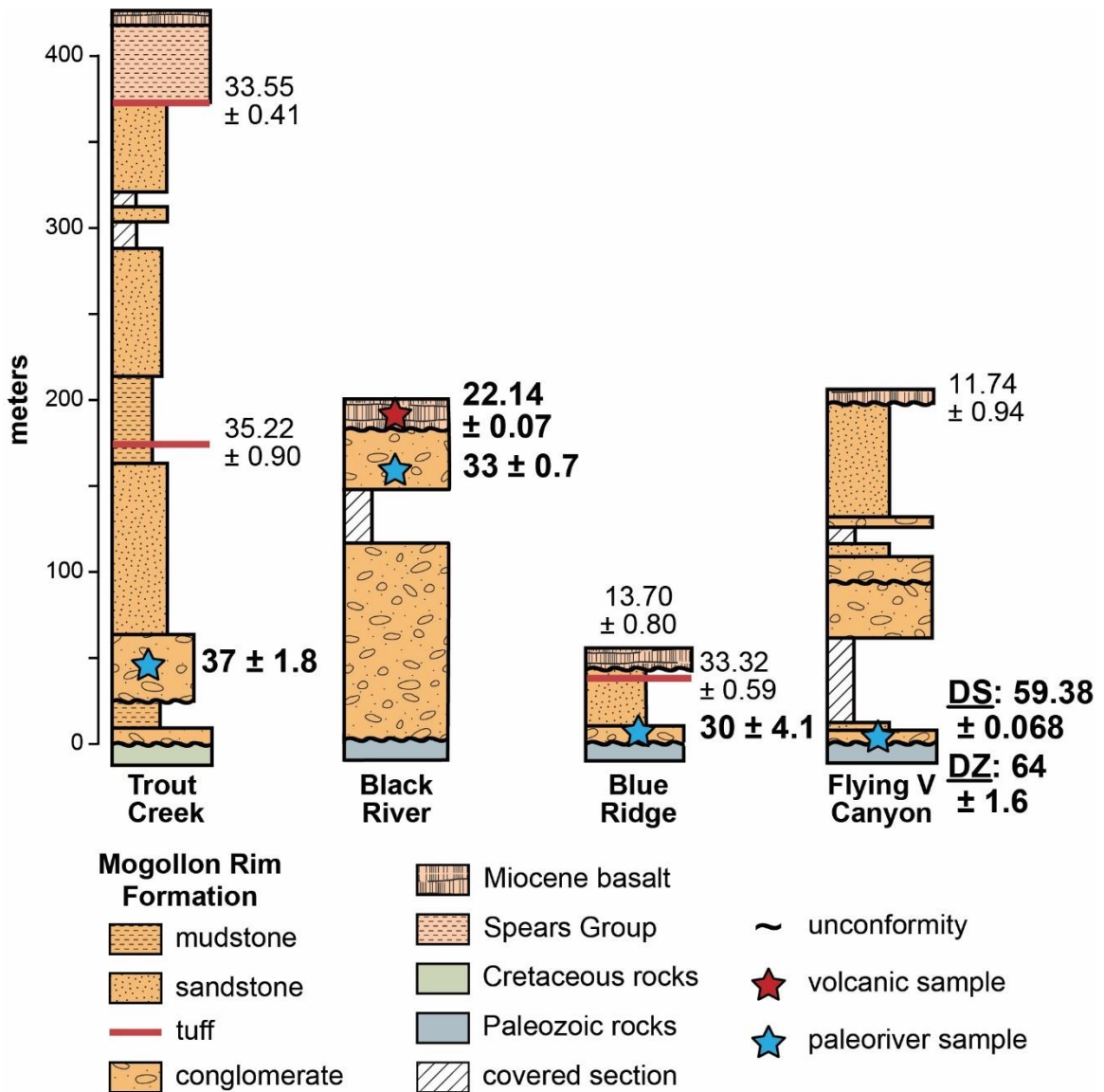
Sample	Latitude	Longitude	Elev. (m)	Age (Ma)	Description
JA18-BLK-2	33.69101	-110.23486	1648	22.14	Natanes Plateau Basalt overlying Mogollon Rim Fm.
K16-Salt-3	33.79786	-110.67399	1181	21.8	Canyon Creek Butte dacite overlying Whitetail Cong.

**Table 2:** Locations, ages and descriptions of volcanic samples. The Elev. column represents the sample's elevation above sea level in meters.

normalized by dividing the area beneath the curve by the total number of grain analysis per sample. These curves form distinctive age peaks that can be linked to various sources.

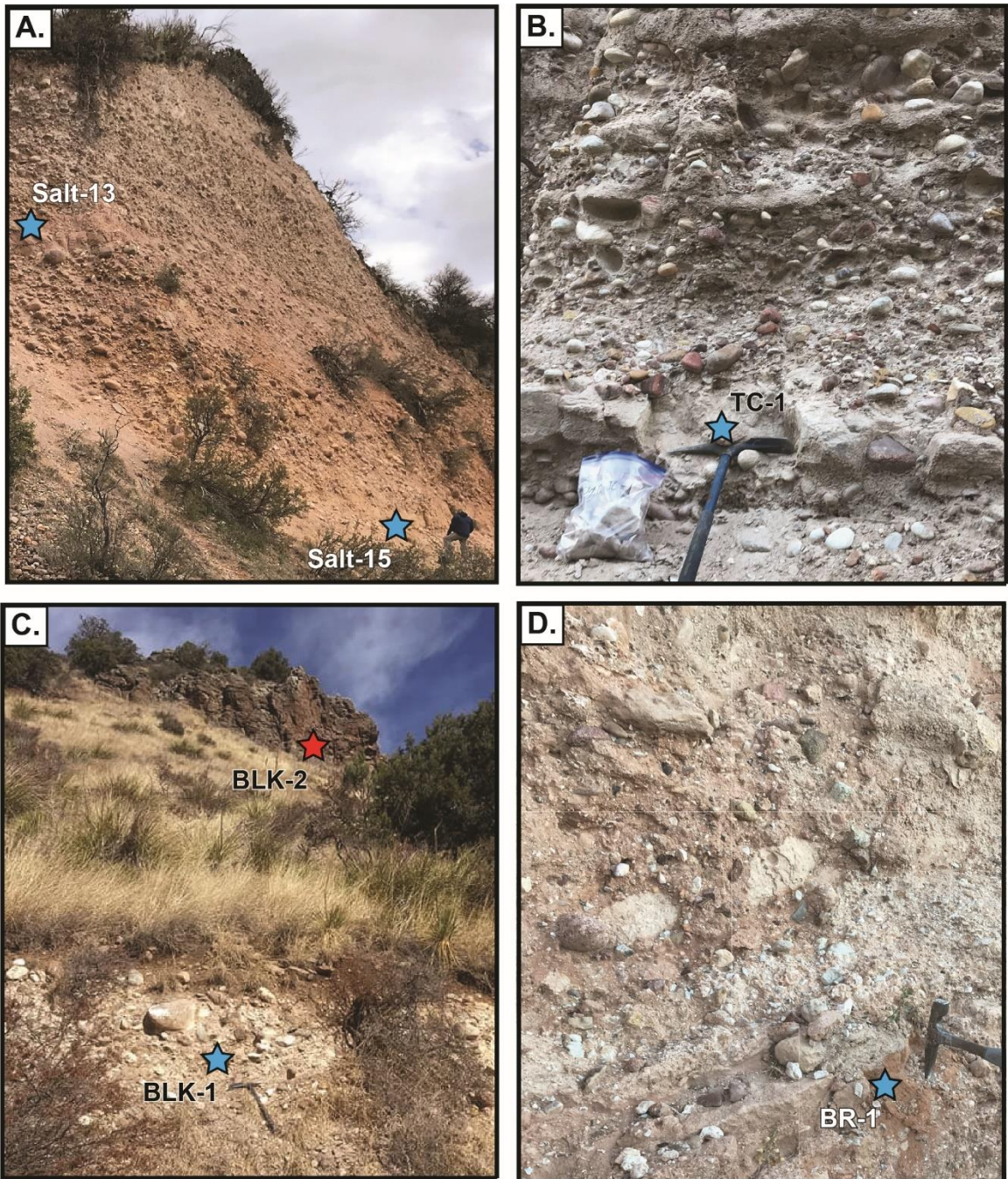
### *Mogollon Rim Formation Results*

Figure 9 shows the stratigraphic columns of Mogollon Rim Formation sample locations. Figure 10 shows photographs of the Mogollon Rim Formation sample locations. Figure 11 shows the detrital zircon results from the Mogollon Rim Formation samples. Each sample contains age peaks around 1440 and 1650 Ma. Sample K16-Salt-13, taken 10 m above the base of the formation on the west side of Highway 60 in the Flying V Canyon area, has additional age peaks at 73 Ma and 168 Ma with the youngest grain at 64 Ma. Sample JA17-TC-1 is from the Trout Creek area where Potochnik (1989)



**Figure 9:** Stratigraphic columns of the Mogollon Rim Formation. Trout Creek, Black River and Flying V Canyon columns are modified from Potochnik, 1989 and Blue Ridge column is modified from Potochnik, 2001a. Maximum depositional ages in millions of years listed next to paleoriver samples. Detrital zircon (DZ) and detrital sanidine (DS) maximum depositional ages listed for the Flying V Canyon sample.  $^{40}\text{Ar}/^{39}\text{Ar}$  age listed next to volcanic samples. Tuff ages at the Trout Creek section are from Potochnik and Faulds, 1998. Basalt and tuff ages at Blue Ridge section are from Potochnik, 2001a. Basalt age at Flying V Canyon section is from Damon et al., 1996.

identified a 375-m type section for the Mogollon Rim Formation. This sample is approximately 40 m above the base of the unit. It has peaks at 69 Ma, 78 Ma, 99 Ma, 165 Ma, 500 Ma and 1089 Ma. The youngest 3 grains form an age peak at 37 Ma. Sample



**Figure 10:** Photographs of Mogollon Rim Formation sample locations (Facies A Potochnik, 1989.) **Figure 10A:** Gravels at Flying V Canyon with the locations of samples K16-Salt-13 and JA18-Salt 15. Photograph by Jacob Thacker. **Figure 10B:** Gravels from Trout Creek and sample JA17-TC-1. **Figure 10C:** Gravels above Black River (JA18-BLK-1) and the overlying Natanes Plateau basalt (JA18-BLK-2). **Figure 10D:** Gravels at Blue Ridge and sample JA17-BR-1.

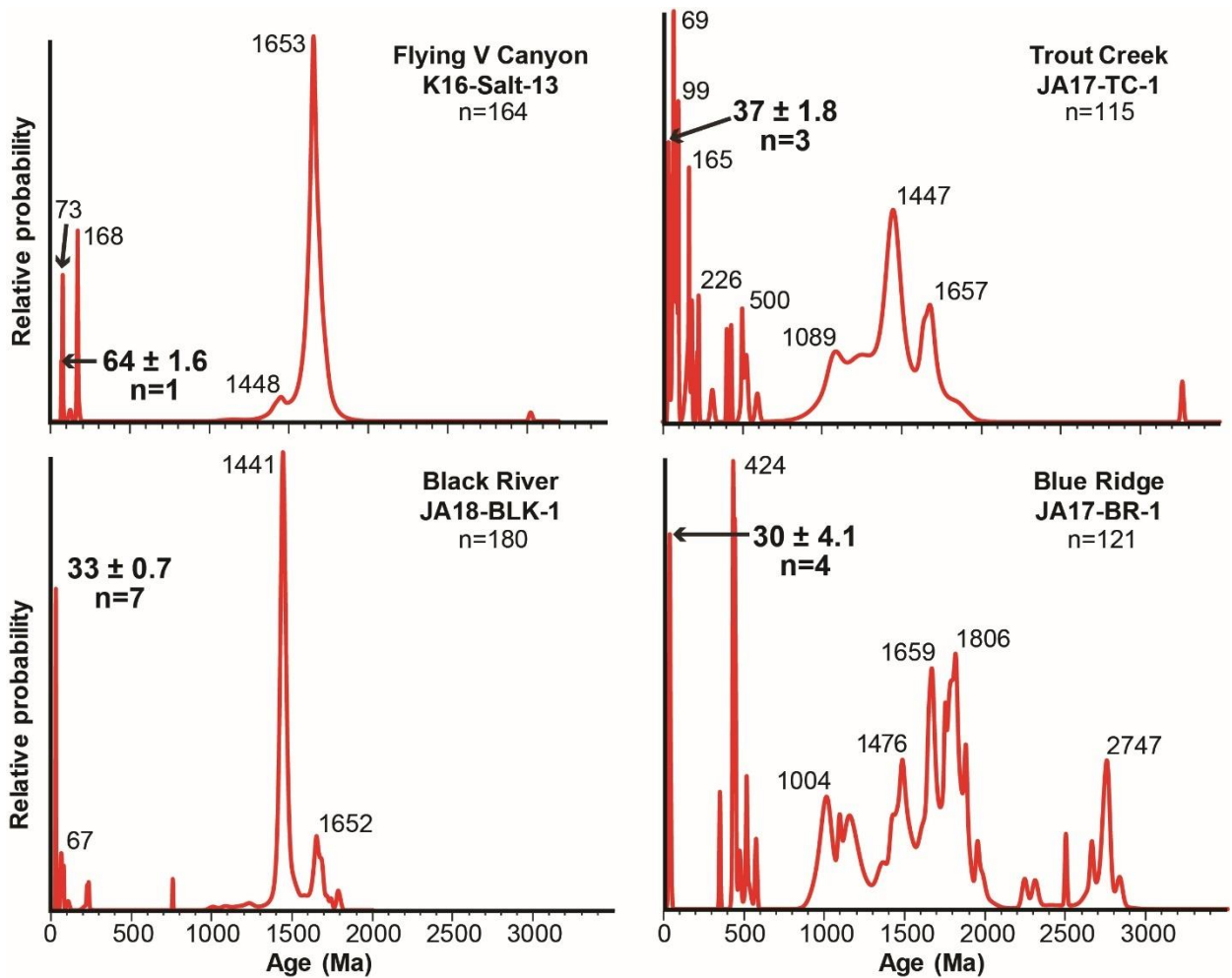


**Figure 11:** Detrital zircon relative probability spectra for Mogollon Rim Formation samples. In the upper right hand corner, the n= number indicates the number of zircon grains analyzed for each sample. The bold number next to the youngest age peak represents the sample’s maximum depositional age. The n= number beneath it indicates the number of grains used to calculate the weighted mean age.

JA18-BLK-1 was taken 30 m beneath Natanes Plateau basalt in Bronco Canyon, a tributary of the Black River. Potochnik (1989) described a section near this location which he named Tick Flack. This sample has an additional peak at 67 Ma. The youngest 7 grains form an age peak at 33 Ma. Sample JA17-BR-1 is from Blue Ridge, a location north of the physiographic Mogollon Rim (Figure 3). Potochnik (2001a) correlated the gravels here with the Mogollon Rim Formation due to their northeast dispersal patterns

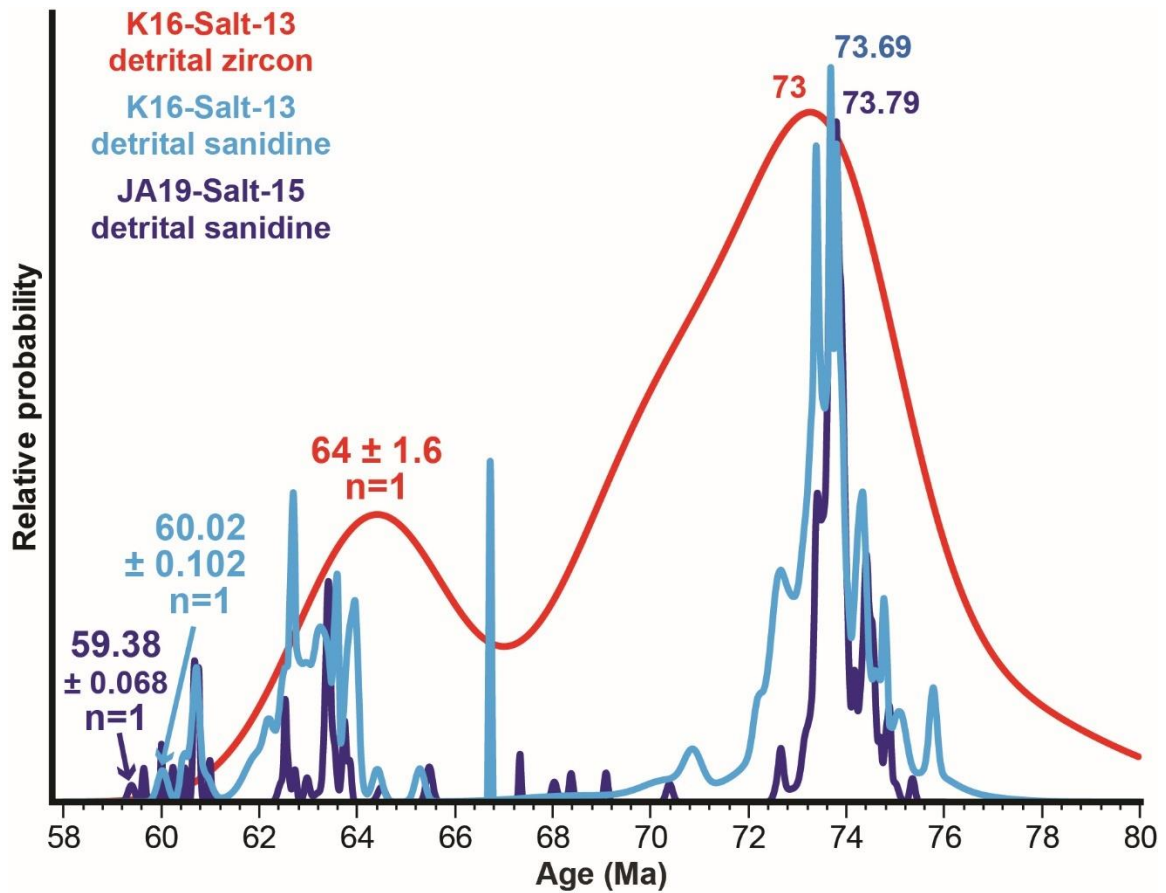


**Figure 12:** Detrital zircon (red) and detrital sanidine (light blue) relative probability spectrums from Flying V Canyon sample K16-Salt-13 as well as detrital sanidine relative probability spectrum (dark blue) for sample JA19-Salt-15. The bold number next to the youngest age peak represents the sample's maximum depositional age. The n= number beneath it indicates the number of grains used to calculate the weighted mean age.

and location of the Colorado Plateau. This sample was taken 20 m beneath the overlying erosional contact with a Miocene basalt flow (Potochnik, 2001a). It has additional detrital zircon age peaks at 424 Ma, 1004 Ma, 1476 Ma, 1659 Ma, 1806 Ma, and 2747 Ma. The youngest four grains form a peak at 30 Ma.

Figure 12 displays the results of two Mogollon Rim Formation samples analyzed for detrital sanidine. Two sanidine grains analyzed from sample K16-Salt-13 taken from Flying V Canyon are younger than 10 Ma. However, these grains cannot be in-situ

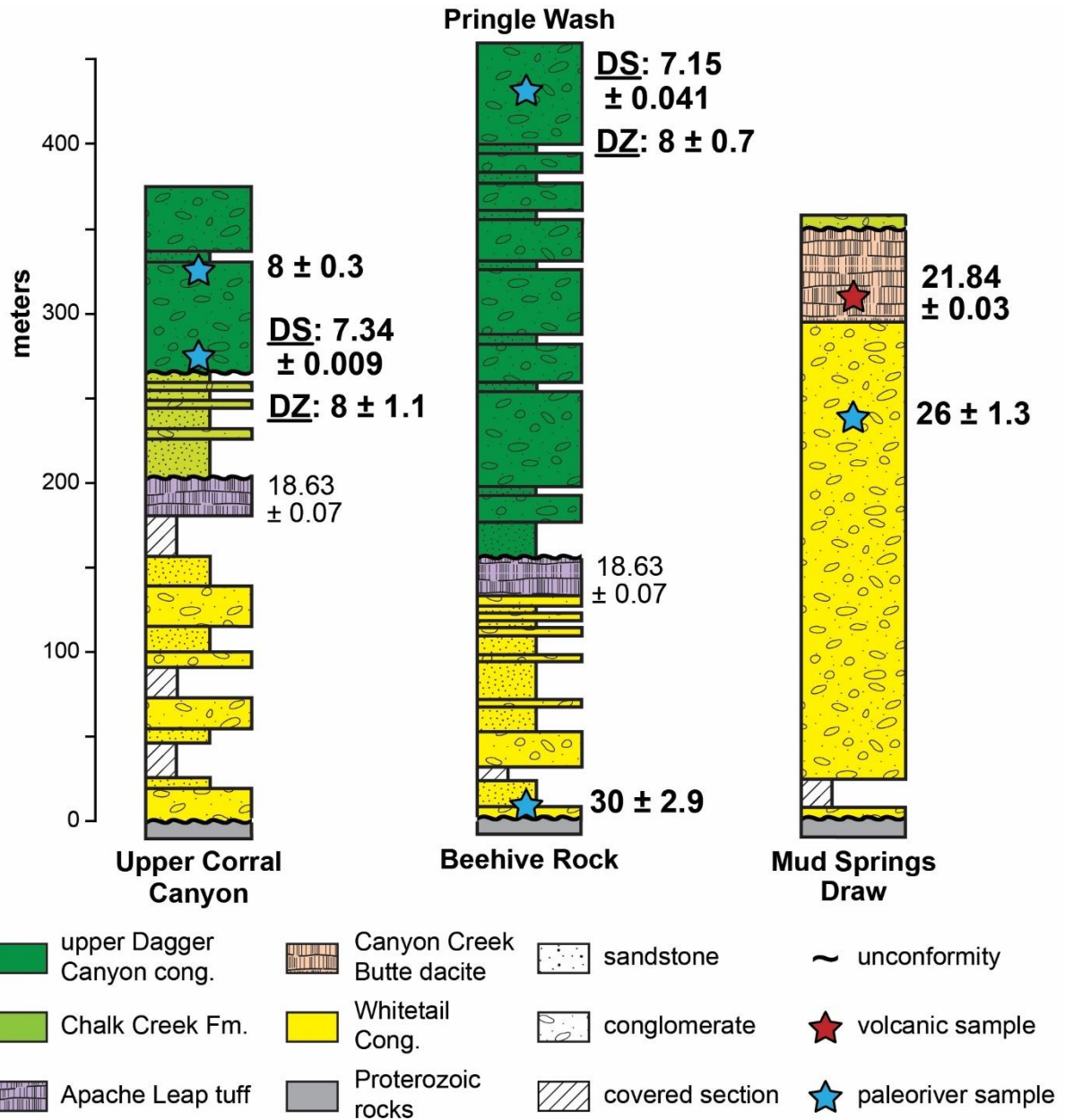


**Figure 13:** Stratigraphic columns from sample locations in the Salt River paleocanyon showing the relative stratigraphic positions of the Whitetail Conglomerate, Canyon Creek Butte dacite, Apache Leap tuff, Chalk Creek Formation and the upper Dagger Canyon Conglomerate. Maximum depositional ages are listed next to paleoriver samples. Detrital zircon (DZ) and detrital sanidine (DS) maximum depositional ages listed next to samples.  $^{40}\text{Ar}/^{39}\text{Ar}$  age are listed next to volcanic sample. Stratigraphic columns modified from Potochnik 2001a. Apache Leap tuff ages are from Potochnik 2001a.

because the formation is overlain by an 11.7 Ma basalt flow (Damon et al., 1996). The next youngest sanidine grain from this sample is 60.02 Ma. Other age peaks are present at 60.7 Ma, 62.7 Ma, and 73.69 Ma. Sample JA19-Salt-15 was taken approximately 5 m beneath K16-Salt-13 and approximately 2 m above the base of the formation (Figure 10). It contains age peaks at 62.7 Ma and 73.79 Ma. The youngest sanidine grain is 59.38 Ma.

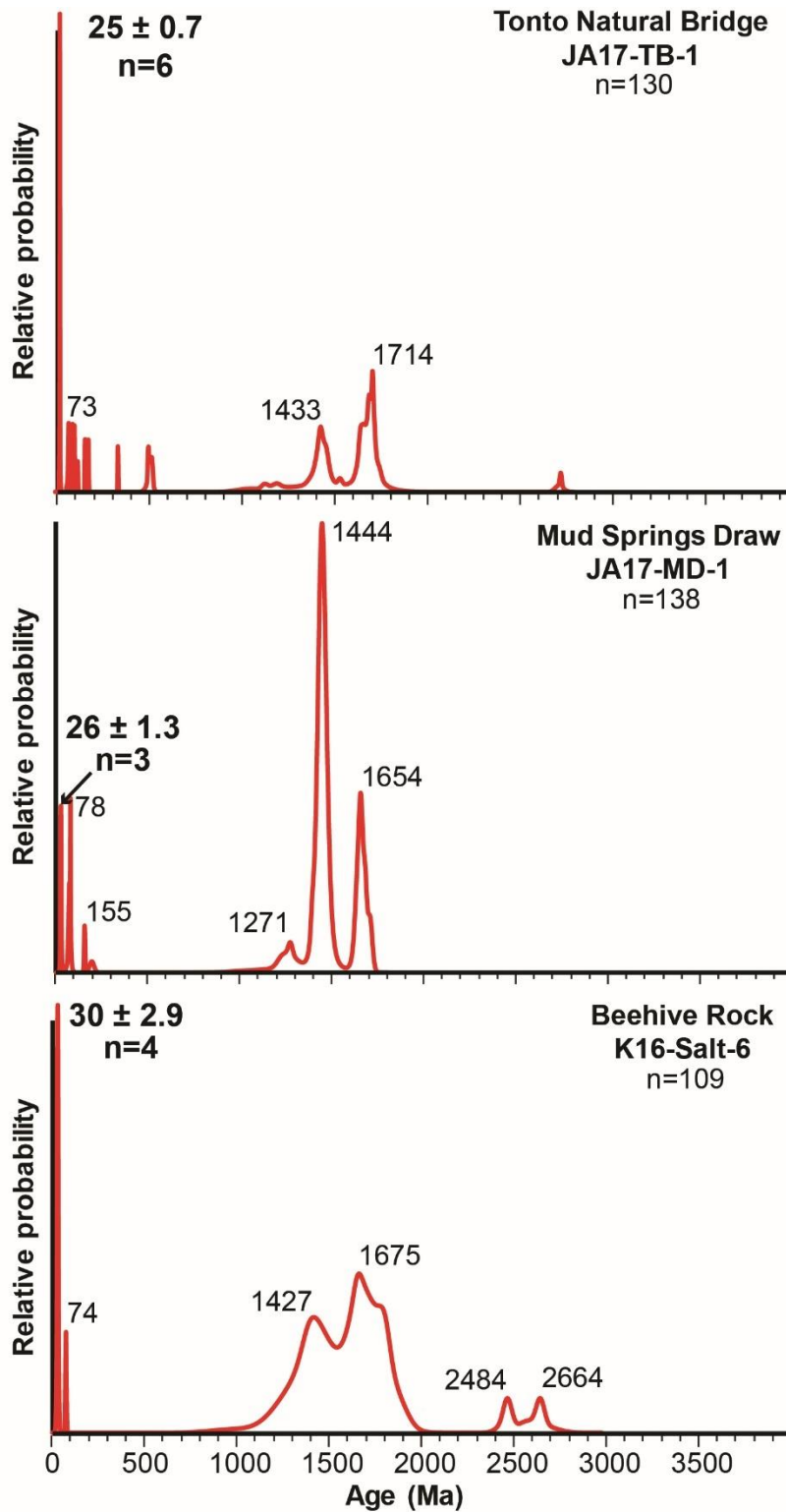
#### *Whitetail Conglomerate Results*

Figure 13 shows the stratigraphic columns for Whitetail Conglomerate sample locations. Figure 14 shows photographs of the Whitetail Conglomerate sample locations. Figure 15 shows the detrital zircon results from two samples of the Whitetail Conglomerate and the valley gravel sample at Tonto Natural Bridge analyzed for detrital zircon. Each sample contains age peaks around 1440 and 1650-1700 Ma. Sample K16-Salt-6 is from Beehive Rock near the base of the Whitetail Conglomerate and near the modern level of the Salt River. It has additional age peaks at 2485 Ma and 2663 Ma. The youngest 4 grains form an age peak at 30 Ma. Sample JA17-MD-1 is from Mud Springs Draw, 66 meters below the overlying Canyon Creek Butte dacite. It has additional peaks at 78 Ma and 1271 Ma. The youngest 3 grains form a peak at 26 Ma. Sample JA17-TB-1 was taken from valley gravel near Tonto Natural Bridge, 15 m below the erosional contact with overlying Miocene basalt. This location is north of the Salt River paleocanyon (Figure 3). Pierce (1979) determined the gravels in this area were deposited after development of the Colorado Plateau based on their geomorphically low position in the landscape. This sample has additional peaks at 73 Ma, 500 Ma, and 1714 Ma. The youngest 6 grains form a peak at 25 Ma. Due to its similar maximum depositional age it is included with the Whitetail Conglomerate detrital zircon spectrums (Figure 15).



**Figure 14:** Photographs of Whitetail Conglomerate, sample locations. **Figure 14A:** Beehive Rock sample location (K16-Salt-6) near the modernriver level and overlying Salt River terrace sample location (K18-BH-2) 83 m above the modern river level.

**Figure 14B:** Mud Springs Draw sample location showing the subangular, locally derived clasts of the Whitetail Conglomerate and the overlying Canyon Creek Butte dacite (K16-Salt-3).



**Figure 15:** Detrital zircon relative probability spectrum for Whitetail Conglomerate samples. In top right corner, the n= number indicates the number of grains analyzed for each sample. The bold number next to the youngest age peak represents the sample's maximum depositional age. The n= number beneath it indicates the number of grains used to calculate the weighted mean age.

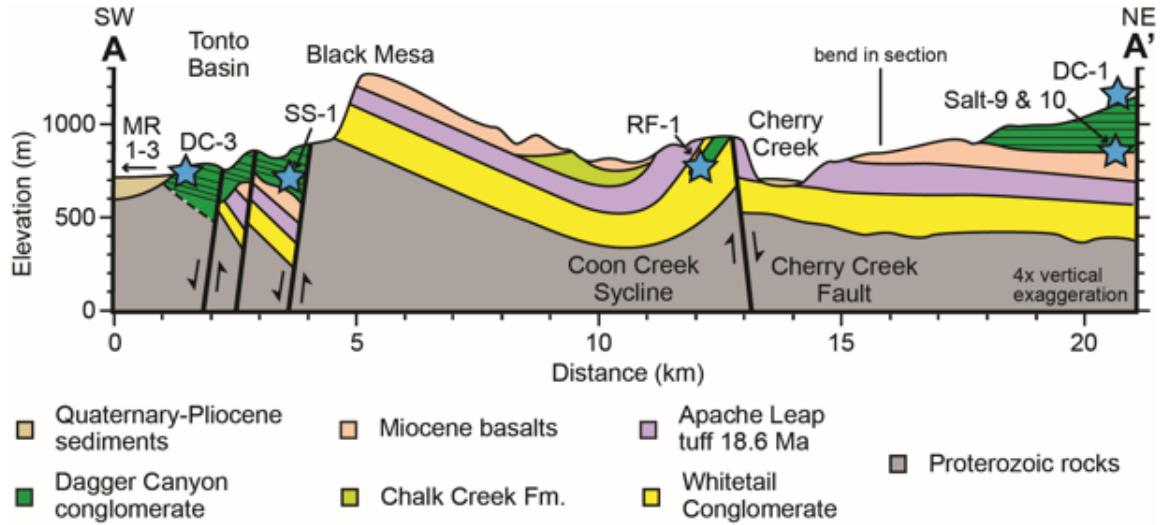


**Figure 16:** Geologic cross section of the Black Mesa area including the flat-lying terrane east of the Cherry Creek Fault, the Coon Creek syncline, Black Mesa and the eastern boundary of the Tonto Basin; shows relative position of upper Dagger Canyon conglomerate samples (K16-Salt-9 & 10) and lower Dagger Canyon conglomerate samples (JA19-RF-1, JA19-SS-1, JA18-DC-3). Locations of upper Dagger Canyon conglomerate, Tonto Basin mudstone and Tonto Basin sandstone samples (K18-MR1-3) are southwest of this cross section. Location of the cross section is outlined on the Figure 4A geologic map; modified from Skotnicki, 2002.

### *Dagger Canyon Conglomerate Results*

The Figure 16 cross section shows the structural and stratigraphic distinction between the tilted lower Dagger Canyon Conglomerate and the un-tilted upper Dagger Canyon conglomerate along with sample locations. Figure 17 shows photographs of the lower Dagger Canyon conglomerate. Figure 18 shows photographs of the upper Dagger Canyon conglomerate in the Salt River paleocanyon and Figure 19 shows photographs of the upper Dagger Canyon conglomerate in the Tonto Basin along with the underlying mudstone and sandstone.

Figure 20 shows the detrital sanidine results from all of the lower and upper Dagger Canyon conglomerate samples along with the Tonto Basin sandstone and mudstone samples. Sample JA19-SS-1 was taken from the lower Dagger Canyon

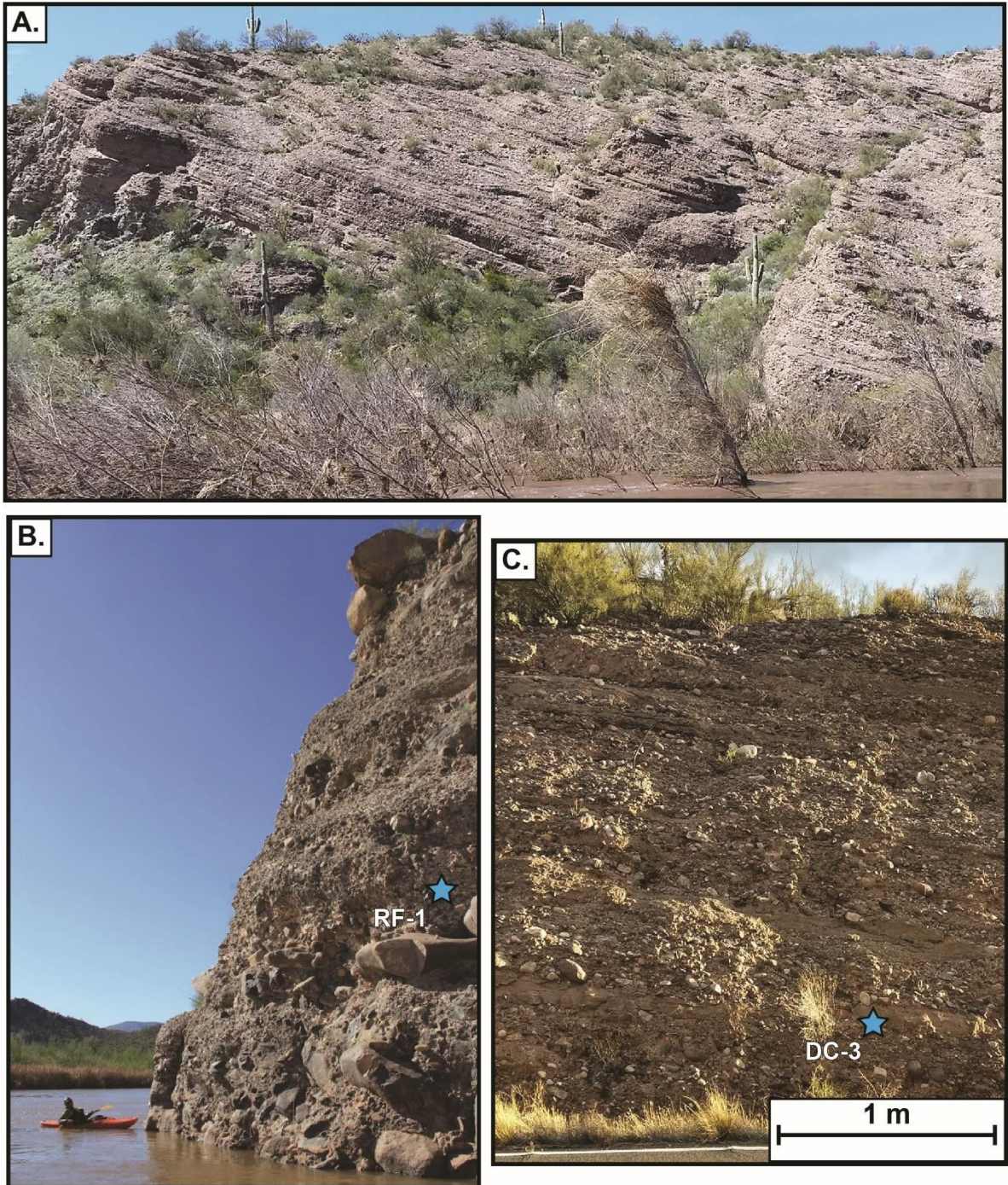


**Figure 17:** Photographs of lower Dagger Canyon conglomerate sample locations. **Figure 17A:** Photograph taken near Shute Springs Creek showing the east dipping lower Dagger Canyon conglomerate beds. **Figure 17B:** Redmond Flat sample location showing the pebble to boulder clast sizes. Photograph by Laura Crossey. **Figure 17C:** Location of Tonto Basin sample showing the east dipping beds. Photograph by Camille Dwyer.

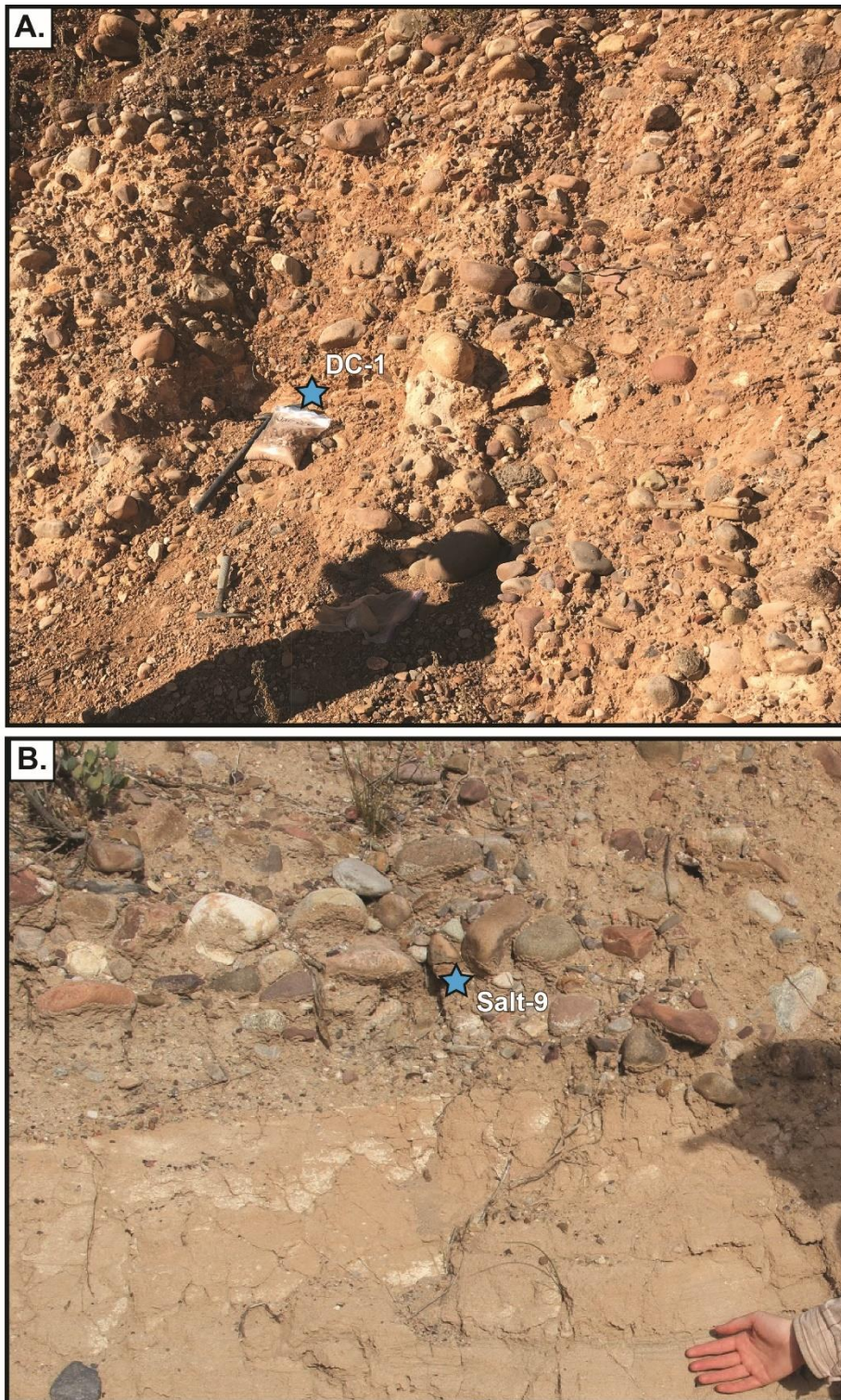


**Figure 18:** Photographs of upper Dagger Canyon conglomerate sample locations in the Salt River paleocanyon. **Figure 18A:** Location of sample JA17-DC-1 near the top of the upper Dagger Canyon conglomerate. **Figure 18B:** Location of sample K16-Salt-9 at the base of the upper Dagger Canyon conglomerate showing the underlying Chalk Creek Formation. Photograph by Laura Crossey.

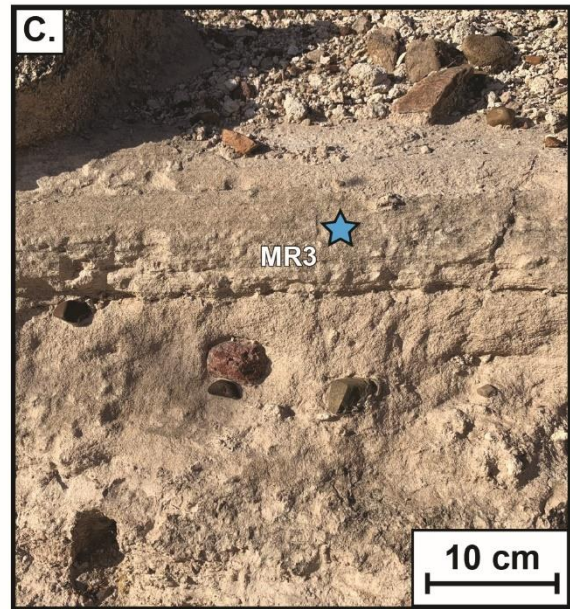
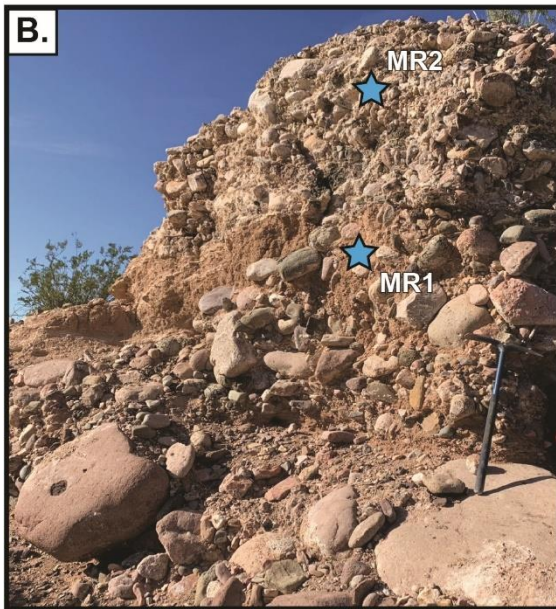


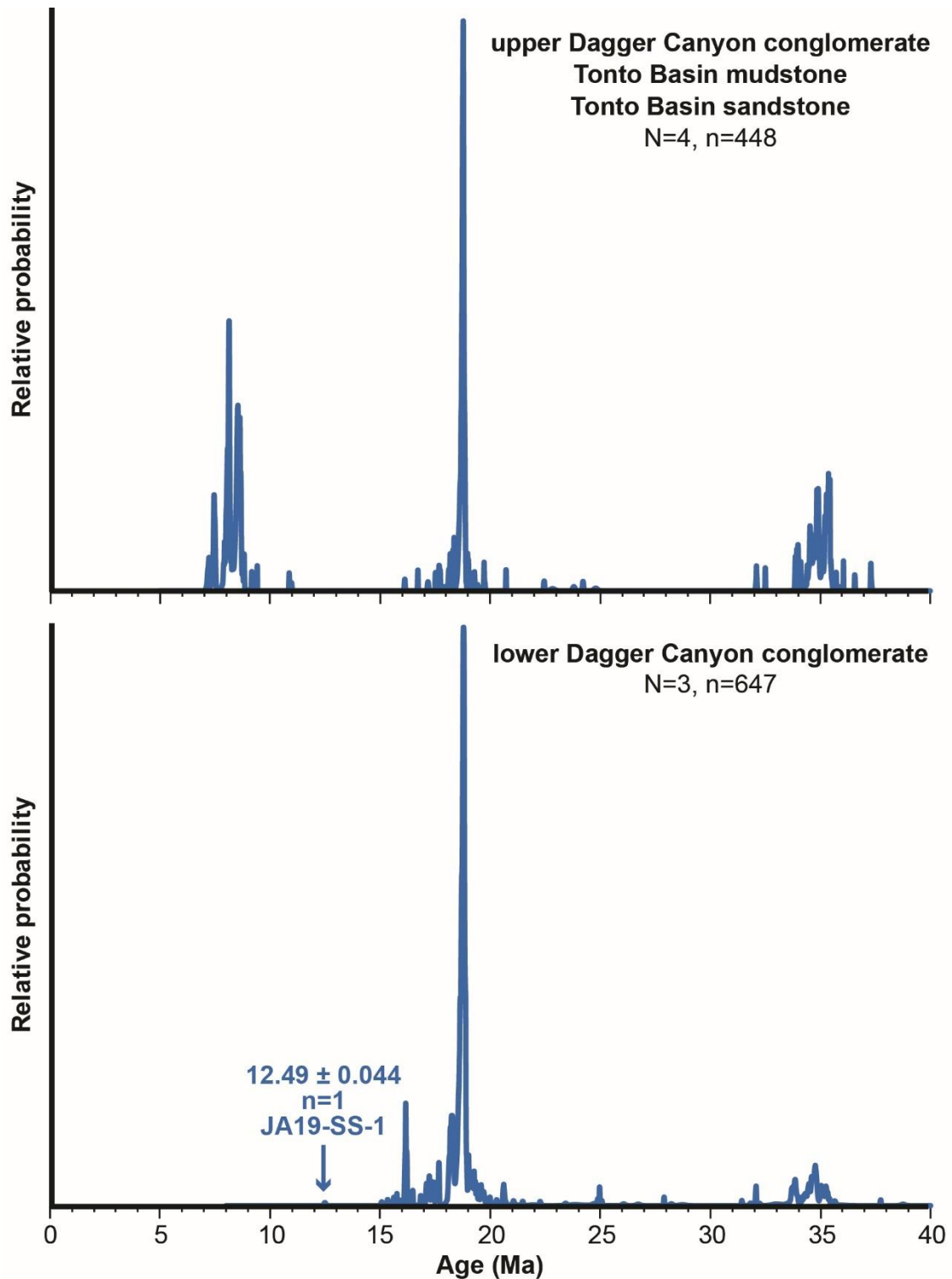
**Figure 19:** Photographs showing the locations of samples K18-MR1-3. **Figure 19A:** Photograph of the Tonto Basin and locations of K18-MR1-3 on the prominent hill. Roosevelt Lake and the Mazatzal Mountains can be seen in the background. **Figure 19B:** Location of the upper Dagger Canyon conglomerate sample (K18-MR2) and the underlying Tonto Basin mudstone sample (K18-MR-1) with interbedded pebble to boulder clasts. **Figure 19C:** Location of Tonto Basin sandstone sample (K18-MR3) 10 m below the upper Dagger Canyon conglomerate and the Tonto Basin mudstone.

conglomerate tilted by the Amer Mountain fault on the north side of the Salt River near river level. It contains age peaks at 24.96 Ma, 18.8 Ma, 18.33 Ma, 16.15 Ma. The youngest grain from this sample is 12.49 Ma. Sample JA19-RF-1 was taken from

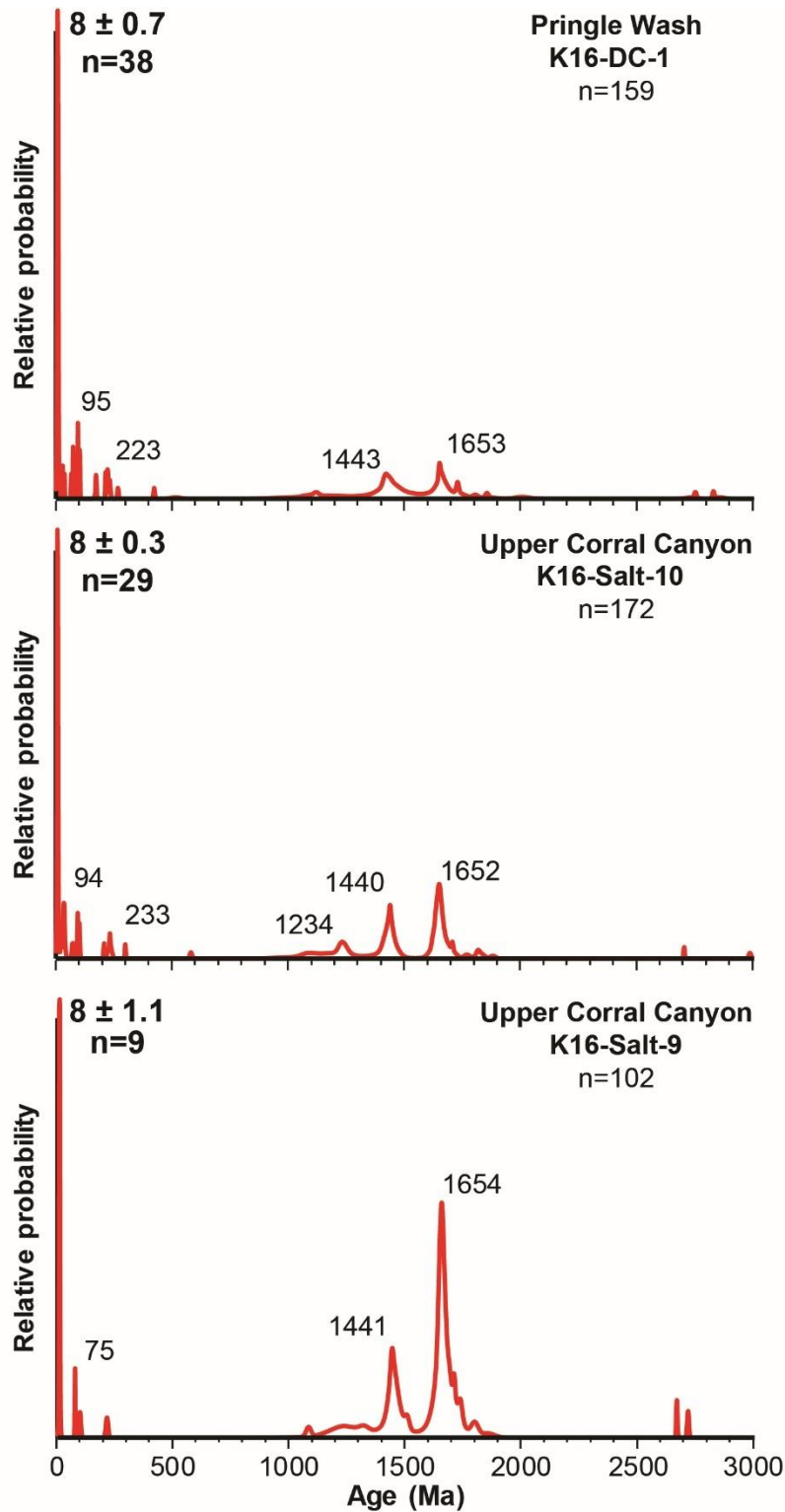
Redmond Flat in a tilted fault block exposed on the east side of the modern Salt River near river level. It contains age peaks at 33.84 Ma, 32.06 Ma, 20.61 Ma, 18.77 Ma, 18.1 Ma, 16.15 Ma and the youngest grain is 15.69 Ma. Sample JA19-DC-3 was taken from in a tilted fault block on the eastern edge of the Tonto Basin. This sample contains seven grains between 60.01 Ma to 72.67 Ma. It also contains age peaks at 34.75 Ma, 33.74 Ma, 18.7 Ma, and 18.2 Ma. The youngest grain is 15.34 Ma.

Figure 21 shows results from three upper Dagger Canyon conglomerate samples analyzed for detrital zircon. All three samples were taken from the Salt River paleocanyon between the Cherry Creek and Canyon Creek faults and all three contain age peaks around 1440 and 1650 Ma. Sample K16-Salt-9 taken near the base of the upper Dagger Canyon conglomerate in the Upper Corral Canyon and has additional age peaks between 1080-1320 Ma in age. The youngest 9 grains form an age peak at 8 Ma. Sample K16-Salt-10 was taken approximately 40 m above K16-Salt-9 in the Upper Corral Canyon. It has additional age peaks at 94 Ma, 233 Ma and 1234 Ma. The youngest 29 grains form a peak at 8 Ma. Sample K16-DC-1 was taken near the top of the upper Dagger Canyon conglomerate approximately 186 m above K16-Salt-10. It has additional age peaks at 95 Ma, and 233 Ma. The youngest 38 grains form an age peak at 8 Ma.

Figures 22 and 23 display the detrital sanidine results of two upper Dagger Canyon conglomerate samples. Figure 22 displays the detrital sanidine and zircon results from both samples. Sample K16-Salt-9 from the base of the upper Dagger Canyon conglomerate contains age peaks at 73.5 Ma, 60.8 Ma, 35.42 Ma, 34.89 Ma, 33.98 Ma, 18.83 Ma, 8.6 Ma and 8.13 Ma. The youngest grain is 7.34 Ma. Sample JA17-DC-1 from near the top of the upper Dagger Canyon conglomerate contains age peaks at 74.5 Ma,



**Figure 20:** Composite detrital sanidine age spectrums for upper and lower Dagger Canyon conglomerate between 40-0 Ma. The top graph includes Tonto Basin mudstone (K18-MR-1) and Tonto Basin sandstone (K18-MR-3) because of their similar maximum depositional ages. The N= number indicates the number of samples used for the composite spectrums and the n= number indicates the total number of grains analyzed for each composite spectrum.



**Figure 21:** Detrital zircon spectrum for upper Dagger Canyon conglomerate samples. In top right corner, n= indicates the number of zircon grains analyzed for each sample. The bold number next to the youngest age peak represents the sample's maximum depositional age. The n= number beneath it indicates the number of grains used to calculate the weighted mean age.

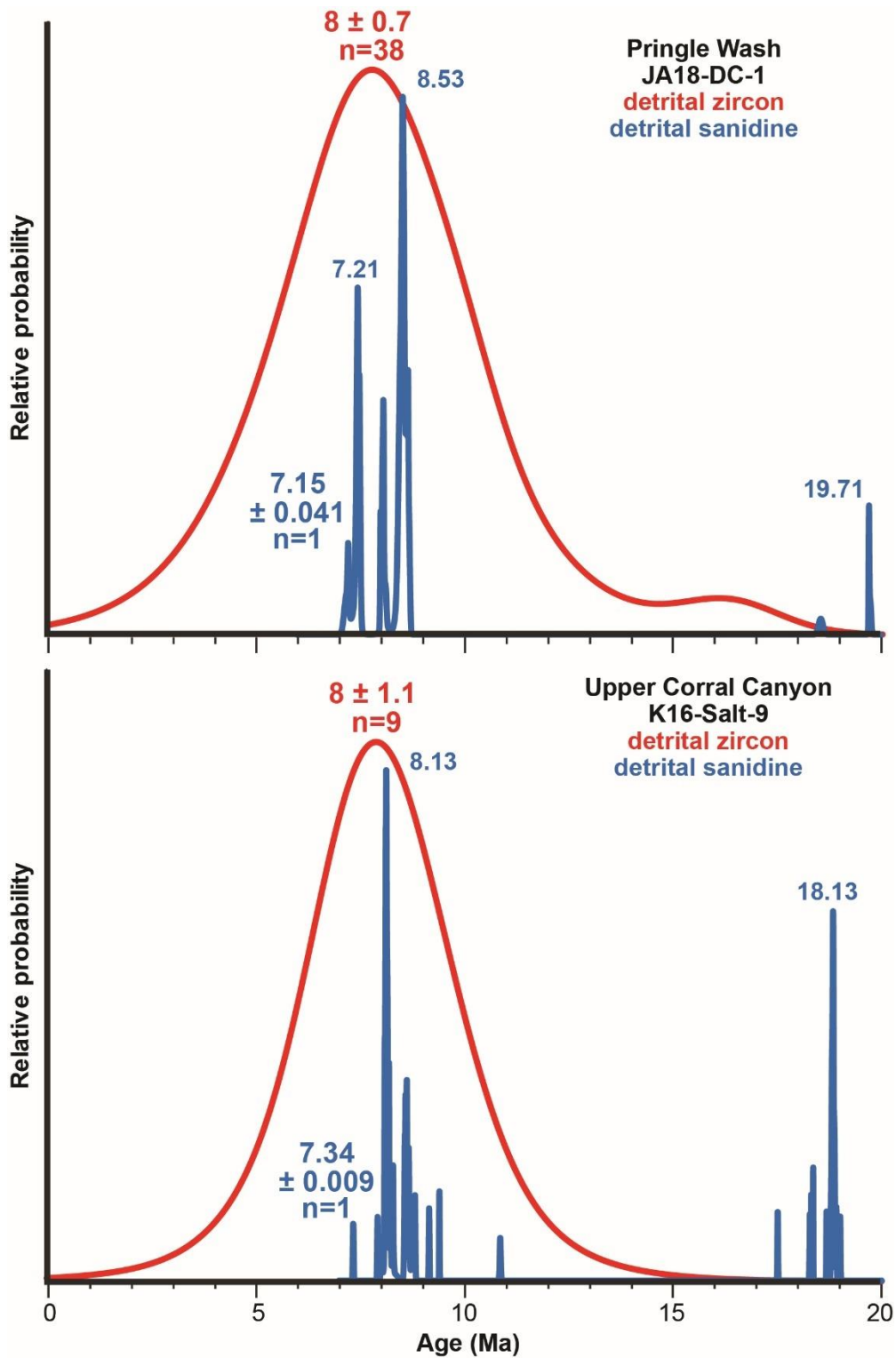


**Figure 22:** Detrital zircon (red) and sanidine (blue) spectrums between 20-0 Ma for the base (K16-Salt-9) and the top (JA18-DC-1) of the upper Dagger Canyon conglomerate. The bold number next to the youngest age peak represents the sample's maximum depositional age. The n= number beneath it indicates the number of grains used to calculate the weighted mean age.

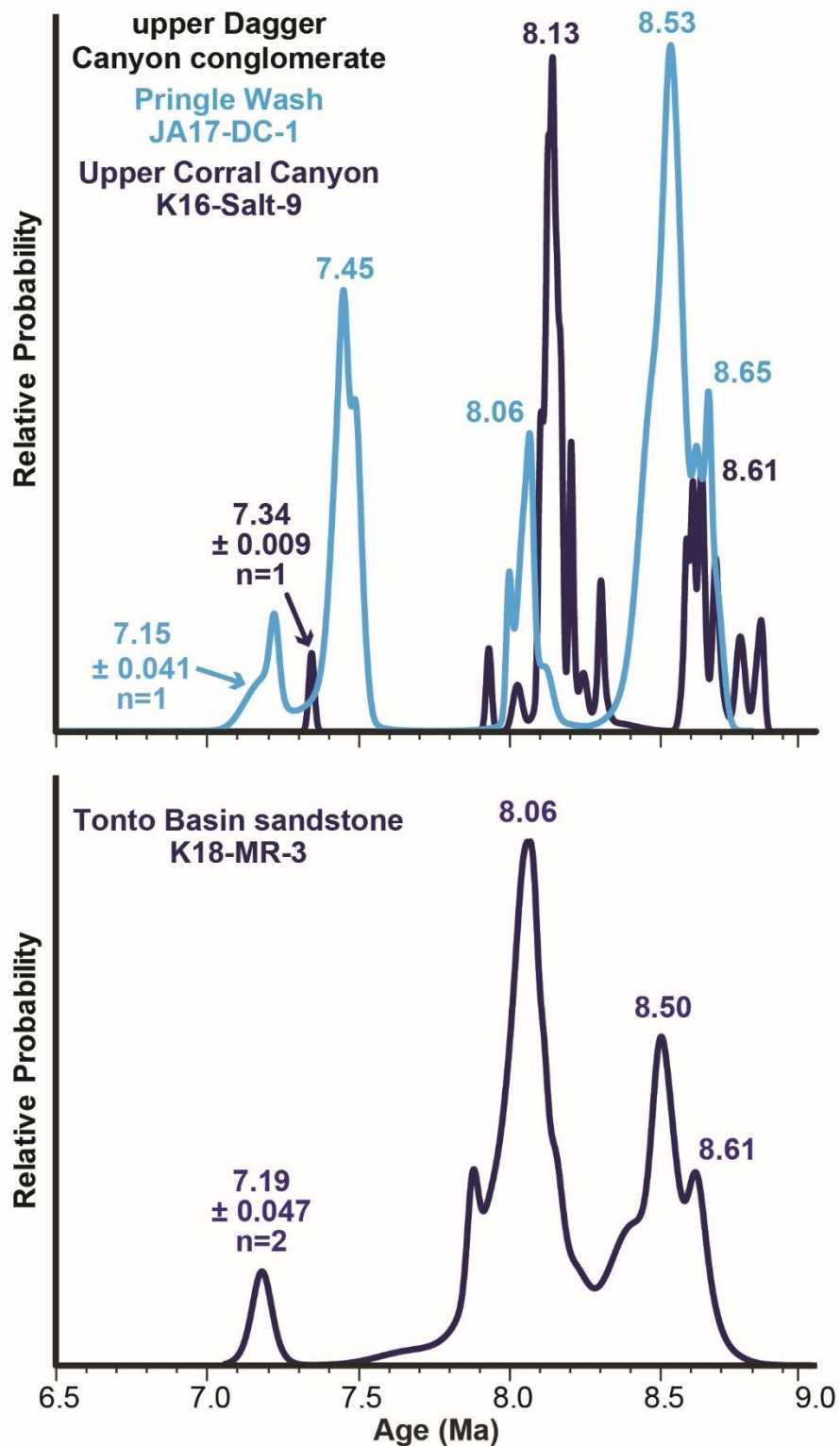


**Figure 23:** Detrital sanidine age spectrums of the upper Dagger Canyon conglomerate and Tonto Basin sandstone between 6.5-9 Ma. The bold number next to the youngest age peak represents the sample's maximum depositional age. The n= number beneath it indicates the number of grains used to calculate the weighted mean age.

35.33 Ma, 34.88 Ma, 33.88, 19.17 Ma, 8.53 Ma, 8.06 Ma and 7.45 Ma and 7.21 Ma. The youngest grain is 7.15 Ma. Sample K18-MR2 was taken from upper Dagger Canyon conglomerate on the east side of the Tonto Basin (Figure 9A). This sample has one age peak at 18.85 Ma and the youngest grain is 17.01 Ma. Due to the small number of grains analyzed (n=63) and lack of grains younger than 17.01 Ma this sample is not included in Dagger Canyon conglomerate detrital sanidine age spectrums.

Samples of Tonto Basin mudstone and sandstone were sampled to compare to upper Dagger Canyon conglomerate sample K18-MR2 and analyzed for detrital sanidine (Figure 19). Sample K18-MR1 was taken directly underneath K18-MR2 from Tonto Basin mudstone with sub-rounded, cobble to boulder clasts. It has a peak at 18.77 Ma and has one grain younger than 14 Ma at 8.83 Ma. Sample K18-MR1 has a similar youngest age peak as the upper Dagger Canyon conglomerate samples and is included with the upper Dagger Canyon Conglomerate composite spectrum for Figure 20. Since this sample has only one grain younger than 14 Ma it is not included in Figure 23. Sample K18-MR3 was taken 10 m below K18-MR1 from Tonto Basin sandstone with interbedded subangular to subrounded pebble to cobble clasts. This sample contains 6 grains between 73.73-58.85 Ma. It contains age peaks at 35.24 Ma, 34.67 Ma 18.76 Ma, 8.53 Ma, and 8.07 Ma. The youngest two grains form a peak at 7.19 Ma. Sample K18-MR3 has a similar youngest age peak and detrital sanidine spectrum to the upper Dagger Canyon conglomerate (Figure 23) and is included in the compilation of upper Dagger Canyon conglomerate age spectrums (Figure 20).

Figure 24 shows photographs of Salt River Terrace sample locations and Figure 25 shows the detrital sanidine results from these samples. Sample K19-MT is from the

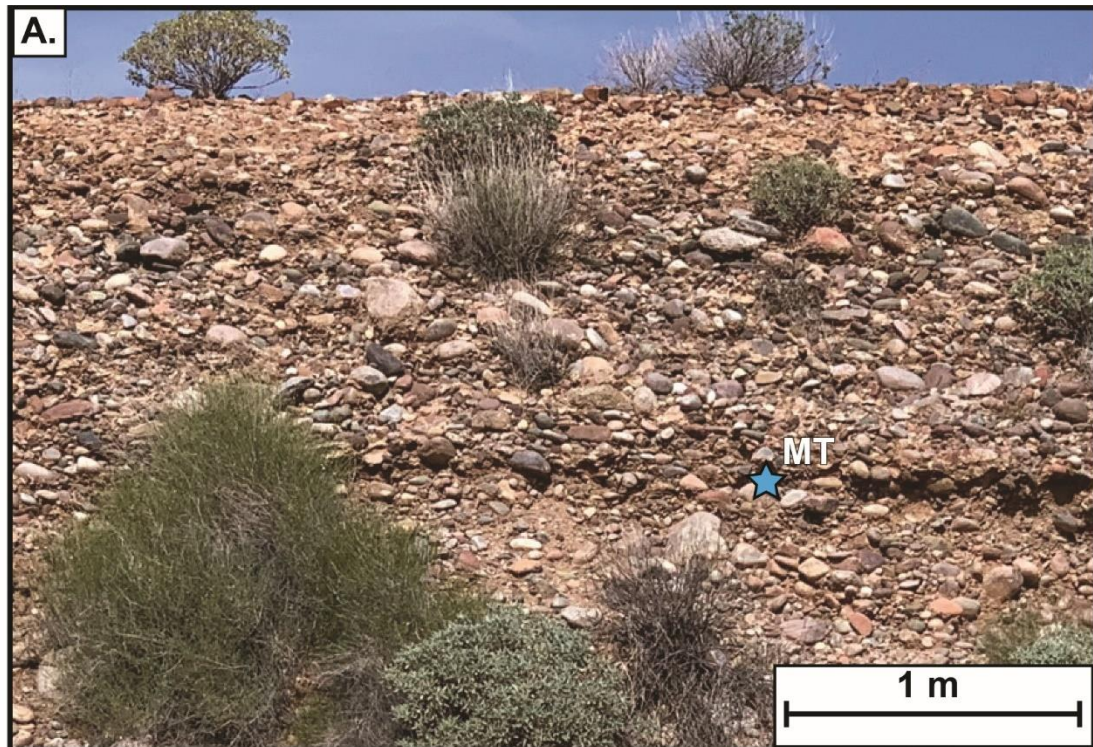


**Figure 24:** Photograph of Salt River terrace sample locations. Photograph of Beehive Rock sample location is on Figure 13A. **Figure 24A:** The Mesa Terrace (K18-MT) sample location is approximately 50 m above the modern river. **24B:** The Salt River terrace at Butte Creek (JA18-BC-1) is approximately 5 m above the modern Salt River.

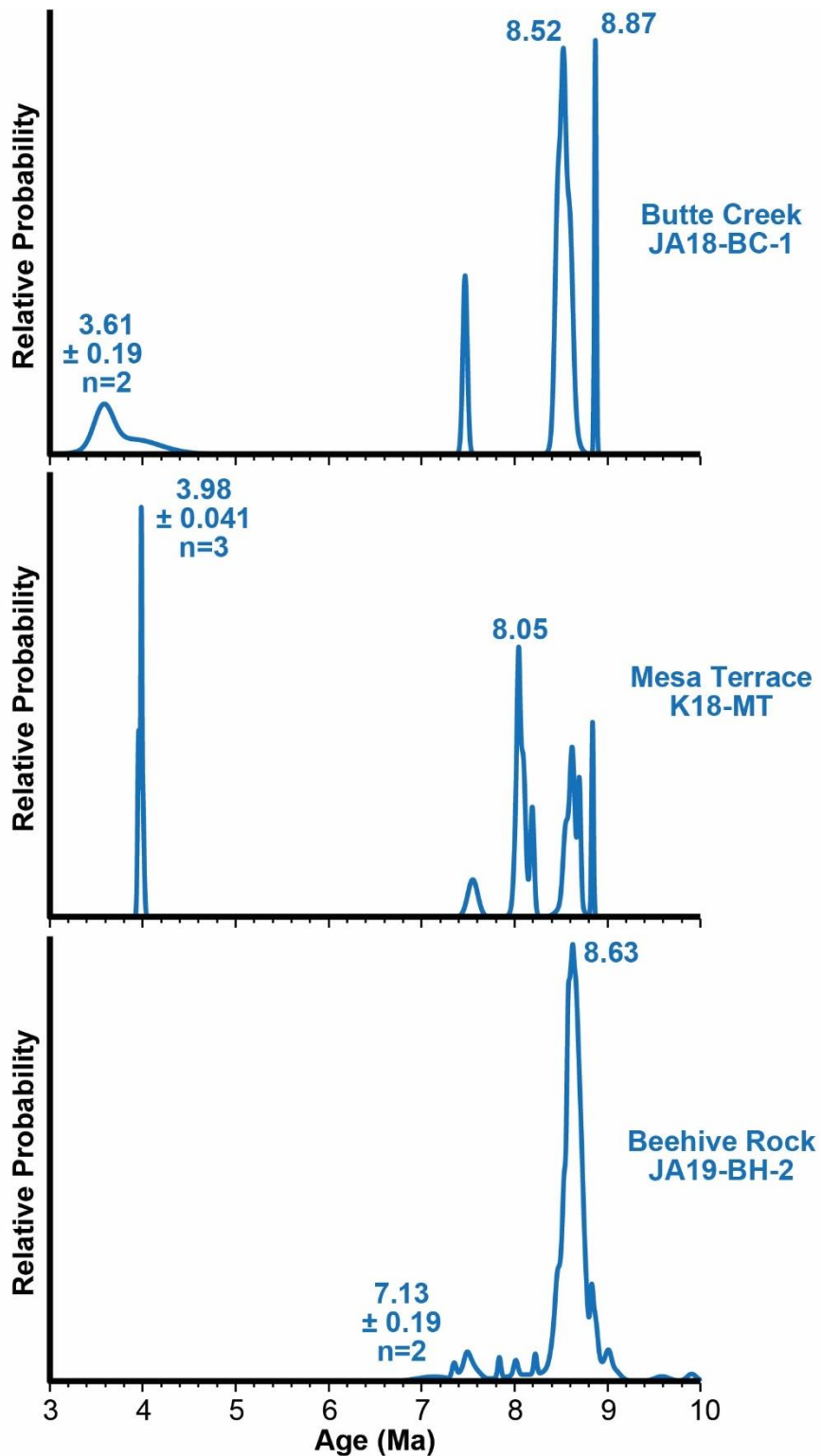


**Figure 25:** Detrital sanidine age spectrums of Salt River terraces between 3-10 Ma. The bold number next to the youngest age peak represents the sample's maximum depositional age. The n= number beneath it indicates the number of grains used to calculate the weighted mean age.

Mesa Terrace, the Salt River's third highest terrace (Péwé, 1978). The sample was taken off of N. Beeline Highway in the Basin and Range east of Phoenix (Figure 3) 50 m above the modern river level. There are age peaks at 18.7 Ma, 10 Ma at 8.62 Ma 8.05 Ma. The youngest three grains form a peak at 3.99 Ma. Sample JA18-BC-1 is from a terrace in the Salt River paleocanyon along Butte Creek 5 m above the modern river level (Figure 4A). This sample contains age peaks at 1353 Ma, 1220 Ma, 1111 Ma, and 1041 Ma, 32.46 Ma and 8.52 Ma. The youngest two grains form a peak at 3.61 Ma. Sample JA19-BH-2 is from a terrace at Beehive Rock overlying the Whitetail Conglomerate 83 m above the modern river level. Figure 14A shows a picture of the Beehive Rock sample location. This sample contains a peak at 34.74 Ma and 8.63 Ma. The youngest two grains form a peak at 7.13 Ma.

#### *<sup>40</sup>Ar/<sup>39</sup>Ar volcanic sample results*

Two volcanic samples were taken above paleoriver sample locations to constrain the minimum depositional age of the paleoriver sediments. <sup>40</sup>Ar/<sup>39</sup>Ar spectrum diagrams for volcanic samples are presented in Figure 26. Sample K16-Salt-3 is from Canyon Creek Butte dacite that overlies Whitetail Conglomerate sample JA17-MD-1 (Figure 12B). The <sup>40</sup>Ar/<sup>39</sup>Ar spectrum of this sample shows 90% of the <sup>39</sup>Ar gas released gives a plateau age of 21.84 ± 0.03 Ma in nine step-heating increments. Sample JA18-BLK-2 is from a Natanes Plateau basalt flow 35 m southeast rim gravel sample JA18-BLK-1. The <sup>40</sup>Ar/<sup>39</sup>Ar spectrum of this sample shows 30% of the oldest <sup>39</sup>Ar gas released gives a plateau age of 22.14 Ma ± 0.07 over 3 step-heating increments.

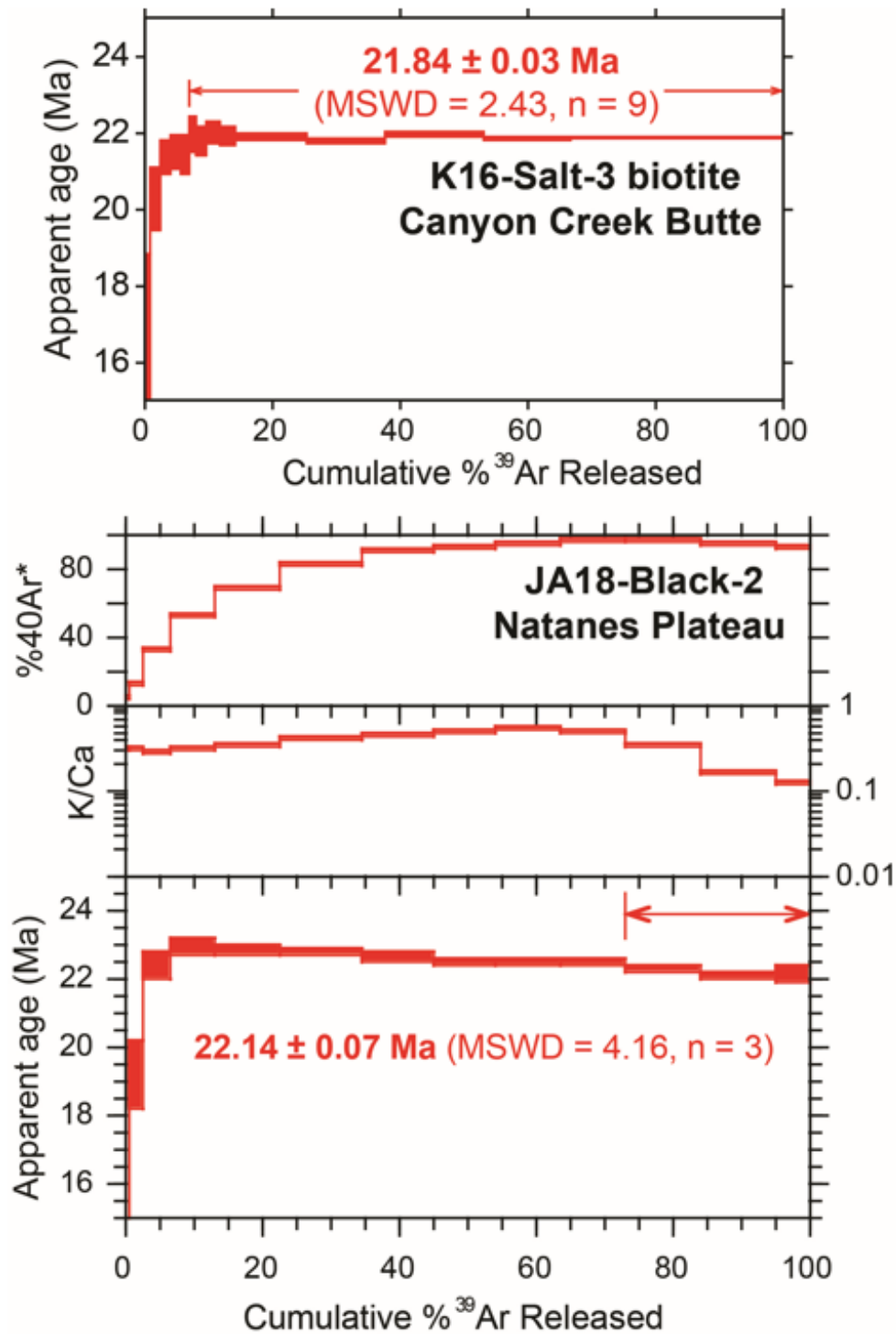


**Figure 26:** <sup>40</sup>Ar/<sup>39</sup>Ar spectrum for basalt and dacite samples used to constrain minimum depositional ages of the Whitetail Formation at Canyon Creek Butte (K16-Salt-3) and the Mogollon Rim Formation at Black River (JA18-Black-2). Sample information available in Table 2.

## INTERPRETATIONS

### *Source of Detrital Zircon and Sanidine*

Every paleoriver sample from this study contains distinct detrital zircon age groups that of 1440 Ma and 1650 Ma. The ~1650 Ma grains are sourced from Mazatzal province basement rocks (Shaw and Karlstrom, 1999; Whitmeyer and Karlstrom, 2007). The ~1440 Ma grains are sourced from the  $1436 \pm 2$  Ma Ruin Granite (Isachsen et al., 1999) and other Mesoproterozoic granites in the area (Anderson, 1989; Conway and Silver, 1989). The majority of paleoriver samples contain detrital zircon and sanidine age peaks between 60-75 Ma. These grains were sourced from Laramide porphyry deposits in the Globe-Miami and Superior area (Leveille and Stegen, 2012; Favorito and Seedorff, 2017; Seedorff et al., 2019). 69-61 Ma zircon grains have been found in porphyry dikes and granite in the Superior and Globe-Miami mining district (Seedorff et al., 2019). Two populations of zircons have been found in the Ray porphyry copper deposit to the south, one at 69 Ma and other at 66 Ma. 74-73 Ma zircon grains have been found in porphyry copper deposits at the Kelvin-Riverside and Troy districts further to the south in the Dripping Springs and Tortilla Mountains (Seedorff et al., 2019). 65 Ma zircon grains have been found in the Christmas porphyry copper deposit in the Dripping Springs Mountains southeast of the Ray deposit (Seedorff et al., 2019). The majority of the paleoriver samples also contain detrital zircon and sanidine age peaks between 36-26 Ma. These grains were likely sourced from the Mogollon-Datil Volcanic Field (McIntosh et al., 1990; McIntosh et al., 1991, 1992). The detrital sanidine age peaks between 20-15 Ma in the Dagger Canyon conglomerate, Tonto Basin deposits and Salt River terrace samples were sourced from the Superstition volcanic field and the prominent 18.6 Ma peak is

from the Apache Leap Tuff (McIntosh and Ferguson, 1998; Potochnik, 2001a). The 7-9 Ma detrital zircon and sanidine peaks from the upper Dagger Canyon conglomerate Tonto Basin and Salt River terrace samples were likely sourced from the Mount Baldy volcanic field (Merrill and Pewe, 1977; Condit and Shafiqullah, 1985).

The detrital zircon spectrum of the Blue Ridge Mogollon Rim Formation sample (JA17-BR-1) contains a cosmopolitan distribution of ages that differs from other Mogollon Rim Formation samples (Figure 11). The Blue Ridge sample contains an Archean detrital zircon age peak at 2747 Ma, a Paleoproterozoic age peak at 1806 Ma, a Mesoproterozoic age peak at 1089 Ma, a range of Neoproterozoic grains between 566 to 996 Ma, and several Paleozoic age peaks at 523 Ma, 436 Ma and 507 Ma. These peaks are not present in other Mogollon Rim Formation samples with the exception of four Paleozoic grains from the Trout Creek sample that are not close enough in age to form a peak. The Blue Ridge sample also lacks Laramide zircon grains between 60-75 Ma that are present in other Mogollon Rim Formation samples.

#### *Age of Northeast-Flowing Rivers and Whitetail Conglomerate*

Northeast-flowing rivers in the Salt River area deposited the Mogollon Rim Formation during the Paleogene (Potochnik, 1989; Potochnik and Faulds, 1998; Potochnik, 2001a). Detrital zircon maximum depositional ages range from 64 Ma at Flying V Canyon (K16-Salt-13), 37 Ma at Trout Creek (JA17-TC-1), 33 Ma at Black River (JA18-BLK-1) and 30 Ma at Blue Ridge (JA17-BR-1) (Figure 11). The maximum depositional age from Trout Creek is similar to the maximum depositional age estimated from Potochnik and Faulds (1998) made by projecting aggradation rates between the  $33.55 \pm 0.41$  Ma and  $35.22 \pm 0.90$  Ma tuffs to the bottom of the section. The  $33.55 \pm 0.41$

tuff at the top of this section defines its minimum depositional age (Figure 9). This indicates deposition of the Mogollon Rim Formation at this location occurred between 37-33.55 Ma and deposition of the lower conglomeratic member occurred between 37-35.22 Ma. The 33 Ma maximum depositional age of the sample at Black River is close to the minimum depositional age at Trout Creek. The 22.14 Ma Natanes Plateau basalt sample (JA18-BLK-2) taken above sample JA18-BLK-1 (Figure 9) is similar in age to previously reported Natanes Plateau basalt ages between 25.3 to 17.7 Ma (Damon et al., 1996; Wrucke et al., 2004). This age is likely younger than the gravels' depositional age due to the petrocalcic paleosol between the Mogollon Rim Formation and Natanes Plateau basalt in this area (Potochnik, 1989). The 30 Ma maximum depositional age of the Blue Ridge sample is younger than the 33.32 Ma tuff interbedded near the top of the formation (Potochnik, 2001a) (Figure 9). There could be multiple reasons for the apparent discrepancy between the maximum and minimum depositional ages. However, the age of tuff is within the error of the 30 Ma detrital zircon peak meaning gravels here were likely deposited quickly around 33 Ma.

The 64 Ma detrital zircon maximum depositional age of the Flying V Canyon sample (K16-Salt-13) is significantly older than the other depositional ages of the Mogollon Rim Formation (Figures 8 and 10). An 11.7 Ma basalt overlies the section at Flying V Canyon (Damon et al., 1996) that is not useful for constraining its minimum depositional age and no other interbedded volcanic units have been identified (Figure 9). The youngest detrital sanidine grain from K16-Salt-13 refines its maximum depositional age to 60.02 Ma, only 4 Ma younger than the youngest detrital zircon grain (Figure 12). Another sample was taken at Flying V Canyon (JA19-Salt-15) 5 m beneath K16-Salt-13

and 2 m above the base of the formation (Figure 10A) to verify this older maximum depositional age was not a result of sampling bias. Detrital sanidine from JA19-Salt-15 show similar age peaks as K16-Salt-13 at 73.79 Ma, 60.07 Ma and 60.02 Ma (Figure 12). This sample's youngest sanidine grain is 59.38 Ma, giving it a very similar maximum depositional age to K16-Salt-13 with a difference of only 0.64 Ma. The best maximum depositional age for the gravels at this location is 59.38 Ma.

The Whitetail Conglomerate represents the transition from northeast-flowing rivers to internally draining conditions in the Salt River paleocanyon region during the Oligocene (Peirce et al., 1979; Faulds, 1986; Potochnik and Faulds, 1998; Potochnik, 2001a). Maximum depositional ages of the Whitetail Conglomerate decrease up section from 30 Ma at Beehive Rock (K16-Salt-6) near the base of the unit to 26 Ma near the top of the unit's maximum thickness at Mud Springs Draw (Figure 13). The maximum depositional age of valley gravels near Tonto Natural Bridge (25 Ma) is similar to these ages (Figure 15). The minimum depositional age the Whitetail Conglomerate is now constrained by the overlying  $21.84 \pm 0.03$  Ma Canyon Creek Butte dacite (K16-Salt-3) (Figure 13). Most of the Whitetail Conglomerate in the Salt River paleocanyon is overlain by the  $18.63 \pm 0.07$  Ma Apache Leap tuff (Faulds, 1986; Potochnik, 2001a) but the Canyon Creek Butte dacite indicates that Whitetail Conglomerate deposition along the Salt River paleocanyon axis was complete by 21.84 Ma.

#### *Age of Southwest-Flowing Rivers*

The initial southwest-flowing paleoriver in the Salt River paleocanyon (proto-Salt river) incised 200 m into the Black Mesa and Chalk Creek Formation before depositing the Dagger Canyon conglomerate. The Dagger Canyon conglomerate must be younger

than the 14.67 Ma Black Mesa basalts weathered by the proto-Salt River (Potochnik and Faulds, 1998). The apparent absence of interbedded and overlying volcanic units makes the Dagger Canyon conglomerate's minimum depositional age difficult to constrain.

The lower Dagger Canyon conglomerate consists of well consolidated, pebble to boulder conglomerate located in northwest trending fault blocks west of Cherry Creek fault and in eastern Tonto Basin (Faulds, 1986; Potochnik, 2001a) (Figure 16). The decreasing dip of bedding up-section from 27° to 0° indicates deposition corresponded with Basin and Range normal faulting in this area (Potochnik, 2001a). Detrital sanidine from three samples of lower Dagger Canyon conglomerate indicate maximum depositional ages range from of 15.69 Ma at Redmond Flat (JA19-RF-1), 15.34 Ma at the western edge of Tonto Basin (JA19-DC-3), and 12.49 Ma near Shute Springs creek (JA19-SS-1) (Figure 20). The proto-Salt River developed after 14.67 Ma so the 12.39 Ma age near Shute Springs Creek is the only useful maximum depositional age for the lower Dagger Canyon conglomerate.

Detrital zircon and sanidine maximum depositional ages indicate the upper Dagger canyon conglomerate is distinctly younger than the lower Dagger Canyon conglomerate (Figures 20-23). The upper Dagger canyon conglomerate consists of flat-lying, poorly consolidated, pebble to cobble conglomerate located between the Cherry Creek and Canyon Creek faults and in the eastern Tonto Basin (Figure 16). Detrital zircon from the base and top of the upper Dagger Canyon conglomerate (K16-Salt-9, K16-Salt-10 and JA17-DC-1) indicate a maximum depositional age of 8 Ma (Figure 21). Detrital sanidine from the base (K16-Salt-9) and top (JA17-DC-1) of the member refine the maximum depositional ages to 7.34 Ma and 7.15 Ma respectively (Figure 22). Detrital

sanidine maximum depositional ages are similar and within error of the 8 Ma detrital zircon age peaks. Unfortunately, none of the detrital sanidine analyzed from the upper Dagger Canyon conglomerate sample from Tonto Basin (K18-MR2) were younger than 17.01 Ma.

Detrital sanidine analyzed from sample K18-MR2 did not constrain the maximum depositional age of the upper Dagger Canyon conglomerate in the Tonto Basin however, detrital sanidine from the underlying mudstone and sandstone provide additional opportunities to constrain its maximum depositional age. Mudstone deposits containing sub-rounded, cobble to boulder clasts are present directly beneath the upper Dagger Canyon conglomerate in the Tonto Basin (Figure 19). Detrital sanidine indicate the maximum depositional age of these sediments is 8.83 Ma (K18-MR1). Sandstone deposits 10 m beneath K18-MR1 and K18-MR2 contain subangular to subrounded, pebble to cobble clasts (Figure 19) and detrital sanidine indicate a maximum depositional age of 7.19 Ma (K18-MR3) (Figure 23). Therefore, the upper Dagger Canyon conglomerate in the Tonto Basin is also younger than 7.19 Ma, similar to the upper Dagger Canyon conglomerate in the Salt River paleocanyon. The Tonto Basin sandstone (K18-MR3) also contains similar peaks as the upper Dagger Canyon conglomerate samples from the Salt River paleocanyon, around 35 Ma, 18.8 Ma, 18.3 Ma (Figure 20 and 23), 8.5 Ma, and 8.1 Ma (Figures 21 and 23).

Detrital sanidine results from Salt River terraces are useful for constraining the Salt River spill-over event from Tonto Basin the Phoenix basin. The spillover event happened before 2.8 Ma based on the cosmogenic burial age of the now buried, oldest Salt River gravels in the Phoenix Basin (Skotnicki et al., 2016). The maximum

depositional ages of the terraces range from 7.13 Ma at Beehive Rock (JA19-BH-2), 3.99 Ma at Mesa terrace and 3.61 Ma at Butte Creek (JA18-BC-1) (Figure 25). The Beehive Rock terrace and the Butte Creek terrace are located in the Salt River paleocanyon and may have been deposited before the spillover. The Mesa terrace is located in the Phoenix Basin (Figure 3) and had to have been deposited after the spillover event. Therefore, the age of the spillover event is now constrained between 3.99-2.8 Ma. The Butte Creek terrace has previously been identified as gravels deposited by northeast-flowing rivers through the Salt River paleocanyon (Potochnik, 2001a). The 10 detrital sanidine grains younger than 10 Ma and the 3.61 maximum depositional age indicate these gravels were instead deposited by the modern Salt River (Figure 25).

## **DISCUSSION**

### *Mogollon Rim Formation*

The near agreement in maximum depositional ages between both samples from Flying V Canyon, for both detrital zircon and sanidine, suggests these gravels are distinctly older than the rest of the Mogollon Rim Formation (Figure 9). The maximum depositional age of the Flying V Canyon gravels based detrital sanidine is 59.38 Ma and 64 Ma based on detrital zircon. These age are similar to the youngest clast ( $54.56 \pm 1.17$  Ma) dated by Peirce (1979) from the Mogollon Rim Formation near Round Top Mountain and similar to the youngest detrital zircon grains found in Baca Formation samples between 56-57 Ma (Donahue, 2016). The depositional age for the rest of the Mogollon Rim Formation is between 37-33.55 Ma. Without a minimum depositional age constraint at Flying V Canyon it is impossible to determine the exact depositional age difference. However, several lines of evidence support an older depositional age at this

location. The lower conglomeratic member here contains interbedded and well-indurated petrocalcic paleosols that are not present in member at other locations (Potochnik, 1989). Also the clast provenance at Flying V Canyon does not significantly change up-section and no clast of volcanic porphyries are present (Potochnik, 1989). The modal abundance of volcanic porphyry clasts increases up-section at other Mogollon Rim Formation locations studied by Potochnik (1989). This means either the northeast-flowing paleoriver's drainage area did not include the Globe-Miami area or the porphyry deposits had not been unroofed during deposition of the gravels at Flying V Canyon. The upper portion of the Flying V Canyon section contain sandstones with scour-and-fill structures and narrow conglomerate-filled channels (Potochnik, 1989). This indicates that NE flowing rivers were still present in the Salt River paleocanyon after deposition of the Flying V Canyon gravels. Thus, we hypothesize the paleoriver responsible for carving the Salt River paleocanyon and depositing the gravels at Flying V Canyon is an older system with a smaller source area than ones responsible for depositing the rest of the Mogollon Rim Formation. Further fieldwork and sample collection are required to test this hypothesis.

Detrital zircon results indicate the paleoriver responsible for depositing the Blue Ridge gravels had a different source area than the paleorivers that deposited the rest of the Mogollon Rim Formation. This sample contains several Precambrian and Paleozoic peaks that are not present in other southeast rim gravel samples (Figure 11). It also lacks Laramide zircon grains between 60-75 Ma from the copper porphyries deposits in the Globe-Miami and Superior area. The 30 Ma maximum depositional age at Blue Ridge and the  $33.32 \pm 0.59$  Ma tuff at the top of the section indicates these gravels were

deposited around the same time as the Trout Creek and Black River gravels. However, the detrital zircon results show the paleoriver at Blue Ridge had a separate source area and was not a tributary of the paleorivers that deposited the gravels at Trout Creek.

#### *The Dagger Canyon Conglomerate Disconformity*

The maximum depositional ages between the Dagger Canyon conglomerate samples indicates a significant disconformity exists between the upper and lower Dagger Canyon Conglomerate (Figure 8). The maximum depositional age of the lower Dagger Canyon conglomerate is 12.49 Ma (Figure 20). This age is within error of the  $11.74 \pm 0.94$  Ma basalt (Damon et al., 1996) overlying un-weathered Mogollon Rim Formation at Flying V Canyon that Potochnik (2001a; 2001b) used as a possible older age constraint for the proto-Salt River. This age is also consistent with the lower Dagger Canyon conglomerate being deposited during Basin and Range normal faulting in this area (Faulds, 1986; Potochnik and Faulds, 1998; Potochnik, 2001a). The maximum depositional ages of the upper Dagger Canyon conglomerate range from 7.34 Ma near its base (K16-Salt-9) to 7.15 Ma near its top (JA17-DC-1) (Figure 13). It is possible the 7.34 Ma detrital sanidine grain from the base of the upper Dagger Canyon conglomerate is close to the depositional age because this sample does not have the 7.2 Ma peak present in the top of the unit (JA17-DC-1) and in the Tonto Basin sandstone (K18-MR3) (Figure 23). Therefore, we consider the 7.34 Ma age to represent the maximum depositional age for the entire upper Dagger Canyon conglomerate. The difference in maximum depositional ages between the lower and upper Dagger Canyon conglomerate is 5.15 Ma. However, differences in maximum depositional ages can also be the result of a lack of nearby volcanic activity instead of a disconformity. The upper Dagger Canyon

conglomerate, Tonto Basin mudstone and Tonto Basin sandstone contain several age peaks younger than 9 Ma including 8.5 Ma, 8.1 Ma, 7.45 Ma and 7.2 Ma that are not present in the lower Dagger Canyon conglomerate (Figures 20 and 23). These multiple peaks rule out the possibility that the difference in maximum depositional ages is purely the result of a gap in volcanic activity since the upper Dagger Canyon conglomerate contains detrital sanidine from several eruptions that are not present in the lower Dagger Canyon conglomerate.

The disconformity between the lower and upper Dagger Canyon conglomerate has significant implications for southern Colorado Plateau evolution. Without minimum depositional age constrains the exact duration of this disconformity cannot be determined however, the estimated minimum depositional ages from this study indicate the disconformity could represent a pause in fluvial deposition between 10.98 to 7.34 Ma. The position of the lower Dagger Canyon conglomerate in tilted fault blocks and its maximum depositional age are evidence that the proto-Salt River initially developed in response to Basin and Range extension. The maximum depositional age of the upper Dagger Canyon conglomerate indicates the proto-Salt River was rejuvenated after 7.34 Ma, well after Basin and Range extension had waned in this area. The potential drivers for this rejuvenation are southern Colorado Plateau uplift from the White Mountains-Mount Baldy volcanic complex between 9-8 Ma and the development of the North American Monsoon season around 6 Ma. Further field work and sampling is required to test this hypothesis.

## CONCLUSIONS

The first goal of this study was to constrain the timing of the drainage reversal from northeast to southwest-flowing river in the Salt River area by providing additional age constraints for sediments deposited before, during and after the reversal. Northeast-flowing rivers deposited the Mogollon Rim Formation on the Colorado Plateau between 59.38-33.55 Ma based on the detrital sanidine maximum depositional age of gravels at Flying V Canyon and the overlying tuff at Trout Creek (Potochnik and Faulds, 1998). Results indicate the Mogollon Rim Formation at Flying V Canyon is older than other locations and deposition began after 59.38 Ma. Deposition in the Trout Creek area occurred between 37-33.55 Ma. Deposition began after 33 Ma in the Black River area. Deposition occurred around 33 Ma in the Blue Ridge area and rivers here were not connect to the rivers that deposited the rest of the Mogollon Rim Formation. The Whitetail Conglomerate signals the shift from northeast-flowing rivers to internal drainage in the Salt River paleocanyon. Whitetail Conglomerate deposition in the paleocanyon tributaries began around 37.60 Ma based on a rhyodacite flow interbedded in the lower Whitetail Conglomerate along the Canyon Creek fault tributary (Potochnik, 2001a). Deposition in the axis of the paleocanyon occurred between 30 Ma-21.84 Ma based on detrital zircon and the overlying Canyon Creek Butte dacite. Internally draining conditions continued in the Salt River paleocanyon until after 14.67 Ma based on the Black Mesa basalts that interfingers the upper member of the Chalk Creek Formation (Faulds, 1986; Potochnik and Faulds, 1998; Potochnik, 2001a). The initial southwest-flowing proto-Salt River system began after 14.67 Ma, integrating the modern Salt River drainage area from the Tonto Basin to the Mogollon Rim (Potochnik and Faulds, 1998).

The proto-Salt River system deposited the lower Dagger Canyon conglomerate after 12.49 Ma according to detrital sanidine. This unit's maximum depositional age and position in tilted fault blocks confirm the proto-Salt River was initiated by Basin and Range extension in this area. Deposition of the upper Dagger Canyon conglomerate began after 7.34 Ma, well after Basin and Range extension had waned in this area. Without an interbedded or overlying volcanic unit the exact difference in depositional ages cannot be determined. However, if these maximum depositional ages are close to the actual depositional ages then the disconformity between the upper and lower Dagger Canyon conglomerate could represent 5.15 Ma of time.

This study also provides additional age constraints for the Salt River's spillover event from the Arizona Transition zone into the Basin and Range. This spillover event represents the Salt River's integration as a tributary of the Gila River and its final major baselevel-lowering event. The Mesa terrace in the Basin and Range was deposited after the spill over and has a maximum depositional age of 3.99 Ma. The event occurred before 2.8 Ma based on the cosmogenic burial age oldest Salt River gravels in the buried Phoenix Basin (Skotnicki et al., 2016). The spillover event is now constrained between 3.99-2.8 Ma.

Constraints provided by this study are useful for understanding the evolution of the southern Colorado Plateau. The minimum depositional age constraints for the Mogollon Rim Formation and the maximum depositional age of the Black River sample indicate northeast-flowing rivers ended around 33 Ma. The maximum depositional age of the Whitetail Conglomerate in the axis of the Salt River paleocanyon indicates internal drainage in the Salt River paleocanyon began 30 Ma. This leads us to the conclusion that

the southern edge of the Colorado Plateau between 33-30 Ma. This means that Oligocene normal faulting and formation of the Mogollon-Datil volcanic field were responsible for the demise of northeast flowing rivers and the development of the Mogollon Rim. Results from the Dagger Canyon conglomerate indicate two stages of southwest-flowing proto-Salt River occurred in the Salt River paleocanyon before the river's spill over event into the Basin and Range. The first stage responsible for integrating the drainage area began after 14.67 Ma and deposited the lower Dagger Canyon conglomerate after 12.49 Ma. Basin and Range extension in this area initiated this first stage. The second stage deposited the 300 m of the upper Dagger Canyon conglomerate after 7.34 Ma. This second stage occurred after Basin and Range extension had waned and before the final Salt River base level fall between 3.99-2.8 Ma. The most likely drivers this second stage include headwater uplift during Mount Baldy volcanic development between 9-8 Ma and the opening of Gulf of California around 6 Ma which intensified the North American monsoon (Chapin, 2008). Further field work and sampling are required to verify this interpretation and differentiate the potential effects of both drivers; however, this second stage of the proto-Salt River raises the likelihood of post-10 Ma uplift of the southern Colorado Plateau.

## REFERENCES

- Anderson, J.L., 1989, Proterozoic anorogenic granites of the southwestern United States, *in* Jenney, J.P. and Reynolds, S.J. eds., *Geologic Evolution of Arizona: Arizona Geological Society Digest 17*, p. 211–238.
- Bilodeau, W.L., 1986, The Mesozoic Mogollon Highlands, Arizona: An Early Cretaceous Rift Shoulder: *The Journal of Geology*, v. 94, p. 724–735.
- Cather, S.M., 2004, Laramide orogeny in central and northern New Mexico and southern Colorado, *in* Mack, G.H. and Giles, K.A. eds., *The geology of New Mexico: A geologic history*, New Mexico Geological Society Special Publication 11, p. 203–248.
- Cather, S.M., Chamberlin, R.M., and Ratte, J.C., 1994, Tertiary stratigraphy and nomenclature for western New Mexico and eastern Arizona, *in* Chamberlin, R.M., Kues, B.S., Cather, S.M., Barker, J.M., and McIntosh, W.C. eds., *Mogollon slope (West-Central New Mexico and East-Central Arizona)*, New Mexico Geological Society 45th Annual Fall Field Conference Guidebook, p. 259–266.
- Cather, S.M., Chapin, C.E., and Kelley, S.A., 2012, Diachronous episodes of Cenozoic erosion in southwestern North America and their relationship to surface uplift, paleoclimate, paleodrainage, and paleoaltimetry: *Geosphere*, v. 8, p. 1177–1206.
- Cather, S.M., and Johnson, B.D., 1984, Eocene tectonics and depositional setting of west-central New Mexico and eastern Arizona: New Mexico Bureau of Mines and Mineral Resources Circular 192, p. 5–33.
- Cather, S.M., McIntosh, W.C., and Chapin, C.E., 1987, Stratigraphy, age, and rates of deposition of the Datil Group (Upper Eocene-Lower Oligocene), west-central New Mexico: *New Mexico Geology*, v. 9, p. 50–54.
- Chapin, C.E., 2008, Interplay of oceanographic and paleoclimate events with tectonism during middle to late Miocene sedimentation across the southwestern USA: *Geosphere*, v. 4, p. 976–991.
- Cobban, W.A., Merewether, E.A., Fouch, T.D., and Obradovich, J.D., 1994, Some Cretaceous Shorelines in the Western Interior of the United States, *in* Caputo, M. V., Peterson, J.A., and Franczyk, K.J. eds., *Mesozoic Systems of the Rocky Mountain Region, USA*, p. 393–414.
- Condit, C.D., and Shafiqullah, M., 1985, K-Ar ages of late Cenozoic rocks of the western part of the Springerville volcanic field, east-central Arizona: *Isochron/West*, v. 44, p. 3–5.
- Conway, C.M., and Silver, L.T., 1989, Early Proterozoic rocks (1710–1615 Ma) in central to southeastern Arizona, *in* Jenney, J.P. and Reynolds, S.J. eds., *Geologic Evolution of Arizona: Arizona Geological Society Digest 17*, p. 165–186.
- Cooley, M.E., 1958, Physiography of the Black Mesa Basin area, Arizona, *in* Black Mesa Basin (Northeastern Arizona), New Mexico Geological Society 9th Annual Fall

- Field Conference Guidebook, p. 146–149.
- Cooley, M.E., and Davidson, E.S., 1963, The Mogollon Highlands-their influence on Mesozoic and Cenozoic erosion and sedimentation, *in* Gray, S.I. ed., Arizona Geological Society Digest, Tucson, Arizona, v. VI, p. 7–35.
- Crow, R., Karlstrom, K., Asmerom, Y., Schmandt, B., Polyak, V., and Dufrane, S.A., 2011, Shrinking of the Colorado Plateau via lithospheric mantle erosion: Evidence from Nd and Sr isotopes and geochronology of Neogene basalts: *Geology*, v. 39, p. 27–30.
- Crow, R., Karlstrom, K., Darling, A., Crossey, L., Polyak, V., Granger, D., Asmerom, Y., and Schmandt, B., 2014, Steady incision of Grand Canyon at the million year timeframe: A case for mantle-driven differential uplift: *Earth and Planetary Science Letters*, v. 397, p. 159–173.
- Cumella, S.P., 1983, Relation of Upper Cretaceous Regressive Sandstone Units of the San Juan Basin to Source Area Tectonics, *in* Reynolds, M.W. and Dolly, E.D. eds., Mesozoic paleogeography of the west-central United States: SEPM Rocky Mountain Section, Rocky Mountain Paleogeography Symposium 2, Denver, Colorado, The Rocky Mountain Section Society of Economic Paleontologist and Mineralogist, p. 189–199.
- Damon, P.E., Shafiqullah, M., Ramond, H.C., and Spencer, J.E., 1996, K-Ar Dates From The University Of Arizona Laboratory Of Isotope, 1971-1991: Arizona Geological Survey Open File Report, OFR-96-18, 53 p.
- Davis, G.H., 1979, Laramide folding and faulting in southeastern Arizona: *American Journal of Science*, v. 279, p. 543–569.
- Davis, G.H., 1981, Regional strain analysis of the superimposed deformations in southeastern Arizona and the eastern Great Basin: *Arizona Geological Society Digest*, v. 14, p. 155–172.
- Davis, G.H., Showalter, S.R., Benson, G.S., McCalmont, L.S., and Faulds, J.E., 1982, The Apache uplift, heretofore unrecognized Colorado Plateau uplift, *in* Abstracts with Programs, Geological Society of America, 472 p.
- Davis, G.H., Showalter, S.R., Benson, G.S., and S, M.L., 1981, Guide to the Geology of the Salt River Canyon Region, Arizona: *Arizona Geological Society Digest*, v. 15, p. 49–97.
- Dickinson, W.R., 2015, Integration of the Gila River drainage system through the Basin and Range province of southern Arizona and southwestern New Mexico (USA): *Geomorphology*, v. 236, p. 1–24.
- Dickinson, W.R., Fiorillo, A.R., Hall, D.L., Monreal, R., and Potochnik, A.R., 1989, Cretaceous Strata of Southern Arizona, *in* Jenney, J.P. and Reynolds, S.J. eds., *Geologic Evolution of Arizona*, Arizona Geological Society, p. 447–461.
- Dickinson, W.R., and Gehrels, G.E., 2010, Implications of U-Pb ages of detrital zircons in Mesozoic strata of the Four Corners region for provenance relations in space and

- time, *in* *Geology of the Four Corners Country*, New Mexico Geological Society, p. 135–146.
- Donahue, M.M., 2016, Episodic uplift of the Rocky Mountains: evidence for U-Pb detrital zircon geochronology and low-temperature thermochronology with a chapter on using mobile technology for geoscience education: The University of New Mexico, Ph.D thesis, 201 p.
- Douglass, J., Meek, N., Dorn, R.I., and Schmeckle, M.W., 2009, A criteria-based methodology for determining the mechanism of transverse drainage development, with application to the southwestern United States: *GSA Bulletin*, v. 121, p. 586–598.
- Eaton, J.G., and Nations, D.J., 1991, Introduction; Tectonic setting along the margin of the Cretaceous Western Interior Seaway, southwestern Utah and northern Arizona, *in* Nations, D.J. and Eaton, J.G. eds., *Stratigraphy, depositional environments, and sedimentary tectonics of the western margin, Cretaceous Western Interior Seaway*, Boulder, Colorado, Geological Society of America, p. 1–8.
- Farmer, G.L., Bailey, T., and Elkins-tanton, L.T., 2008, Mantle source volumes and the origin of the mid-Tertiary ignimbrite flare-up in the southern Rocky Mountains, western U.S.: *Lithos*, v. 102, p. 279–294.
- Faulds, J., 1986, Tertiary geologic history of the Salt River Canyon region, Gila County, Arizona: The University of Arizona, Master's Thesis, 318 p.
- Favorito, D.A., and Seedorff, E., 2017, Characterization and reconstruction of Laramide shortening and superimposed Cenozoic extension, Romero Wash–Tecolote Ranch area, southeastern Arizona: *Geosphere*, v. 13, p. 577–607.
- Gastil, G., Wraher, M., Strand, G., Lee Kear, L., Eley, D., Chapman, D., and Anderson, C., 1992, The tectonic history of the southwestern United States and Sonora, Mexico during the past 100 m.y.: *Tectonics*, v. 11, p. 990–997.
- Gehrels, G., 2011, Detrital zircon U-Pb geochronology: current methods and new opportunities, *in* Busby, C. and Azor, A. eds., *Tectonics of Sedimentary Basins: Recent Advances*, Hoboken, New Jersey, Blackwell Publishing, p. 47–62.
- Gehrels, G.E., Blakey, R., Karlstrom, K.E., Timmons, J.M., Dickinson, B., and Pecha, M., 2011, Detrital zircon U-Pb geochronology of Paleozoic strata in the Grand Canyon, Arizona: *Lithosphere*, v. 3, p. 183–200.
- Gootee, B.F., 2019, Revised depth-to-bedrock and depth-to base of Gila River deposits along the southern Higley and northern Picacho Basin boundary, Pinal County, Arizona: Arizona Geological Survey, Open-File Report OFR-19-01, 18 p.
- Haq, B.U., Hardenbol, J., and Vail, P.R., 1987, Chronology of Fluctuating Sea Levels Since the Triassic: *Science*, v. 235, p. 1156–1167.
- Heizler, M.T., 2012, Higher Precision: Opening A new  $^{40}\text{Ar}/^{39}\text{Ar}$  can of worms, Abstract V21E-02, *in* 2012 Fall Meeting, San Francisco, California, AGU.

- Hereford, R., Beard, L.S., Dickinson, W.R., Karlstrom, K.E., Heizler, M.T., Crossey, L.J., Amoroso, L., House, P.K., and Pecha, M., 2016, Reevaluation of the Crooked Ridge River — Early Pleistocene (ca. 2 Ma) age and origin of the White Mesa alluvium, northeastern Arizona: *Geosphere*, v. 12, p. 768–789.
- Hilgendorf, Z., Wells, G., Larson, P.H., Millett, J., and Kohout, M., 2020, Geomorphology From basins to rivers : Understanding the revitalization and significance of top-down drainage integration mechanisms in drainage basin evolution: *Geomorphology*, v. 352, p. 1–17.
- Humphreys, E.D., 1995, Post-Laramide removal of the Farallon slab, western United States: *Geology*, v. 23, p. 987–990.
- Hunt, C.B., 1956, Cenozoic Geology of the Colorado Plateau: Geological Survey Professional Paper 270, 99 p.
- Huntoon, P.W., 1990, Phanerozoic Structural Geology of the Grand Canyon, *in* Beus, S.S. and Morales, M. eds., *Grand Canyon Geology*, Oxford University Press, p. 261–310.
- Huybers, P., and Molnar, P., 2007, Tropical cooling and the onset of North American glaciation: *Climate of the Past*, v. 3, p. 549–557.
- Isachsenl, C.E., Gehrels, G.E., Riggs, N.R., Spence, J.E., Ferguson, C.A., Skotnicki, S.J., and Richard, S.M., 1999, U-Pb geochronologic data from zircons from eleven granitic rocks in central and western Arizona: Arizona Geological Survey Open-File Report 99-5, 27 p.
- Karlstrom, K.E. et al., 2012, Mantle-driven dynamic uplift of the Rocky Mountains and Colorado Plateau and its surface response: Toward a unified hypothesis: *Lithosphere*, v. 4, p. 3–22.
- Karlstrom, K.E., Crow, R., Crossey, L.J., Coblenz, D., and Van Wijk, J.W., 2008, Model for tectonically driven incision of the younger than 6 Ma Grand Canyon: *Geology*, v. 36, p. 835–838.
- Keith, S.B., and Wilt, J.C., 1985, Late Cretaceous and Cenozoic orogenesis of Arizona and adjacent Regions: a strato-tectonic approach, *in* Flores, R.M. and Kaplan, S.S. eds., *Cenozoic Paleogeography of the west-central United States*, Denver, Colorado, Rocky Mountain Section S.E.P.M., p. 403–438.
- Lance, J.F., Downey, J.S., and Alford, M., 1962, Cenozoic sedimentary rocks of Tonto Basin, *in* Weber, R.H. and Pierce, H.W. eds., *Mogollon Rim Region (East-Central Arizona) New Mexico Geological Society 13th Annual Fall Field Convergence Guidebook*, New Mexico Geological Society, p. 98–99.
- Larson, P.H., Dorn, R.I., Douglass, J., Gootee, B.F., and Arrowsmith, R., 2010, Stewart Mountain Terrace: A New Salt River Terrace with Implications for Landscape Evolution of the Lower Salt River Valley, Arizona: *Journal of the Arizona-Nevada Academy of Science*, v. 42, p. 26–35.
- Levander, A., Schmandt, B., Miller, M.S., Liu, K., Karlstrom, K.E., Crow, R.S., Lee,

- C.T.A., and Humphreys, E.D., 2011, Continuing Colorado plateau uplift by delamination-style convective lithospheric downwelling: *Nature*, v. 472, p. 461–465.
- Leveille, R.A., and Stegen, R.J., 2012, The southwestern North America Porphyry Copper Province, *in* Hedenquist, J.W., Harris, M., and Camus, F. eds., *Geology and Genesis of Major Copper Deposits and Districts of the World: A Tribute to Richard H. Sillitoe*: Society of Economic Geologists Special Publication, p. 361–401.
- Lipman, P.W., and Glazner, A.F., 1991, Introduction to middle Tertiary Cordilleran volcanism-magma sources and relations to regional tectonics: *Journal of Geophysical Research: Solid Earth and Planets*, v. 91, p. 6329–6345.
- Lowry, A.R., Ribe, N.M., and Smith, B., 2000, Dynamic elevation of the Cordillera, western United States: *Journal of Geophysical Research*, v. 105, p. 23,371–23,390.
- Mahon, K.L., 1996, Mahon The New York Regression Application of an Improved Statistical Method to Geochemistry: *International Geology Review*, v. 38, p. 293–303.
- McIntosh, W.C., Chapin, C.E., Ratte, J.C., and Sutter, J.F., 1992, Time-stratigraphic framework for the Eocene-Oligocene Mogollon-Datil volcanic field, southwest New Mexico: *Geological Society of America Bulletin*, v. 104, p. 851–871.
- McIntosh, W.C., and Ferguson, C.A., 1998, Sanidine, Single Crystal, Laser-Fusion  $^{40}\text{Ar}/^{39}\text{Ar}$  Geochronology Database for the Superstition Volcanic Field, Central Arizona: Arizona Geological Survey Open Report, OFR-98-27, 74 p.
- McIntosh, W.C., Heizler, M., Peters, L., and Esser, R., 2003,  $^{40}\text{Ar}/^{39}\text{Ar}$  Geochronology at the New Mexico Bureau of Geology and Mineral Resources: New Mexico Bureau of Geology and Mineral Resources, Open File Report OF-AR-1, 7 p.
- McIntosh, W.C., Kedzie, L.L., and Sutter, J.F., 1991, Paleomagnetism and  $^{40}\text{Ar}/^{39}\text{Ar}$  ages of ignimbrites, MogolionDatil volcanic field, southwest New Mexico: *New Mexico Bureau of Mines and Mineral Resources Bulletin* 135, 99 p.
- Mckee, E.D., and Mckee, E.H., 1972, Pliocene Uplift of the Grand Canyon Region- Time of Drainage Adjustment: *Geological Society of America Bulletin*, v. 83, p. 1923–1932.
- McIntosh, W.C., Sutter, J.F., and Chapin, C.E., 1990, High-precision  $^{40}\text{Ar}/^{39}\text{Ar}$  sanidine geochronology of ignimbrites in the Mogolion-Datil volcanic field, southwestern New Mexico: *Bulletin of Volcanology*, v. 52, p. 584–601.
- Menges, C.M., and Pearthree, P.A., 1989, Late Cenozoic tectonism in Arizona and its impact on regional landscape evolution, *in* Jenney, J.P. and Reynolds, S.J. eds., *Geologic Evolution of Arizona*, Arizona Geological Society Digest 17, p. 649–680.
- Merrihue, C., and Turner, G., 1966, Potassium-Argon dating by Activation with Fast Neutrons: *Journal of Geophysical Research*, v. 71, p. 2852–2857.
- Merrill, R.K., and Pewe, T.L., 1977, Late Cenozoic Geology of the White Mountains Arizona, *in* Special Paper No. 1, State of Arizona Bureau of Geology and Mineral

- Technology, 65 p.
- Morgan, P., and Swanberg, C.A., 1985, On the Cenozoic uplift and tectonic stability of the Colorado Plateau: *Journal of Geodynamics*, v. 3, p. 39–63.
- Moucha, R., Forte, A.M., Rowley, D.B., Mitrovica, J.X., Simmons, N.A., and Grand, S.P., 2009, Deep mantle forces and the uplift of the Colorado Plateau: v. 36, p. 1–6.
- Moucha, R., Forte, A.M., Rowley, D.B., Mitrovica, J.X., Simmons, N.A., and Grand, S.P., 2008, Mantle convection and the recent evolution of the Colorado Plateau and the Rio Grande Rift valley: *Geology*, v. 36, p. 439–442.
- Nations, J.D., 1989, Cretaceous history of northeastern and east-central Arizona, *in* Jenney, J.P. and Reynolds, S.J. eds., *Geologic Evolution of Arizona*, Arizona Geological Society, p. 435–446.
- Nations, J.D., 1987, Report on the Tertiary stratigraphy of the Tonto basin, central Arizona: unpublished report prepared for the U.S. bureau of Reclamation, Denver Colorado, 27 p.
- Nations, D., Wilt, J.C., and Hevly, R.H., 1985, Cenozoic Paleogeography of Arizona, *in* Flores, R.M. and Kaplan, S.S. eds., *Cenozoic Paleogeography of the west-central United States*, Denver, Colorado, Rocky Mountain Section S.E.P.M., p. 335–355.
- Pecha, M.E., Gehrels, G.E., Karlstrom, K.E., Dickinson, W.R., Donahue, M.S., Gonzales, D.A., and Blum, M.D., 2018, Provenance of Cretaceous through Eocene strata of the Four Corners region: Insights from detrital zircons in the San Juan Basin, New Mexico and Colorado: *Geosphere*, v. 14, p. 785–811.
- Peirce, H.W., 1985, Arizona's Backbone: The Transition Zone: Arizona Bureau of Geology and Mineral Technology Fieldnotes, v. 14, p. 2–6.
- Peirce, H.W., Damon, P.E., and Shafiqullah, M., 1979, An Oligocene (?) Colorado Plateau Edge in Arizona: *Tectonophysics*, v. 61, p. 1–24.
- Péwé, T.L., 1978, Terraces of the Lower Salt River Valley in Relation to the Late Cenozoic History of the Phoenix Basin, Arizona: *Guidebook to the Geology of Central Arizona*, v. 2, p. 1–13.
- Potochnik, A.R., 2001a, Cenozoic Structural and Paleogeographic Evolution of the Transition Zone, Central Arizona: Arizona State University, Ph.D Thesis, 173 p.
- Potochnik, A.R., 1989, Depositional style and tectonic implications of the Mogollon Rim Formation (Eocene), east-central Arizona: *New Mexico Geological Society 40th Annual Field Conference Guidebook*, p. 107–118.
- Potochnik, A.R., 2001b, Paleogeomorphic evolution of the Salt River region: Implications for Cretaceous-Laramide inheritance for ancestral Colorado River drainage: *Colorado River: Origin and evolution: Grand Canyon*, Arizona, Grand Canyon Association, p. 17–22.
- Potochnik, A.R., and Faulds, J.E., 1998, A tale of two rivers: mid-tertiary structural

- inversion and drainage reversal across the southern boundary of the Colorado Plateau: *Geologic Excursions in Northern and Central Arizona, Fieldtrip Guidebook for the Geological Society of American Rocky Mountain Section meeting, Flagstaff AZ*, p. 149–174.
- Roy, M., Jordan, T.H., and Pederson, J., 2009, Colorado Plateau magmatism and uplift by warming of heterogeneous lithosphere: *Nature*, v. 459, p. 978–982.
- Schmidt, K., 1991, Tertiary palaeoclimatic history of the southeastern Colorado Plateau: *Palaeogeography, Paleoclimatology, Palaeocology*, v. 86, p. 283–296.
- Seedorff, E., Barton, M.D., Gehrels, G.E., Valencia, V.A., Johnson, D.A., and Maher, D.J., 2019, Temporal evolution of the Laramide arc: U-Pb geochronology of plutons associated with porphyry copper mineralization in east-central Arizona, *in Geological Society of America, Field Guide 55*, p. 369–400.
- Shafiqullah, M., Damon, P.E., Lynch, D.J., Reynolds, S.J., and Raymond, R.N., 1980, K-Ar Geochronology and Geologic History of Southwestern Arizona and Adjacent Areas by: *Arizona Geological Society Digest*, v. XII, p. 201–260.
- Shaw, C.A., and Karlstrom, K.E., 1999, The Yavapai-Mazatzal crustal boundary in the Southern Rocky Mountains: *Rocky Mountain Geology*, v. 34, p. 37–52.
- Skotnicki, S., Deponty, J., and Dorn, R.I., 2016, Developing a Better Understanding of the Evolution of Water Resources in the East Salt River Valley , Arizona: Special Research Project Report for Modification 35 to Cooperative Agreement 98-153C, 71 p.
- Skotnicki, J. S., 2002, Geologic Map of the Sierra Ancha, Central Arizona: Arizona Geological Survey Digital Geologic Map DGM-24, version 1.0, map scale 1:24,000, 31 p., 2 plates.
- Slattery, J.S., Cobban, W.A., Mckinney, K.C., Harries, P.J., and Sandness, A.L., 2015, Early Cretaceous to Paleocene Paleogeography of the Western Interior Seaway: The Interaction of Eustasy and Tectonism, *in Bingle-Davis, M. ed., Wyoming Geological Association Guidebook, 68th Annual Field Conference, Casper, Wyoming*, p. 22–60.
- Whitmeyer, S.J., and Karlstrom, K.E., 2007, Tectonic model for the Proterozoic growth of North America: *Geosphere*, v. 3, p. 220–259.
- Wijk, J.W., Baldrige, W.S., Hunen, J. Van, Goes, S., Aster, R., Coblenz, D.D., Grand, S.P., and Ni, J., 2010, Small-scale convection at the edge of the Colorado Plateau: Implications for topography, magmatism, and evolution of Proterozoic lithosphere: *Geology*, v. 38, p. 611–615.
- Williams, G.D., and Stelck, C.R., 1975, Speculations on the Cretaceous paleogeography of North America, *The Cretaceous System in the Western Interior of North America: Geological Association of Canada Special Paper*, v. 13, p. 1–20.
- Wrucke, B.C.T., Bromfield, C.S., Simons, F.S., Greene, R.C., Brenda, B., Miller, R.J., and Gray, F., 2004, Geologic Map of the San Carlos Indian Reservation , Arizona:

U.S. Geologic Survey, Geologic Investigations Series I-2780, 27 p.

Young, R.A., and Mckee, E.H., 1978, Early and middle Cenozoic drainage and erosion in west-central Arizona: Geological Society of America Bulletin, v. 89, p. 1745–1750.

## **CHAPTER 2: COLORADO PLATEAU UPLIFT IN THE SALT RIVER AREA**

### **ABSTRACT**

The Colorado Plateau is a unique geologic province because of its high average elevation (2 km) and relatively undeformed Paleozoic and Mesozoic rock strata. The region was near sea level until about 75 million years ago. Colorado Plateau uplift occurred over multiple stages, one during the Laramide Orogeny (80-50 Ma) and another during the ignimbrite flareup (35-25 Ma). Several lines of evidence support a third and possibly ongoing stage of uplift in the past 10 Ma. The proposed mechanism for driving this recent stage of uplift is dynamic topography supported by convecting asthenosphere bringing warmer and less dense mantle beneath the edges of the Colorado Plateau. The goal of this study is to test and quantify the post-10 Ma surface uplift hypothesis for the southern Colorado Plateau using differential incision rates of the Salt River.

A southwest-flowing proto-Salt River first established itself from the rim of the Colorado Plateau to the Tonto Basin around 12 Ma, and aggraded the 300-m-thick upper Dagger Canyon conglomerate east of and within Tonto Basin after 8 Ma. The modern Salt River achieved its present pathway via a major base level lowering event when the river spilled over from the Tonto Basin in the Arizona Transition Zone to join the Gila River around 2.8 Ma. The Gila had previously been graded to sea level likely around the same time as the Colorado River. Incision rates are calculated using the age and height of four Springerville Volcanic Field basalt flows emplaced as long run-outs within paleochannels of the Salt River's headwaters and tributaries between 3 and 0.52 Ma. Results indicate that the Salt River has incised its headwaters near the rim of the southern Colorado Plateau at a near-steady rate of 95 m/Ma since 3 Ma. The incision rate of the

Gila River at the Sentinel-Arlington volcanic field over the past 2.37 Ma has been 10 m/Ma, indicating a differential incision rate of 85m/Ma between the Salt River's headwaters and its base level. This 85 m/Ma differential incision rate is interpreted to represent a proxy for southern Colorado Plateau uplift estimating a total of 275 m of uplift over the past 3 Ma. This uplift was likely driven partly by the construction of the Springerville Volcanic Field volcanic but more fundamentally by mantle-driven epeirogenic uplift of the southern edge of the Colorado Plateau. Other regional differential incision studies for rivers draining the Colorado Plateau (Virgin River 338 m/Ma, Grand Canyon 140 m/Ma, and Verde River 100-160 m/Ma) are somewhat higher than Salt River rates suggesting a west to east decrease in differential incision/uplift rates along the southern Colorado Plateau over the past few million years.

## **INTRODUCTION**

The Colorado Plateau is a unique geologic province in the western United States because its rock layers record minimal deformation compared to the surrounding geologic provinces despite experiencing about 2 kilometers of uplift since the late Cretaceous. The Colorado Plateau is bordered by the Rocky Mountains to the north and east, the Basin and Range to the south and west, and the Rio Grande rift to the east. The Arizona Transition Zone is a transitional boundary between the Colorado Plateau and the Basin and Range and marks the location of the now collapsed mountain range known as the Mogollon Highlands. These highlands uplifted Precambrian rocks that were structurally higher than the Colorado Plateau until Basin and Range normal faulting down-dropped the Arizona Transition zone such that it is now topographically lower than the Colorado Plateau.

The Colorado Plateau region has experienced several stages of uplift since it was near sea level around 75 Ma (Karlstrom et al., 2011; Cather et al., 2012). The first stage occurred during the Laramide Orogeny 70 to 40 Ma due to the flat-slab subduction of the Farallon Plate and the resulting hydration and minor thickening of the North American lithosphere (Coney, 1978; Humphreys et al., 2003; Liu and Gurnis, 2010). The second stage occurred during the Oligocene ignimbrite flare-up which was the result of Farallon plate delamination and its replacement by warm and buoyant asthenosphere underneath the Colorado Plateau (Lipman and Glazner, 1991; Humphreys, 1995; Farmer et al., 2008; Roy et al., 2009; Cather et al., 2012; Karlstrom et al., 2012). In the southern Colorado Plateau area ignimbrite volcanism occurred in the Mogollon-Datil volcanic field ~40 Ma to 24 Ma (McIntosh et al., 1992). The Colorado Plateau has likely experienced a third stage of uplift over the past 10 Ma. This most recent and possibly ongoing stage is proposed to be the result of asthenospheric convection beneath the Colorado Plateau and other dynamic mantle processes (Morgan and Swanberg, 1985; Lowry et al., 2000; Karlstrom et al., 2008; Moucha et al., 2008, 2009; Wijk et al., 2010; Crow et al., 2011; Levander et al., 2011; Cather et al., 2012; Karlstrom et al., 2012; Crow et al., 2014). Several studies have invoked dynamic mantle processes to explain the elevation and relief in the western United States in general (Humphreys and Dueker, 1994; Wernicke et al., 1996; Braun, 2010; Donahue et al., 2013). Other studies have found evidence for epeirogenic, mantle-driven uplift along sections of the Jemez lineament based on river incision rates and analysis of river paleoprofiles (Wisniewski and Pazzaglia, 2002; Nereson et al., 2013; Channer et al., 2015; Repasch et al., 2017).

Multiple studies have used long-term (i.e. > 0.3 Ma) differential incision rates of rivers draining the Colorado Plateau as evidence for post-10 Ma Colorado uplift (Hamblin et al., 1981; Karlstrom et al., 2007, 2008, 2017; Crow et al., 2014; Walk et al., 2019). Several interacting factors control a river's incision rate including climate, base level fall, headwater uplift, changes in sediment load, and bedrock erodibility (Kirby et al., 2001; Sklar and Dietrich, 2004; Gilfillan et al., 2008; Phillips and Lutz, 2008; Pederson and Tressler, 2012). The interaction between these factors is complex but certain patterns of incision rates can indicate the dominant controls. Rivers responding to relative headwater uplift/ base level fall are more likely to have steady incision rates over periods of millions of years. The benefit of measuring river incision rates over a scale of millions of years is climate complexities like glacial-interglacial aggradation-incision cycles are averaged out (Karlstrom et al., 2012; Walk et al., 2019). Modeling suggests that river incision generated by headwater uplift will propagate upstream resulting in steeper river channel gradient while river incision generated by climatic changes will propagate downstream resulting in a decrease in river channel gradient (Wobus et al., 2010).

The Salt River is one of the largest river systems in southern Arizona. It flows southwest from the southern edge of the Colorado Plateau, through the Arizona Transition Zone, and into the Basin and Range where it becomes the largest tributary of the Gila River near Phoenix (Chapter 1 Figure 1 this study). The Gila River continues to flow southwest through the Basin and Range until it meets the Colorado River near Yuma, AZ. The Salt River begins at the confluence of the White and Black Rivers (Figure 1A). Its

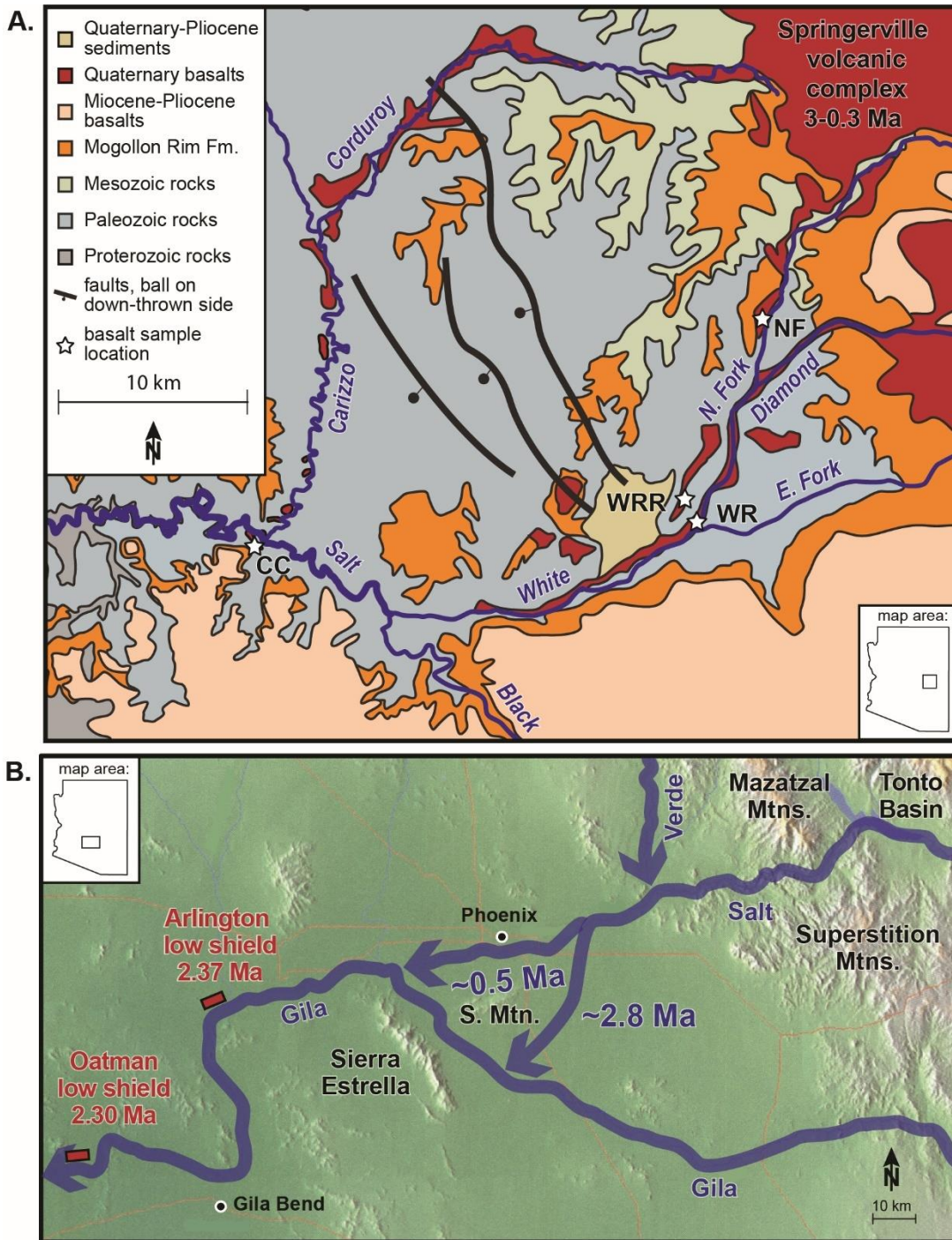


**Figure 1A:** Simplified geologic map for the headwaters of the Salt River showing the Springerville Volcanic complex basalt sample locations for this study. Modified from Skotnicki, 2002 and Faulds, 1986. CC stands for Carrizo Creek, WRR stands for White River Ridge, WR stands for White River and NR stands for North Fork. **Figure 1B:** Digital elevation map of the Phoenix Basin depicting the original path of the Salt River after it spilled over from the Tonto Basin around 2.8 Ma and the present path of the Salt River taken around 0.5 (Laney and Hahn, 1986; Block, 2007; Skotnicki et al., 2016). Red boxes are the locations of Sentinel-Arlington volcanic field flows used to calculate Gila River incision rates since 2.37 Ma (Cave, 2015).

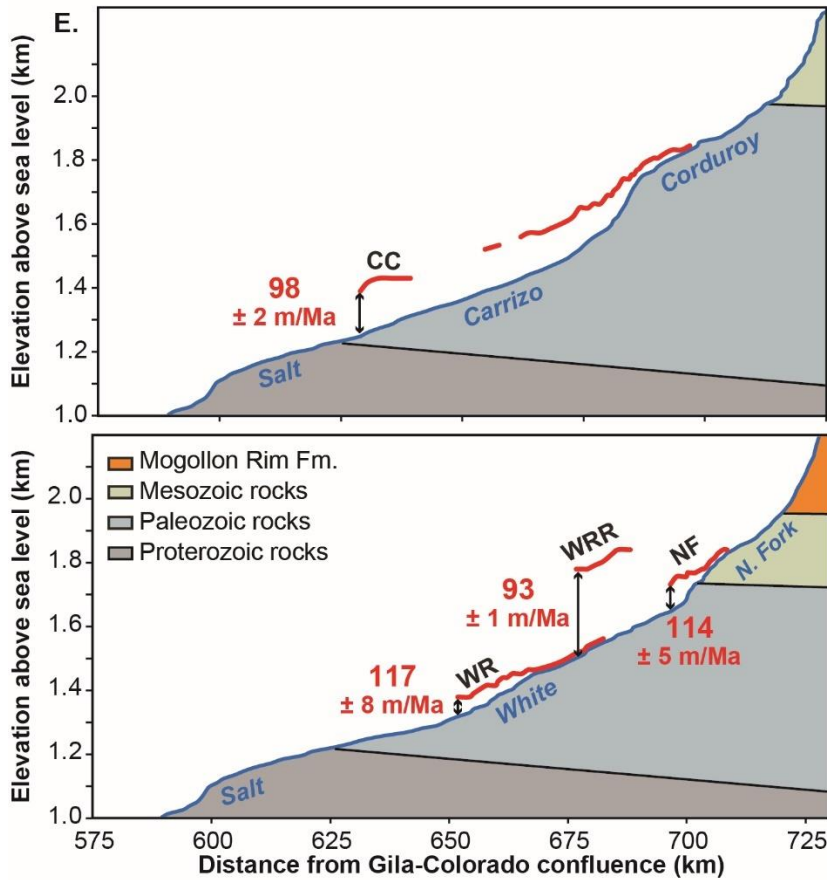
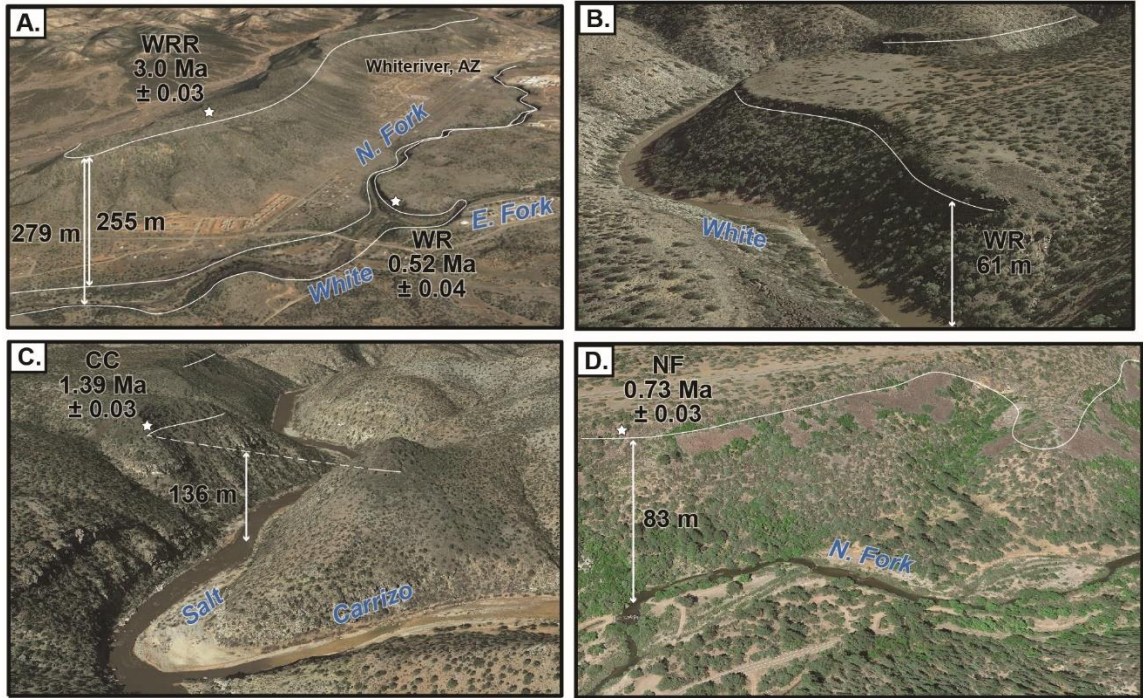
headwaters drain the Mogollon Rim escarpment, the White Mountains, and Springerville Volcanic Field.

The Salt River became a tributary of the Gila River around 2.8 Ma according to cosmogenic burial ages of the first arriving Salt River gravels in the Phoenix Basin (Skotnicki et al., 2016). These gravels indicate the Salt River originally flowed on the east side of South Mountain and then took its modern course around 0.5 Ma (Laney and Hahn, 1986; Block, 2007; Skotnicki et al., 2016) (Figure 1B). The Gila River was already fully integrated from the Safford Basin to sea level by this time (Dickinson, 2015; Skotnicki et al., 2016; Gootee, 2019). This integration represents the last major base level fall along the Salt River

The goal of this study is to evaluate if this young Salt River system is responding to post-10 Ma southern Colorado Plateau uplift by calculating incision rates of the Salt River's headwaters since its final major base level fall around 2.8 Ma (Skotnicki et al., 2016). Incision rates are calculated by dating basalt flows that infilled paleochannels of the Salt River and its tributaries then dividing their age by their height above the modern river (Figure 2). The elevation profiles of the Salt River, its tributaries and the basalt flows are also analyzed to understand how the incision is propagating through the river system.

## **METHODS**

The headwaters of the Salt River provide an excellent opportunity to test the post-10 Ma Colorado Plateau uplift hypothesis for the southern Colorado Plateau. The headwaters drain the Springerville Volcanic Complex (Figure 1A). Four far-traveled basalt flows infilled paleochannels of the Salt River's headwaters (Figure 2). The profiles



**Figures 2 A-D:** Google Earth images of basalt sample locations along with their age in Ma, analytical error and height above the river in meters. WR stands for White River, WRR stands for White River Ridge, CC stands for Carrizo Creek and NF stands for North Fork. **Figure 2E:** Elevation profiles of the Salt River and its tributaries along with the elevation profiles of Springerville Volcanic complex basalt flows that infilled their paleochannels. Incision rates listed in red next to each flow along with their associated analytical error.

of these basalt flows represent the paleoprofile of the river they flowed into and provide excellent incision rate constraints. The headwaters are incising similar strata of Paleozoic shale, sandstone and limestone at each location (Figure 1A and 2E) which minimizes rock erodibility complexities.

Bedrock incision rates represent how much vertical distance a river has cut into bedrock after the eruption of a basalt that flowed into a river channel. Basalt flows into the lowest topographic area in a landscape, often along river beds. To calculate incision rates, a sample of basalt was collected near the bottom of the basalt flow to approximate the elevation of the strath at the time of the flow. The height of the base of the flow above the modern river was measured using a range finder or GPS and confirmed with USGS topography maps or Google Earth. The basalt samples were dated using  $^{40}\text{Ar}/^{39}\text{Ar}$  techniques and the age of the sample is divided by its height above the modern river in meters giving a bedrock incision rate in meters per million years (m/Ma). Basalts can be more difficult to erode through than many lithologies, perhaps dampening long term bedrock incision rate, but studies on numerous rivers of the Grand Canyon region follow this same approach and show that multiple basalt or lava dam emplacement episodes do not seem to alter long term steady bedrock incision rates (Crow et al., 2014; Karlstrom et al., 2017; Walk et al., 2019).

Basalt samples were dated at the New Mexico Geochronology Research Laboratory using  $^{40}\text{Ar}/^{39}\text{Ar}$  methods (McIntosh et al., 2003). This method produces more precise ages than K/Ar methods previously used to date these basalt flows. Samples were crushed and cleaned with hydrochloric acid before grains of the groundmass were separated from phenocrysts. Argon gas was extracted from the groundmass by a process

of step heating using a resistance furnace and analyzed using a Thermo Scientific Helix Multicollector noble gas mass spectrometer. Ages were calculated by weighting each heating step by the inverse of the variance to test the statistical precision of contiguous heating steps (Mahon, 1996).

## RESULTS

The location, description, age and calculated incision rates of basalt samples are listed in Table 1.  $^{40}\text{Ar}/^{39}\text{Ar}$  spectrum diagrams for volcanic samples are presented in Figure 3. Sample locations are shown on Figure 1A.

Sample	Latitude	Longitude	Elev. (m)	H.A.R. (m)	Age (Ma)	I.R. (m/Ma)	Description
JA18-WRR-1	33.79827	-110.00648	1766	279	3	93	Springerville basalt from White River ridge west of Whiteriver, AZ
JA18-CC-1	33.78626	-110.33261	1364	136	1.39	98	Springerville basalt along Carrizo Creek above Salt River
JA18-NF-1	33.92369	-109.93939	1728	83	0.73	114	Springerville basalt along North Fork White River
JA18-WR-1	33.79188	-109.99433	1528	61	0.52	117	Springerville basalt along White River

**Table 1:** Basalt sample location, elevation (Elev.) in meters, age in Ma, height above river (H.A.R.) in meters, and incision rate (I.R.) in m/Ma.

The highest basalt flow is located 279 m above the modern White River and west of the town of Whiteriver, AZ (Figure 2A). This flow originated from a vent near Mount Baldy and flowed west around 4 km until it entered a southwest-flowing paleo-White River. River gravels are present beneath this flow in float however no outcrops of the gravels or the strath were identified. Sample JA18-WRR-1 was taken from this flow which is informally referred to as the White River ridge basalt flow in this study. The  $^{40}\text{Ar}/^{39}\text{Ar}$  age of this flow is  $3.0 \pm 0.03$  Ma giving an incision rate of  $93 \pm 1$  m/Ma. This refines the 86 m/Ma incision rate at this location from a previously obtained  $3.25 \pm 0.08$  Ma K/Ar age (Damon et al., 1996).

The second highest basalt flow traveled east from the Springerville Volcanic Field along a paleo-Corduroy Creek then flowed southwest 27 km along a paleo-Carrizo Creek

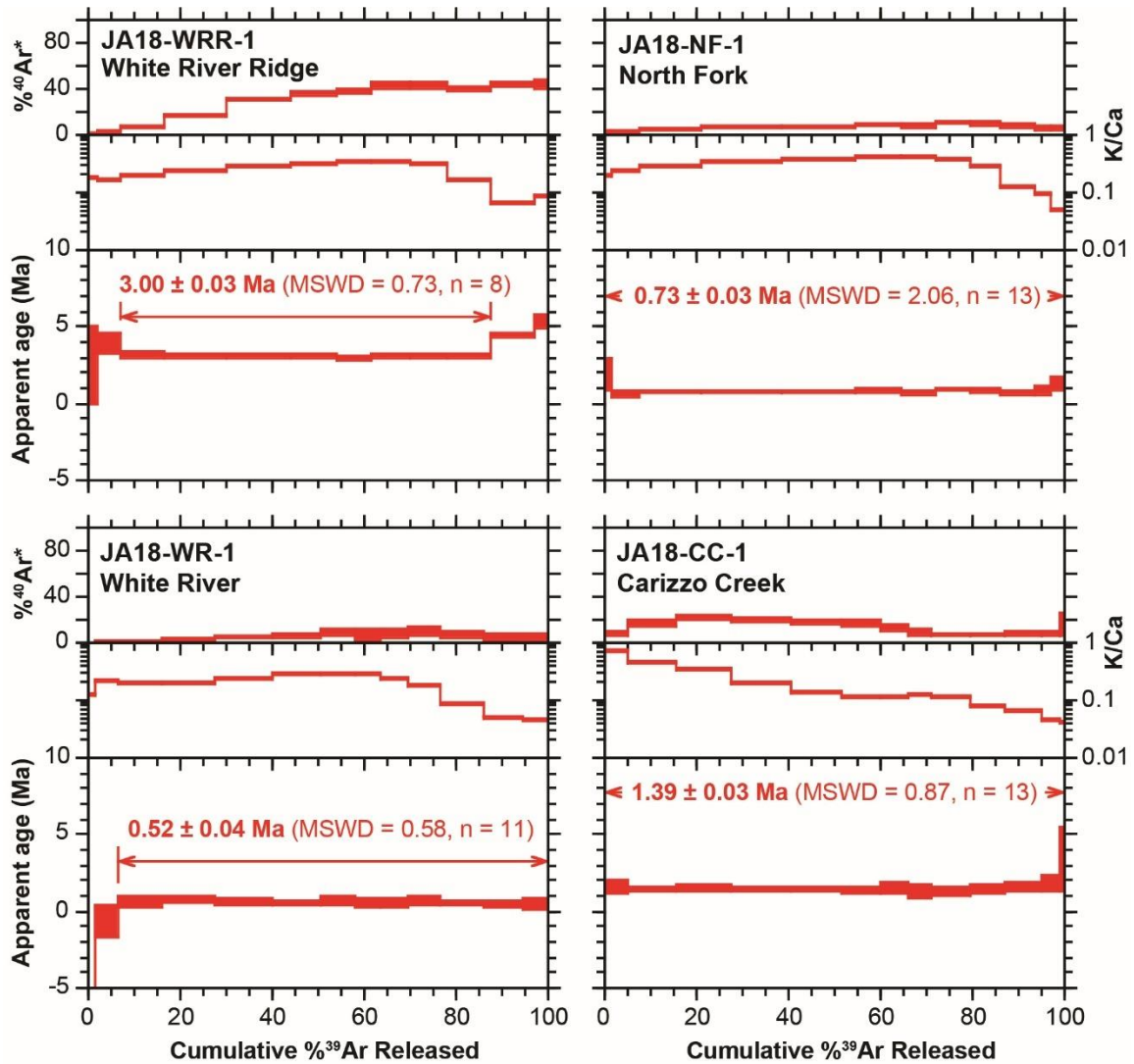


**Figure 3:**  $^{40}\text{Ar}/^{39}\text{Ar}$  step heated release spectra and apparent plateau ages for basalt samples along with %  $^{40}\text{Ar}^*$  released and K/Ca ratio for each heating step. Sample information available in Table 1.

until it met a paleo-Salt River near the modern Salt River-Carrizo Creek confluence (Figure 2C). A range finder was utilized at the Salt-Carrizo confluence during sample collecting to measure the 136 m height of the base of the flow above the river. USGS topography maps and Google Earth also confirmed the base of the flow at its terminus is 136 m above the river. Sample JA18-CC-1 was taken from this flow above the Carrizo Creek-Salt River confluence. The  $^{40}\text{Ar}/^{39}\text{Ar}$  age of  $1.39 \pm 0.03$  Ma gives an incision rate

of  $98 \pm 2$  m/Ma. Condit and Mayer (1991) previously obtained a K-Ar age of  $1.90 \pm 0.06$  Ma for this flow and calculated an incision rate of 60 m/Ma based on a 115 m height of the flow above the river.

The next highest basalt flowed west and then southwest along a paleo-North Fork White River from the Springville volcanic field (Figure 2D). The base of the flow is 83 m above the modern North Fork White River at its terminus. The lowest basalt flow traveled west and southwest along a paleo-Diamond Creek until it met the paleo-North Fork White River and continued southwest past the White River-Black River confluence. The base of the flow is 61 m above the river at its terminus. Sample JA18-NF-1 was taken from this flow and its  $^{40}\text{Ar}/^{39}\text{Ar}$  age of  $0.73 \pm 0.04$  gives an incision rate of  $114 \pm 5$  m/Ma.

Sample JA18-WR-1 was taken above the confluence of the east and north forks of the White River (Figure 2B). This basalt flowed an additional 12 km downstream along the White River and is 61 m above the modern river at its terminus. The  $^{40}\text{Ar}/^{39}\text{Ar}$  age of this sample is  $0.52 \pm 0.04$  Ma, giving an incision rate of  $117 \pm 8$  m/Ma. This updates a previously obtained K-Ar age of  $0.60 \pm 0.10$  Ma (Damon et al., 1996) that gave an incision rate of 102 m/Ma.

## **INTERPRETATION**

The four Springerville Volcanic Field basalts constrain the incision rates of the upper Salt River. Incision rates calculated from these flows indicate that the Salt River headwaters have incised the southern Colorado Plateau at semi-steady rates around 93-117 m/Ma over the past 3 Ma (Figure 2E). This semi-steady headwater incision result is

also shown by the two basalt flows in the same reach of the river near Whiteriver, AZ. These flows provide a unique opportunity to constrain the Salt River's incision rate between 3.0-0.52 Ma at one location. The base of the 3.0 Ma White River ridge basalt at its terminus is 255 m above the base of the 0.52 Ma White River basalt flow (Figure 2A) indicating that, the White River has incised the underlying bedrock at a rate of  $103 \pm 3$  m/Ma between 3 and 0.52 Ma similar to the 93-117 m/Ma rates calculated relative to the modern river. Figure 4A graphs the age of each basalt flow versus its height above the river. This graph shows a clear trend of near-steady bedrock incision at a rate of  $95 \pm 1.3$  m/Ma over the past 3 Ma.

The maximum amount of bedrock incision under these basalt flows is at the downstream terminus, with incision decreasing to near zero farther upstream (Figure 2E). The modern river elevation profile under the basalt flows is steeper than the paleoprofile of the basalt flows. This suggests that the headwaters have steepened their profile following the emplacement of each flow. Knickpoints are found beneath each flow and are interpreted to reflect a knickpoint from the flow terminus migrating upstream. These features are similar to flows seen in the Virgin River headwaters (Walk et al., 2019) and are interpreted to indicate that the incision is propagating upstream via headward erosion.

Figure 4B summarizes the integration and differential incision rates of the modern Salt River. The Salt River reached the Basin and Range and became a Gila River tributary through a process of lake spillover around 2.8 Ma (Skotnicki et al., 2016). The Gila River was already integrated from the Safford Basin to sea level by this time (Dickinson, 2015; Skotnicki et al., 2016; Gootee, 2019). Based on the now buried Salt River gravels, the initial path of the river ran east of South Mountain (Laney and Hahn,

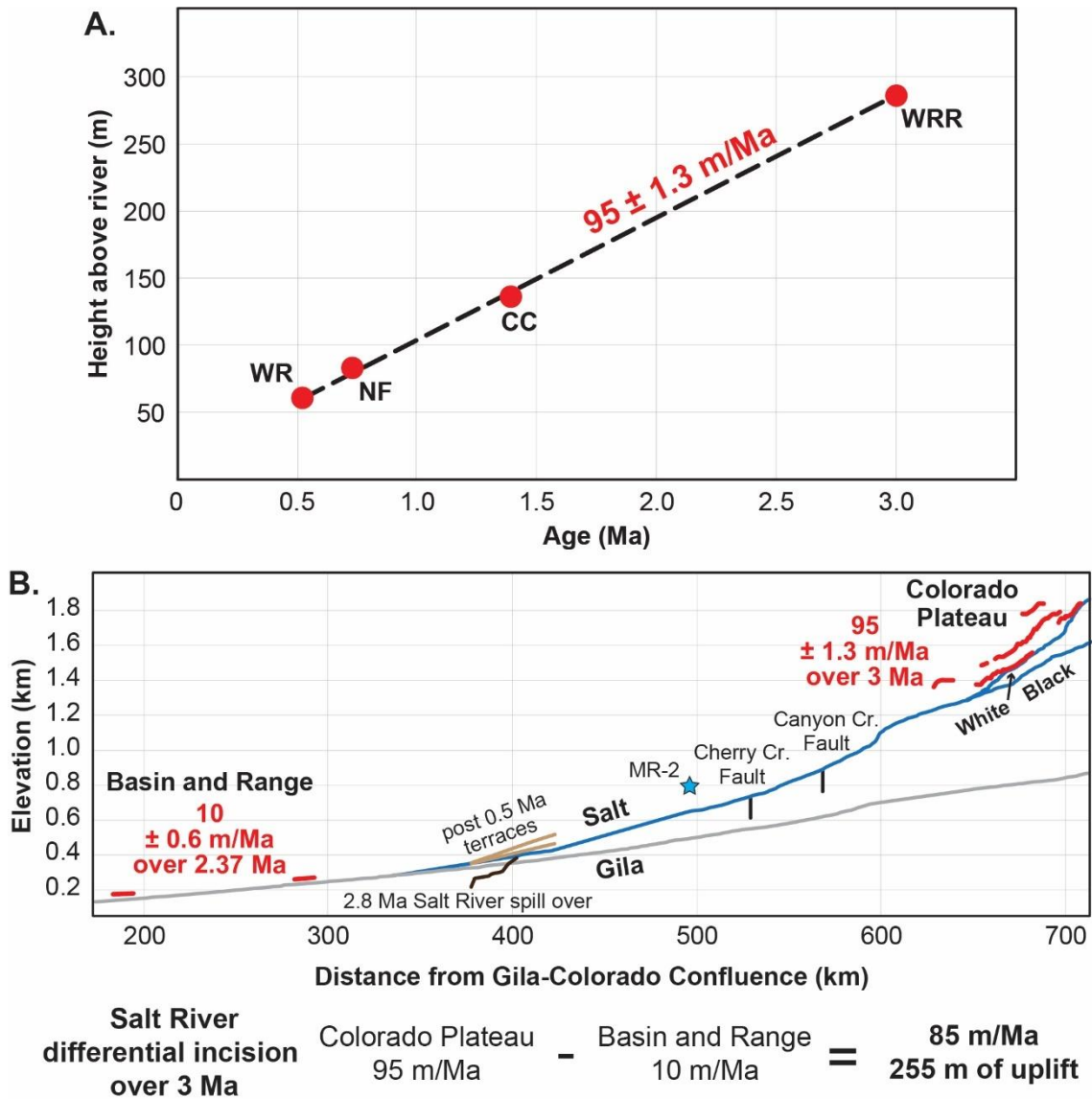


**Figure 4A:** Graph of the age in Ma and height above river in meters for each basalt flow. WR stands for White River, WRR stands for White River Ridge, CC stands for Carrizo Creek and NF stands for North Fork. Trendline shows the near-steady incision rate of  $95 \pm 1.3$  m/Ma over the past 3 Ma. **Figure 4B:** Elevation profile of Salt River, Gila River, White River, and Black River. Shows relative positions of basalt flows used to calculate Colorado Plateau headwater and Basin and Range baselevel incision rates. Also shows Salt River differential incision rate calculation for the past 3 Ma.

1986; Block, 2007) (Figure 1B) The base of these gravels display a steep profile

(Skotnicki et al., 2016) (Figure 4B). The Salt River took its modern course north of South

Mountain around 0.5 Ma (Skotnicki et al., 2016) (Figure 1B). The river then formed a

series of strath terraces with profiles that diverge upstream (Péwé, 1978) (Figure 4B).

The Gila River has minimally incised the Basin and Range downstream of the Salt River confluence since 2.37 Ma based on two Sentinel-Arlington basalt flows that infilled the Gila's channel (Cave, 2014, 2015) (Figure 4B). These basalts show the Gila has incised the Basin and Range at a rate of only 10 m/Ma over the past 2.37 Ma, in contrast to the 95 m/Ma rates over a similar time period in the Salt River headwaters. This indicates an 85 m/Ma differential incision rate for the Salt River since 3 Ma.

The near-steady headwater incision rates can either be driven by base level lowering, an increase in the drainage area or headwater uplift. The rates cannot be due to base level lowering since the Gila and Salt River's base level has not dropped significantly since 2.8 Ma. The drainage area of the Salt River east of Tonto Basin was almost completely integrated before the spillover from Tonto Basin (Chapter 1 this study). This means an increase in drainage area does not sufficiently explain the near-steady incision rates since the majority of its drainage area had previously been intergraded.

In the absence of base level fall and headwater expansion, our interpretation for these observations is that the Salt River headwaters are responding to recent southern Colorado Plateau uplift. The Salt River's differential incision rate of 85 m/Ma since 3 Ma represents a proxy for the uplift over this time, for an estimated 255 m of uplift. Several geomorphic observations reinforce this interpretation that the Salt River is responding to post-10 Ma uplift of the Colorado Plateau. The elevation profile of < 0.5 Ma Salt River terraces in the Phoenix Basin all diverge upstream (Figure 4B) which Péwé (1978) interpreted as evidence for headwater uplift. Also pediments near the Salt River are responding to base level fluctuations at rates similar to rates found in areas experiencing

active tectonism or active base level fall (Larson et al., 2014). The combination of upstream incision propagation and steepening of channel profile are also observed in models for headwater uplift whereas river incision driven by climatic changes may propagate downstream resulting in a decrease in river channel gradient (Wobus et al., 2010).

### *Comparing River Incision and Uplift Across the Southern Colorado Plateau*

Several studies have used long-term differential incision rates of rivers draining other areas of the Colorado Plateau as evidence for post-10 Ma Colorado uplift (Hamblin et al., 1981; Karlstrom et al., 2007, 2008, 2017; Crow et al., 2014; Walk et al., 2019). Figure 5 compiles the bedrock incision rates along different rivers that cross the boundary between the Colorado Plateau and the Basin and Range in Arizona over the past 3-5 Ma. Incision rates are plotted on a map of mantle P-wave velocity at 100 km to emphasize the interpretation that mantle buoyancy variations may be driving differential surface uplift of the southwestern edge of the Colorado Plateau (Karlstrom et al., 2008, 2012, 2017; Crow et al., 2014; Schmandt and Lin, 2014). In more recent papers, the sharp velocity transition imaged inboard of the physiographic Colorado Plateau margin (yellow zone of Figure 5) is envisioned to be the site of ongoing transfer of heat and mass that is driving differential surface uplift, with this active zone having migrated inboard over the past 10 million years at the about the same rate and direction as absolute North American plate motion, of 20 cm/yr towards the southwest (Crow et al., 2011; Walk et al., 2019). Since incision along these rivers is semi-steady at each location over timescales > 1 Ma; and since the Colorado River and Gila River systems were previously graded to Gulf of California sea level (Dickinson, 2015; Crow et al., 2019) the cumulative difference

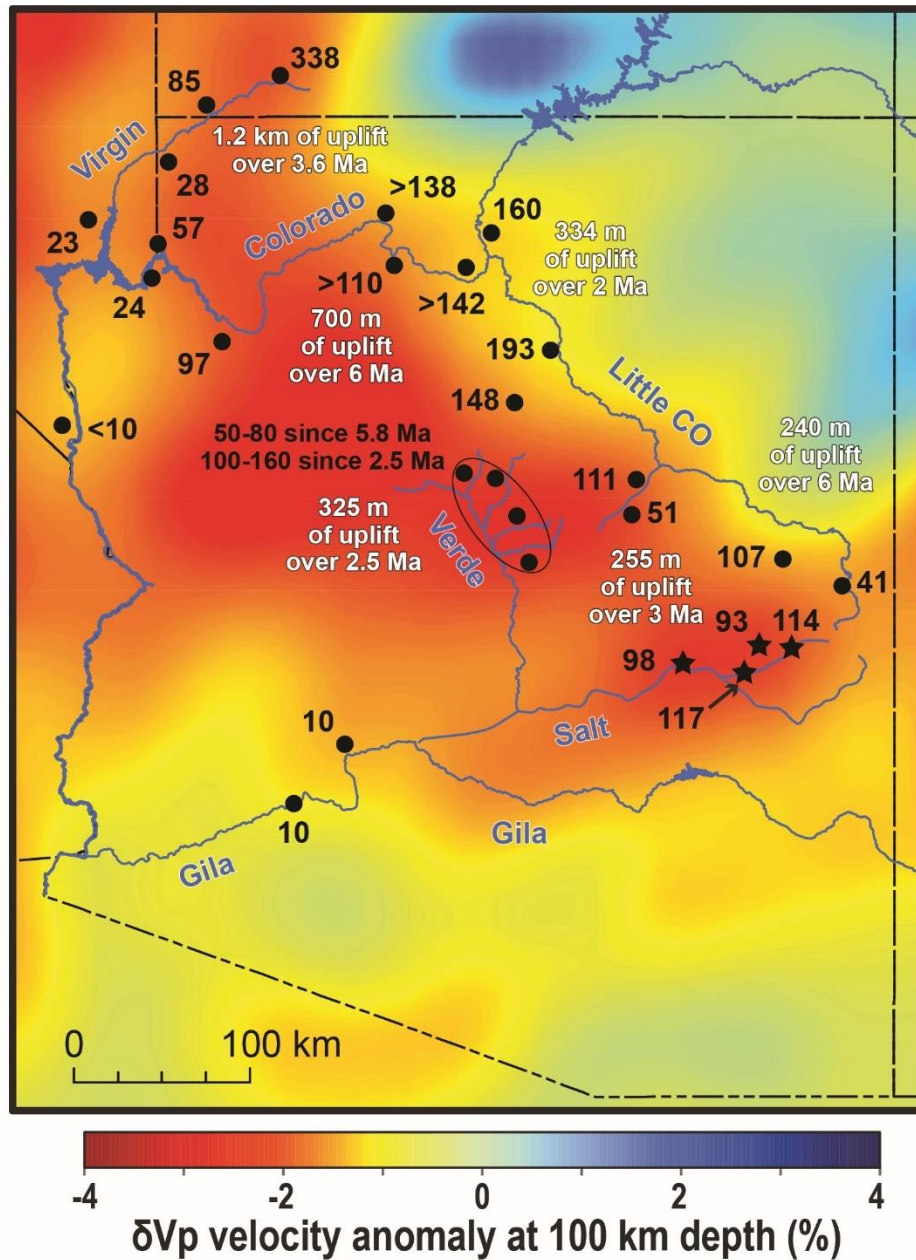


**Figure 5:** Mantle tomography at 100 km depth (Schmandt and Lin, 2014). Warmer colors indicate warmer, less dense, upwelling mantle whereas cooler colors represent denser, colder, downwelling mantle. Black dots and corresponding values are river incision rates between 4 Ma to present. Star locations are incision rates from this study. Incision rates and uplift estimate from Karlstrom et al., 2008 (Colorado River), Karlstrom et al., 2017 (Little Colorado River), Ott et al., 2018 (Verde River), Crow et al., 2019 (Colorado River) and Walk et al., 2019 (Virgin River).

between Colorado Plateau bedrock incision and Basin and Range incision is a proxy of Colorado Plateau uplift (neglecting the <100 m scale baselevel changes since Pliocene higher sea levels (Crow et al., 2014).

Differential incision for the Verde River's headwater tributaries is summarized by Ott et al., (2018). They reported differential incision of 290-464 m over the past 5.8 Ma (~50-80 m/Ma) but noted the majority of the observed differential incision was likely accomplished after the spill over from Verde Valley around 2.5 Ma, meaning incision rates would be closer to 100-160 m/Ma (Ott et al., 2018, p. 1707). Since the base level of the Verde has not changed after 2.5 Ma, the 100-160 m/Ma rates imply 250-400 m of Colorado Plateau uplift in the past 2.5 Ma, somewhat higher than the 255 m of estimated uplift of the Salt River headwaters since 3 Ma.

The Colorado River system through Grand Canyon has received extensive study and near-steady rates in each of the incision locations shown in Figure 4 has been documented over timescale of 3-4 Ma for western Grand Canyon and ~1.5-2.5 Ma for eastern Grand Canyon (Crow et al., 2019). New data indicate a 4.6 Ma maximum depositional age for a Bullhead Alluvium strath near the Nevada border (Crow et al., 2020) which, combined with arguments that sub-surface Bullhead alluvium has been down-dropped (Thacker et al., 2020), suggests that average long term bedrock incision rates in the lower Colorado River corridor are < 10 m/Ma since initial integration around 5 Ma. In contrast, western Grand Canyon has incised at rates 97 m/Ma and eastern Grand Canyon at a rate of 160 m/Ma. This suggests 150 m/Ma of differential incision over 5 Ma and Colorado Plateau uplift amounts of 750 m relative to sea level during this time. This

is similar to (150 m/Ma), or perhaps 1.5 times higher (if 100 m/Ma) than the range of rates reported for the Verde River headwaters.

The Virgin River exhibits differential incision which previous geologists have interpreted as evidence for Colorado Plateau uplift (Hamblin et al., 1981). Work by Walk et al., (2019) applies  $^{40}\text{Ar}/^{39}\text{Ar}$  dating techniques on basalt-filled paleoriver channels along the length of the river and shows a cumulative total of 328 m/Ma differential incision suggesting 1.2 km of differential uplift over the past 3.6 Ma. These rates are double the inferred rates across Grand Canyon.

The Little Colorado River closes the “incision circuit” between the Colorado and Salt River systems because its confluence is located in eastern Grand Canyon and its headwaters are the same Mogollon Rim region of the Salt and Verde rivers (Chapter 1 Figure 2 this study). Its downstream rates of 148-193 m/Ma are similar to the Colorado River over the past 1-2 Ma and its upstream rates of 41-107 m/Ma are similar to the Salt and Verde Rivers (Karlstrom et al., 2017).

Our overall interpretation of the differential incision data is that the Colorado Plateau has been actively uplifting over the past 10 Ma and this uplift has caused rivers to cut deep canyons at its edges. The 41 m/Ma average rate for the Little Colorado River headwaters over the past 7 Ma (Karlstrom et al., 2017) is interpreted to be the background uplift rate for the southern Colorado Plateau. The progressive increase in differential incision/uplift from southeast to northwest along the southwestern margin of the Colorado Plateau is interpreted here to be due to broad warping of the uplifting plateau. Faster incision indicates uplift along the western edge of the Colorado Plateau

mimics higher slip rates and magnitude on the Hurricane fault along the western edge of the Colorado Plateau.

*Supporting Evidence for Active Tectonism and Upwelling Mantle in the Southern Colorado Plateau Area*

Several other lines of evidence support the hypothesis that the southern Colorado Plateau is tectonically active. Between December 21st and 22<sup>nd</sup>, 2003 a swarm of at least twenty earthquakes ranging in magnitude between 3.2-4.2 occurred in eastern Arizona near the Colorado Plateau-Transition zone physiographic boundary (Eagar and Fouch, 2007). The EarthScope USArray Transportable Array in Arizona aided in identifying a zone of elevated seismic activity along the southern edge of the Colorado Plateau (Lockridge et al., 2012). The Transition Zone and the southern edge of the Colorado Plateau correspond with a zone of neotectonic structures, historic earthquake epicenters and regional downcutting-patterns that likely reflect an elongated zone of Pliocene-Quaternary uplift (Menges and Pearthree, 1989). Neotectonic faulting has also deformed Springville volcanic field basalts between the ages of 0.9 to 1.3 Ma (Crumpler et al., 1994).

Mantle tomography models of the present mantle constructed from mantle P-wave velocity variations indicate that the southern edge of the Colorado Plateau and the Transition Zone are underlain by low velocity mantle and the core of the Colorado Plateau is underlain by high velocity mantle (Schmandt and Humphreys, 2010; Schmandt and Lin, 2014) (Figure 5). Low P-wave mantle velocity indicates warmer mantle that contains partial melt while fast velocities indicate cooler mantle temperatures. The combined thermal and compositional aspects of low velocity regions induce uplift

relative to high velocity regions. Springs in the southern Colorado Plateau area that overlie the low P-wave mantle velocity regions contain elevated concentrations of mantle derived helium and CO<sup>2</sup> (Newell et al., 2005; Gilfillan et al., 2008; Crossey et al., 2009, 2016) Thick accumulations of travertine as well as large CO<sub>2</sub> and He gas fields in the Springerville volcanic field area are also evidence for mantle degassing and partial mantle melt beneath the southern Colorado Plateau (Embid, 2009; Priewisch et al., 2014). Springerville volcanic field petrology changes from tholeiitic to evolved alkalic basalt implying that these lavas were sourced from partial melting and the volume of source melt decreased during the eruptions (Condit et al., 1989).

## **CONCLUSIONS**

This study provides evidence for post-10 Ma uplift of the southern Colorado Plateau as quantified by differential incision rates of the Salt River since its last major base level fall around 2.8 Ma (Skotnicki et al., 2016). Incision rates indicate the Salt River has steadily incised the margin of the Colorado Plateau at a rate of around 95 m/Ma over the past 3 Ma. The river's base level has not dropped significantly since then based on the slow incision rate (10 m/Ma) of the Gila River at the Sentinel-Arlington volcanic field over the past 2.37 Ma (Cave, 2014, 2015) and its drainage area east of Tonto Basin has not increased significantly (Chapter 1 this study). Thus, differential incision between the southern Colorado Plateau (95 m/Ma) and the Basin and Range (10 m/Ma) suggests the southern Colorado Plateau has been uplifted at a rate of 85 m/Ma relative to the Basin and Range for a total of 255 m over 3 Ma. This young uplift is interpreted to be due to upwelling asthenosphere associated with the eruptions of the White Mountain and Springville Volcanic complexes on the southern edge of the Colorado Plateau.

## REFERENCES

- Block, J., 2007, 3-D visualization for water resources planning and for Salt River paleogeomorphology in central Arizona: Arizona State University, Master's Thesis, p. 139.
- Braun, J., 2010, The many surface expressions of mantle dynamics: *Nature Geoscience*, v. 3, p. 825–833.
- Cather, S.M., Chapin, C.E., and Kelley, S.A., 2012, Diachronous episodes of Cenozoic erosion in southwestern North America and their relationship to surface uplift, paleoclimate, paleodrainage, and paleoaltimetry: *Geosphere*, v. 8, p. 1177–1206.
- Cave, S.R., 2014, Geologic Map of the Sentinel-Arlington Volcanic Field, Maricopa and Yuma Counties, Arizona: Arizona Geological Survey, Contributed Map CM-14-A, 11 p.
- Cave, S.R., 2015, The Sentinel-Arlington Volcanic Field, Arizona: Arizona State University, Ph.D. Thesis, 98 p.
- Channer, M.A., Ricketts, J., Zimmerer, M., Heizler, M., and Karlstrom, K.E., 2015, Surface uplift above the Jemez mantle anomaly in the past 4 Ma based on  $^{40}\text{Ar}/^{39}\text{Ar}$  dated paleoprofiles of the Rio San Jose, New Mexico, USA: *Geosphere*, v. 11, p. 1384–1400.
- Condit, C.D., Crumpler, L.S., Aubele, J.C., and Elston, W.E., 1989, Patterns of Volcanism along the Southern Margin of the Colorado Plateau: The Springerville Field: *Journal of Geophysical Research*, v. 94, p. 7975–7986.
- Coney, P.J., 1978, The plate tectonic setting of southeastern Arizona, *in* Callender, J.F., Wilt, J.C., and Clemons, R.E. eds., *Land of Cochise (Southeastern Arizona)* New Mexico Geological Society 29th Annual Fall Field Conference Guidebook, New Mexico Geological Society, p. 285–290.
- Crossey, L.J. et al., 2016, Continental smokers couple mantle degassing and distinctive microbiology within continents: *Earth and Planetary Science Letters*, v. 435, p. 22–30.
- Crossey, L.J., Karlstrom, K.E., Springer, A.E., Newell, D., Hilton, D.R., and Fischer, T., 2009, Degassing of mantle-derived CO<sub>2</sub> and He from springs in the southern Colorado Plateau region — Neotectonic connections and implications for groundwater systems: *GSA Bulletin*, v. 121, p. 1034–1053, doi:10.1130/B26394.1.
- Crow, R.S. et al., 2019, Insights into post-Miocene uplift of the western margin of the Colorado Plateau from the stratigraphic record of the lower Colorado River: *Geosphere*, v. 15, p. 1826–1845.
- Crow, R., Karlstrom, K., Asmerom, Y., Schmandt, B., Polyak, V., and Dufrane, S.A., 2011, Shrinking of the Colorado Plateau via lithospheric mantle erosion: Evidence from Nd and Sr isotopes and geochronology of Neogene basalts: *Geology*, v. 39, p. 27–30.

- Crow, R., Karlstrom, K., Darling, A., Crossey, L., Polyak, V., Granger, D., Asmerom, Y., and Schmandt, B., 2014, Steady incision of Grand Canyon at the million year timeframe: A case for mantle-driven differential uplift: *Earth and Planetary Science Letters*, v. 397, p. 159–173.
- Crow, R.S., Schwing, J., Karlstrom, K.E., Heizler, M., Pearthree, P.A., House, P.K., Stelten, M., Dulin, S., and Crossey, L., 2020, Redefining the age of the Colorado River: *Geology*, v. in press.
- Crumpler, L.S., Aubele, J.C., and Condit, C.D., 1994, Volcanics and neotectonic characteristics of the Springerville volcanic field, Arizona, *in* Chamberlin, R.M., Kues, B.S., Cather, S.M., Barker, J.M., and C, M.W. eds., *Mogollon slope (West-Central New Mexico and East-Central Arizona)* New Mexico Geological Society 45th Annual Fall Field Conference Guidebook, p. 147–164.
- Damon, P.E., Shafiqullah, M., Ramond, H.C., and Spencer, J.E., 1996, K-Ar Dates From The University Of Arizona Laboratory Of Isotope, 1971-1991: Arizona Geological Survey Open File Report, OFR-96-18, 53 p.
- Dickinson, W.R., 2015, Integration of the Gila River drainage system through the Basin and Range province of southern Arizona and southwestern New Mexico (USA): *Geomorphology*, v. 236, p. 1–24.
- Donahue, M.S., Karlstrom, K.E., Aslan, A., Darling, A., Granger, D., Wan, E., Dickinson, R.G., and Kirby, E., 2013, Incision history of the Black Canyon of Gunnison, Colorado, over the past ~ 1 Ma inferred from dating of fluvial gravel deposits: *Geosphere*, v. 9, p. 815–826.
- Eagar, K.C., and Fouch, M.J., 2007, Detection of a Unique Earthquake Swarm in Eastern Arizona: *Arizona Geology*, v. 37, p. 5.
- Embid, E.H., 2009, U-series dating, geochemistry, and geomorphic studies of travertines and springs of the Springerville area, east-central Arizona, and tectonic implications: The University of New Mexico, Master's Thesis, p. 103.
- Farmer, G.L., Bailey, T., and Elkins-tanton, L.T., 2008, Mantle source volumes and the origin of the mid-Tertiary ignimbrite flare-up in the southern Rocky Mountains, western U.S.: *Lithos*, v. 102, p. 279–294.
- Gilfillan, S.M. V, Ballentine, C.J., Holland, G., Blagburn, D., Sherwood, B., Stevens, S., Schoell, M., and Cassidy, M., 2008, The noble gas geochemistry of natural CO<sub>2</sub> gas reservoirs from the Colorado Plateau and Rocky Mountain provinces, USA: *Geochimica et Cosmochimica Acta*, v. 72, p. 1174–1198.
- Gootee, B.F., 2019, Revised depth-to-bedrock and depth-to base of Gila River deposits along the southern Higley and northern Picacho Basin boundary, Pinal County, Arizona: Arizona Geological Survey, Open-File Report OFR-19-01, 18 p.
- Hamblin, W.K., Damon, P.E., and Bull, W.B., 1981, Estimates of vertical crustal strain rates along the western margins of the Colorado Plateau: *Geology*, v. 9, p. 293–298.
- Humphreys, E.D., 1995, Post-Laramide removal of the Farallon slab, western United

- States: *Geology*, v. 23, p. 987–990.
- Humphreys, E.D., and Dueker, K.G., 1994, Physical state of the western U.S. upper mantle: *Journal of Geophysical Research*, v. 99, p. 9635–9650.
- Humphreys, E., Hessler, E., Dueker, K., Farmer, G.L., Erslev, E., and Atwater, T., 2003, How Laramide-Age Hydration of North American Lithosphere by the Farallon Slab Controlled Subsequent Activity in the Western United States: *International Geology Review*, v. 45, p. 575–595.
- Karlstrom, K.E. et al., 2012, Mantle-driven dynamic uplift of the Rocky Mountains and Colorado Plateau and its surface response: Toward a unified hypothesis: *Lithosphere*, v. 4, p. 3–22.
- Karlstrom, K.E., Crossey, L.J., Embid, E., Crow, R., Heizler, M., Hereford, R., Beard, L.S., Ricketts, J.W., Cather, S., and Kelley, S., 2017, Cenozoic incision history of the Little Colorado River: Its role in carving Grand Canyon and onset of rapid incision in the past ca. 2 Ma in the Colorado River System: *Geosphere*, v. 13, p. 49–81.
- Karlstrom, K.E., Crow, R., Crossey, L.J., Coblenz, D., and Van Wijk, J.W., 2008, Model for tectonically driven incision of the younger than 6 Ma Grand Canyon: *Geology*, v. 36, p. 835–838.
- Karlstrom, K.E., Crow, R.S., Peters, L., McIntosh, W., Raucchi, J., Crossey, L.J., and Dunbar, N., 2007,  $^{40}\text{Ar}/^{39}\text{Ar}$  and field studies of Quaternary basalts in Grand Canyon and model for carving Grand Canyon: Quantifying the interaction of river incision and normal faulting across the western edge of the Colorado Plateau: *GSA Bulletin*, v. 119, p. 1283–1312.
- Kirby, E., Studies, C., and Barbara, S., 2001, Quantifying differential rock-uplift rates via stream profile analysis: *Geology*, v. 29, p. 415–418.
- Laney, R.L., and Hahn, M.E., 1986, Hydrogeology of the eastern part of the Salt River Valley area, Maricopa and Pinal Counties, Arizona: U.S. Geological Survey, Water Resources Investigations 86-4147, 4 plates.
- Larson, P.H., Bowles, Z., Harrison, E., Diego, S., Kelley, S.B., Schmeeckle, M.W., and Douglass, J., 2014, Pediment response to drainage basin evolution in south-central Arizona: *Physical Geography*, v. 35, p. 369–389.
- Levander, A., Schmandt, B., Miller, M.S., Liu, K., Karlstrom, K.E., Crow, R.S., Lee, C.T.A., and Humphreys, E.D., 2011, Continuing Colorado plateau uplift by delamination-style convective lithospheric downwelling: *Nature*, v. 472, p. 461–465.
- Lipman, P.W., and Glazner, A.F., 1991, Introduction to middle Tertiary Cordilleran volcanism-magma sources and relations to regional tectonics: *Journal of Geophysical Research: Solid Earth and Planets*, v. 91, p. 6329–6345.
- Liu, L., and Gurnis, M., 2010, Dynamic subsidence and uplift of the Colorado Plateau: *Geology*, v. 38, p. 663–666.

- Lockridge, J.S., Fouch, M.J., and Arrowsmith, J.R., 2012, Seismicity within Arizona during the Deployment of the EarthScope USArray Transportable Array: *Bulletin of the Seismological Society of America*, v. 102, p. 1850–1863.
- Lowry, A.R., Ribe, N.M., and Smith, B., 2000, Dynamic elevation of the Cordillera, western United States: *Journal of Geophysical Research*, v. 105, p. 23,371–23,390.
- Mahon, K.L., 1996, Mahon The New York Regression Application of an Improved Statistical Method to Geochemistry: *International Geology Review*, v. 38, p. 293–303.
- Mcintosh, W.C., Chapin, C.E., Ratte, J.C., and Sutter, J.F., 1992, Time-stratigraphic framework for the Eocene-Oligocene Mogollon-Datil volcanic field, southwest New Mexico: *Geological Society of America Bulletin*, v. 104, p. 851–871.
- Mcintosh, W.C., Heizler, M., Peters, L., and Esser, R., 2003, 40Ar/39Ar Geochronology at the New Mexico Bureau of Geology and Mineral Resources: *New Mexico Bureau of Geology and Mineral Resources, Open File Report OF-AR-1*, 7 p.
- Menges, C.M., and Pearthree, P.A., 1989, Late Cenozoic tectonism in Arizona and its impact on regional landscape evolution, *in* Jenney, J.P. and Reynolds, S.J. eds., *Geologic Evolution of Arizona*, *Arizona Geological Society Digest* 17, p. 649–680.
- Morgan, P., and Swanberg, C.A., 1985, On the Cenozoic uplift and tectonic stability of the Colorado Plateau: *Journal of Geodynamics*, v. 3, p. 39–63.
- Moucha, R., Forte, A.M., Rowley, D.B., Mitrovica, J.X., Simmons, N.A., and Grand, S.P., 2009, Deep mantle forces and the uplift of the Colorado Plateau: v. 36, p. 1–6.
- Moucha, R., Forte, A.M., Rowley, D.B., Mitrovica, J.X., Simmons, N.A., and Grand, S.P., 2008, Mantle convection and the recent evolution of the Colorado Plateau and the Rio Grande Rift valley: *Geology*, v. 36, p. 439–442.
- Nereson, A., Stroud, J., Karlstrom, K., Heizler, M., and Mcintosh, W., 2013, Dynamic topography of the western Great Plains: Geomorphic and 40Ar/39 Ar evidence for mantle-driven uplift associated with the Jemez lineament of NE New Mexico and SE Colorado: *Geosphere*, v. 9, p. 521–545.
- Newell, D.L., Crossey, L.J., Karlstrom, K.E., and Fischer, T.P., 2005, Continental-scale links between the mantle and groundwater systems of the western United States: Evidence from travertine springs and regional He isotope data: *GSA Today*, v. 17, p. 4–10.
- Ott, R.F., Whipple, K.X., and Soest, M. Van, 2018, Incision history of the Verde Valley region and implications for uplift of the Colorado Plateau (central Arizona): *Geosphere*, v. 14, p. 1690–1709.
- Pederson, J.L., and Tressler, C., 2012, Colorado River long-profile metrics, knickzones and their meaning: *Earth and Planetary Science Letters*, v. 345–348, p. 171–179, <http://dx.doi.org/10.1016/j.epsl.2012.06.047>.
- Péwé, T.L., 1978, Terraces of the Lower Salt River Valley in Relation to the Late

- Cenozoic History of the Phoenix Basin, Arizona: Guidebook to the Geology of Central Arizona, v. 2, p. 1–13.
- Phillips, J.D., and Lutz, J.D., 2008, Geomorphology Profile convexities in bedrock and alluvial streams: *Geomorphology*, v. 102, p. 554–566.
- Priewisch, A., Crossey, L.J., Karlstrom, K.E., Polyak, V.J., Asmerom, Y., Nereson, A., and Ricketts, J.W., 2014, U-series geochronology of large-volume Quaternary travertine deposits of the southeastern Colorado Plateau: Evaluating episodicity and tectonic and paleohydrologic controls: *Geosphere*, v. 10, p. 401–423.
- Repasch, M., Karlstrom, K., Heizler, M., and Pecha, M., 2017, Birth and evolution of the Rio Grande fluvial system in the past 8 Ma: Progressive downward integration and the influence of tectonics, volcanism, and climate: *Earth-Science Reviews*, v. 168, p. 113–164.
- Roy, M., Jordan, T.H., and Pederson, J., 2009, Colorado Plateau magmatism and uplift by warming of heterogeneous lithosphere: *Nature*, v. 459, p. 978–982.
- Schmandt, B., and Humphreys, E., 2010, Complex subduction and small-scale convection revealed by body-wave tomography of the western United States upper mantle: v. 297, p. 435–445.
- Schmandt, B., and Lin, F., 2014, P and S wave tomography of the mantle beneath the United States: *Geophysical Research Letters*, v. 41, p. 6342–6349.
- Sklar, L.S., and Dietrich, W.E., 2004, A mechanistic model for river incision into bedrock by saltating bed load: *Water Resources Research*, v. 40, p. 1–22.
- Skotnicki, S., Deponty, J., and Dorn, R.I., 2016, Developing a Better Understanding of the Evolution of Water Resources in the East Salt River Valley , Arizona: Special Research Project Report for Modification 35 to Cooperative Agreement 98-153C, 71 p.
- Skotnicki, J. S., 2002, Geologic Map of the Sierra Ancha, Central Arizona: Arizona Geological Survey Digital Geologic Map DGM-24, version 1.0, map scale 1:24,000, 31 p., 2 plates.
- Thacker, J.O., Karlstrom, K.E., Crossey, L.J., Crow, R.S., Cassidy, C.E., Beard, L.S., Singleton, J.S., Strickland, E.D., Seymour, N.M., and Wyatt, M.R., 2020, Post–12 Ma deformation in the lower Colorado River corridor, southwestern USA: Implications for diffuse transtension and the Bouse Formation: *Geosphere*, v. 16, p. 111–135.
- Walk, C.J., Karlstrom, K.E., Crow, R.S., and Heizler, M.T., 2019, Birth and evolution of the Virgin River fluvial system : ~ 1 km of post – 5 Ma uplift of the western Colorado Plateau: v. 15, p. 759–782.
- Wernicke, B. et al., 1996, Origin of High Mountains in the Continents: The Southern Sierra Nevada: *Science*, v. 271, p. 190–193.
- Wijk, J.W. Van, Baldridge, W.S., Hunen, J. Van, Goes, S., Aster, R., Coblenz, D.D.,

- Grand, S.P., and Ni, J., 2010, Small-scale convection at the edge of the Colorado Plateau: Implications for topograph , magmatism, and evolution of Proterozoic lithosphere: *Geology*, v. 38, p. 611–614.
- Wisniewski, P.A., and Pazzaglia, F.J., 2002, Epeirogenic Controls on Canadian River Incision and Landscape Evolution, Great Plains of Northeastern New Mexico: *Journal of Geology*, v. 110, p. 437–456.
- Wobus, C.W., Tucker, G.E., and Anderson, R.S., 2010, Does climate change create distinctive patterns of landscape incision? *Journal of Geophysical Research*, v. 115, p. 1–12.